# IMPROVING THE STRENGTH OF ADDITIVELY MANUFACTURED OBJECTS VIA MODIFIED INTERIOR STRUCTURE

A THESIS SUBMITTED TO
THE GRADUATE SCHOOL OF NATURAL AND APPLIED SCIENCES
OF
MIDDLE EAST TECHNICAL UNIVERSITY

BY

CAN MERT AL

IN PARTIAL FULFILLMENT OF THE REQUIREMENTS
FOR
THE DEGREE OF MASTER OF SCIENCE
IN
MECHANICAL ENGINEERING

JANUARY 2018

Approval of the thesis:

**IMPROVING THE STRENGTH OF ADDITIVELY MANUFACTURED OBJECTS VIA MODIFIED INTERIOR STRUCTURE**

Submitted by **CAN MERT AL** in partial fulfillment of the requirements for the degree of **Master of Science in Mechanical Engineering Department, Middle East Technical University** by,

Prof. Dr. Gülbin Dural Ünver _____
Director, Graduate School of **Natural and Applied Sciences**

Prof. Dr. M. A. Sahir Arıkan _____
Head of Department, **Mechanical Engineering Dept., METU**

Asst. Prof. Dr. Ulaş Yaman _____
Supervisor, **Mechanical Engineering Dept., METU**

**Examining Committee Members:**

Prof. Dr. Haluk Darendeliler _____
Mechanical Engineering Dept., METU

Asst. Prof. Dr. Ulaş Yaman _____
Mechanical Engineering Dept., METU

Prof. Dr. Oğuzhan Yılmaz _____
Mechanical Engineering Dept., Gazi University

Assoc. Prof. Dr. Ender Ciğeroğlu _____
Mechanical Engineering Dept., METU

Asst. Prof. Dr. Orkun Özşahin _____
Mechanical Engineering Dept., METU

**Date:** 30.01.2018

**I hereby declare that all the information in this document has been obtained and presented in accordance with academic rules and ethical conduct. I also declare that, as required by these rules and conduct, I have fully cited and referenced all material and results that are not original to this work.**

Name, Last Name: Can Mert Al

Signature:

# ABSTRACT


IMPROVING THE STRENGTH OF
ADDITIVELY MANUFACTURED OBJECTS
VIA
MODIFIED INTERIOR STRUCTURE

Al, Can Mert
M.S., Department of Mechanical Engineering
Supervisor : Asst. Prof. Dr. Ulaş Yaman

January 2018, 126 pages

This thesis study provides an approach to improve the durability of additively manufactured parts via modified interior structures by considering the stress field results from tensile loading conditions. In other words, the study provides an automated method, i.e., implicit slicing method, which improves the strength of the parts with infill structures modified according to the quasi-static Finite Element Analysis (FEA) results under tensile loadings, automatically.

The parts which are used throughout the work are designed by using Rhinoceros3D® which is Computer Aided Design (CAD) software by considering the ASTM D638 standard. In scope of this study, the interior structures of the designed parts are modified by using the developed algorithm in Grasshopper3D®, which provides the strength improvements by the help of heterogeneous infill structures. The quasi-static FEA is performed in Karamba3D® which works as a plug-in on Grasshopper3D®. Interior structures are constructed by using the stress field results and the first principal stress vector directions under the tensile loading conditions.

The G-Code file which is required to manufacture the parts via 3D printing is also obtained inside the constructed Grasshopper3D® schema by using a Python scripting to be used for a DeltaWASP 3D printer.

For the geometries, different methods were employed to construct the interior structures. Then, the method which gives the most durable parts was applied for different parts to prove the applicability of the approach. The tensile tests were performed by using the ASTM-D638 tensile testing standard.

The first version of the developed method was a kind of manual method. By using the proposed manual algorithm, the durability of the standard part was increased by about 42%.

Regarding the further steps of this thesis study, the method used to construct the infill structure was tried to be automated. In this automated method, the only input is the designed geometry. The method itself obtains the boundaries of the colored meshes, fills the interior of the regions according to their colors by using the lines which connect the first principal stress vectors and generates the G-code file to be submitted to an open source Fused Deposition Modeling (FDM) 3D printed for fabrication. By using this automated algorithm, the ultimate tensile strength of the parts was increased by about 50%. The maximum load per weight ratios of the more complex geometries are improved by about 85%.

*Keywords: Structural Optimization, Query-Based Approach, Implicit Slicing, Stress Modified Infill Structure*

# ÖZ


EKLEMELİ ÜRETİM YÖNTEMİ İLE ÜRETİLEN
PARÇALARIN DAYANIMLARININ
İÇYAPININ DEĞİŞTİRİLMESİYLE ARTTIRILMASI

Al, Can Mert
Yüksek Lisans, Makina Mühendisliği Bölümü
Tez Yöneticisi: Yrd. Doç. Dr. Ulaş Yaman

Ocak 2018, 126 sayfa

Bu tez çalışması, eklemeli üretim yöntemiyle imal edilen parçaların arzu edilen yükleme koşulları altında elde edilen gerilme alanı sonuçlarını göz önüne alarak içyapılarının değiştirilmesiyle dayanıklılığını arttıran bir yaklaşım sunmaktadır. Diğer bir deyişle, bu çalışma, parçaların belirlenen yükleme koşulları altında Sonlu Elemanlar Analizi (SEA) sonuçlarına göre otomatik olarak dolgu yapılarını değiştirerek dayanımlarını artıran bir yöntem sunmaktadır.

Çalışma boyunca kullanılan parçalar, Bilgisayar Destekli Tasarım (BDT) yazılımı olan Rhinoceros3D® kullanılarak ve ASTM D638 standardı göz önünde bulundurularak tasarlanmıştır. Bu çalışma kapsamında, tasarlanan parçaların içyapıları oluşturulan algoritma kullanılarak değiştirilmiş ve bu değişim Grasshopper3D® kullanılarak gerçekleştirilmiştir. Bu yöntem heterojen iç-yapı kullanımı sayesinde dayanım artırımı sağlamıştır. SEA, Grasshopper3D®'de eklenti olarak çalışan Karamba3D® kullanılarak gerçekleştirilmiştir. İç-yapılar eksenel yükleme sonucunda elde edilen gerilme alanı sonuçları ve birinci maksimum gerilme vektörleri kullanılarak oluşturulmuştur.

Parçaların üretimi için DeltaWASP 3D yazıcı tarafından kullanılacak olan G-komut dosyası Grasshopper3D® kullanılarak oluşturulan şema içerisinde Python kodlama dili kullanılarak elde edilir.

Geometrilerin içyapıları oluşturulurken farklı yöntemler kullanılmıştır. Daha sonra, en dayanıklı parçaları oluşturan yöntem, yaklaşımın uygulanabilirliğini kanıtlamak için farklı parçalara uygulanmıştır. Eksenel testler ASTM D638 eksenel test standardı gözetilerek gerçekleştirilmiştir.

İlk geliştirilen yöntem her şeyin kullanıcı tarafından yapıldığı bir yöntemdir. Tasarlanan manuel algoritmayı kullanarak, heterojen gerilme alanı bilgisi kullanılarak değiştirilmiş dolgu yapısı, standart parçanın dayanıklılığını %42 oranında arttırmıştır.

Bu tez çalışmasının ilerleyen aşamalarında, dolgu malzemesinin yapımında kullanılan yöntem otomatikleştirilmiştir. Gerilme alan sonuçlarından elde edilen bölgelerin iç kısımlarını doldurmak için bir Python komut dosyası kullanılmıştır. Bu otomatik yöntemde, tek girdi tasarlanmış geometridir. Yöntemin kendisi, renkli örgülerin sınırlarını elde etmekte, gerilme akış çizgilerini kullanarak bölgelerin içlerini renklerine göre doldurmakta ve üretim için açık kaynaklı Eriyik Yığma Modelleme (EYM) tipi 3B yazıcıya iletilmek üzere G-komut dosyasını üretmektedir. Bu otomatik algoritma kullanılarak parçaların nihai gerilme mukavemeti %50 oranında arttırılmıştır. Karmaşık geometriler için kullanılan maksimum taşınan yükün ağırlığa oranında ise %85 oranında artım sağlanmıştır.

*Anahtar Kelimeler: Yapısal Optimizasyon, Sorguya Dayalı Yaklaşım, Sonlu Elemanlar Analizi, Gerilme Odaklı Dolgu Yapısı*

***To My Love and My Family…***

## ACKNOWLEDGEMENTS

I would like to thank to my supervisor Asst. Prof. Dr. Ulaş Yaman, for invaluable helps and for giving chance to me to work with him.

Besides, testing opportunity for this work is supported by the Material and Processing Laboratory (M&P) of the Turkish Aerospace Industries (TAI). Thus, the author would like to thank a lot to M&P laboratory of the TAI for their superior support during the work.

I would also like to thank to Structural Testing Team of TAI for their golden supports.

**TABLE OF CONTENTS**

## LIST OF TABLES

TABLES

## LIST OF FIGURES

FIGURES

## LIST OF SYMBOLS

| | |
|---|---|
| $F$ | Applied Load |
| $A$ | Cross Sectional Area |
| $U_d$ | Distortion Energy |
| $(U_d)_y$ | Distortion Energy at Yield |
| $\sigma_1$ | First Principal Stress |
| $F_{max}$ | Maximum (Ultimate) Load Applied |
| $A_o$ | Original (Initial) Cross Sectional Area |
| $\gamma$ | Poisson's Ratio |
| $\sigma_2$ | Second Principal Stress |
| $\sigma$ | Stress |
| $\sigma_3$ | Third Principal Stress |
| $\sigma_u$ | Ultimate Tensile Strength |
| $\sigma_{vm}$ | Von Mises Stress |
| $\sigma_y$ | Yield Strength |
| $E$ | Young's Modulus |

## LIST OF ABBREVIATIONS

| | |
|---|---|
| ABS | Acrylonitrile Butadiene Styrene |
| AM | Additive Manufacturing |
| CAD | Computer Aided Design |
| CAM | Computer Aided Manufacturing |
| FDM | Fused Deposition Modeling |
| FEA | Finite Element Analysis |
| FFF | Fused Filament Fabrication |
| M&P | Materials and Processing |
| NURBS | Non-Uniform Rational B-Splines |
| SLA | Stereolithography |
| SLS | Selective Laser Sintering |
| TAI | Turkish Aerospace Industries |

# CHAPTER 1

# INTRODUCTION

Additive Manufacturing (AM), in other words 3D printing, is a process where the sequential addition of material to a domain, generally called building plate, occurs. In 3D printing, the desired object is constructed layer by layer. It is a process which starts from the virtual design of the part to manufacturing of the designed object. This study aims to construct an automated approach which only takes the geometry, boundary conditions and the loading conditions as inputs and generates the G-code file. It includes the trajectory of the printer head for the geometry to be fabricated with the stress modified infill structure, to be conveyed to an open source FDM 3D printer.

## 1.1 Motivation of the Thesis

3D printing is becoming more common each day because of its crucial advantages such as speed, accuracy, etc. over traditional manufacturing methods. Especially, Fused Filament Fabrication (FFF) 3D printing methodology is frequently used because of the fact that the FFF type of desktop 3D printers is highly appropriate for different fields of engineering and science. In spite of the fact that there are significant advantages of AM, the major disadvantage is the lower strength of the fabricated parts, which is still true for the desktop FFF 3D printers utilizing plastic materials such as Acrylonitrile butadiene styrene (ABS), Polylactic acid (PLA), Nylon, etc.

The main motivation of this thesis is to improve the mechanical behaviors of the artifacts under tensile loading. In this study, an alternative method is developed to improve the strength of the AM parts using CAD/CAE/CAM integration. Traditional CAM software of the 3D printers takes only the geometry as an input in triangular

mesh form (stereolithography, STL file) which includes data only about the outer boundaries of the geometry. Besides, by using this traditional software, inner structures are manufactured with homogeneous infill patterns, such as rectilinear, honeycomb, triangular, etc. The developed method throughout the study provides a way to produce parts with heterogeneous infill patterns by using the stress field data which is related with the loading condition that the part is exposed to. This data is taken from a FEA plug-in, such as Karamba3D®. By using heterogeneous infill structures, the strengths of the parts are increased significantly.

## 1.2 Layout of the Thesis

Chapter 2 is devoted to the literature review about AM. Initially, concise information about AM is given. Then, the methodology behind the 3D printing is explained briefly. Besides, the possible study areas such as surface quality, dimensional accuracy and mechanical behavior of the 3D printed parts are considered.

In Chapter 3, the developed methodology and the performed quasi-static FEA are presented in details. First of all, because of the fact that the method starts from the design stage, the design work is mentioned. Then, FEA details are evaluated for the different cases where Abaqus®, Millipede® and Karamba3D® are used as FEA software. Moreover, differences between this software are examined. The developed algorithm which uses the results of the FEA under the tensile loading conditions is mentioned. Finally, the G-code generation method is addressed and a brief conclusion about the chapter is given at the end.

Chapter 4 is dedicated to explain the test cases for ASTM D638-Type 1 specimens that are used for the development of the method in early stages. Throughout the study, tensile tests are performed to develop and verify the method. All the details of the tensile test performance are explained in this chapter. Besides, the detailed information about the tensile testing machine which is used for tensile testing is presented. The problems faced through the study about testing are also examined.

In Chapter 5, the best approach is employed on some other samples. They are randomly chosen geometries named as rectangle with necks, rectangle with slot and s-shaped. The details of the geometries of these samples are defined in this chapter. Then, the tensile tests performed using these artifacts are expressed. The results of the performed tests are evaluated to decide whether the proposed algorithm can be used to improve the mechanical behaviors of more complex parts under tensile loading.

Chapter 6 gives the general conclusions. Additionally, the recommendations for the future work are also addressed. The thesis study briefly concluded in this chapter.

### 1.3 Limitations of the Thesis

In this thesis, the study is limited to basic 2.5-Dimensional geometries. 2.5D geometries mean parts where 2D drawings are extruded through the height direction. So, the complex 3D geometries are not considered throughout the work.

The study is limited to use of plastic material, PLA. No other plastic materials such as nylon, ABS, etc. or metals are not considered throughout the thesis.

The study also focuses on the interior structure modification for the designed parts. So, no topology optimization about the exterior geometry is performed during the study.

The method is optimized to improve the strength characteristics of the 3D printed parts. So, no optimization performed about other mechanical properties, printing time or printing method. Only the FFF 3D printing method is used in scope of this study.

Moreover, the method is developed by using tensile testing. So, the 2.5D geometries which carry tensile loads are in the scope of this thesis study. No more loading type such as transverse loading, torsion, etc. are not issues for this study.

# CHAPTER 2

# LITERATURE REVIEW

In this chapter, literature behind this study is presented. First of all, a brief introduction about AM is given. In this introductory section, little information about the history of additive manufacturing, some related definitions about it and the manufacturing methods behind 3D printing can be found.

Besides, main research areas about AM are presented such as surface quality, dimensional accuracy and mechanical behavior. Literature about these topics is presented under related subsections.

## 2.1 Introduction

AM, also named as 3D printing or rapid prototyping, is a very important and useful fabrication technique whose history is dating back to 1980s [1]. Even though it is known as a pretty new technique, the first 3D printer has been explored in 1983. Because of the fact that the patents of the initial 3D printers are expired in the last decade, the interest about AM technologies is growing rapidly these days [2].

AM is a process where the sequential addition of material to a domain, called building plate, occurs [1]. In this process, during manufacturing a 3D object, the material is added layer by layer, where the material is plastic, metal, concrete, etc. [3]. As a pre-process, a designed 3D geometry is subdivided into collection of meshes, generally triangular meshes. This process is known as STL file conversion. In addition, these meshes created by STL conversion are also subdivided into layers on CAM software of the corresponding 3D printer. After the meshes are sliced into a series of distinct layers, the commands which provide information about the toolpath of the printer head and other related components are generated and written into a G-code file. This process is known as *slicing* which can be processed by an algorithm

known as *slicer* [4]. The basic steps of the conventional design and fabrication pipeline of AM can be seen in Figure 1.

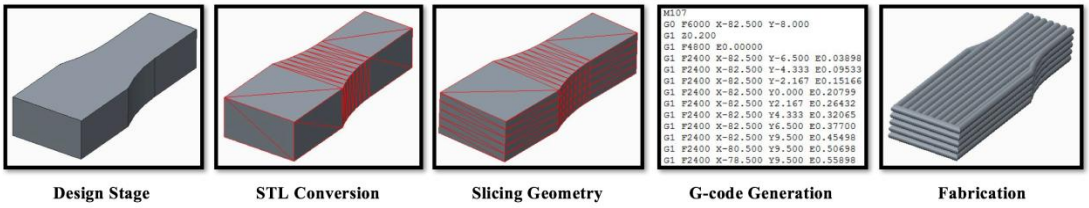


Figure 1: A design and fabrication pipeline for 3D printing

There are three main technologies used for AM; solidification of a liquid material, sintering or fusion of powder materials and deposition of semi-solid materials. The methods using these techniques can be listed as Stereolithography (SLA), Selective Laser Sintering (SLS) and Fused Deposition Modeling (FDM), respectively [1].

### 2.1.1 Stereolithography (SLA)

SLA is an AM process where plastic resin material named as photopolymer is cured by a light source layer by layer. In SLA machines, resin material is usually stored in a tank located under the print bed. The print bed is moving down slowly during the process and photopolymer is cured by mostly an UV laser at each layer of the sliced geometry. When the fabrication is completed, the part is cleaned by using a solvent to remove the uncured resin [5]. The basic structure of an SLA machine can be seen in Figure 2, below.

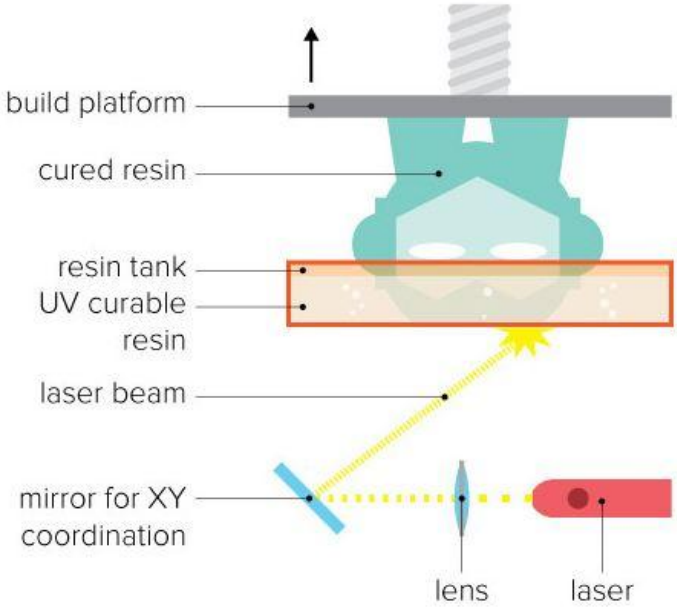


Figure 2: Structure of a SLA machine [6]

SLA is a more precise method than FFF. When very tight tolerances are required, SLA process should be selected. The reason behind this fact is that the focus diameter of the laser is smaller than the nozzle diameter where the material is extruded through [5].

SLA is a slower fabrication method because of the smaller cross sectional area of the laser beam. Moreover, the laser covers the entire cross section for each layer. The speed of the scanning is highly important for fabrication time. In fact, the larger parts take days to be manufactured. Besides, due to the limited availability of the photopolymers, it can be said that the SLA process is a bit expensive method than others. This technique is not preferred in engineering applications due to its low speed and low strength compared to the other AM methodologies. Another reason is the limited number of materials suitable for SLA machines in the manufacturing industry [5].

### 2.1.2 Selective Laser Sintering (SLS)

In SLS manufacturing technique, part fabrication is performed by laser beam which has high density. The laser beam is used to melt and cure the powder material.

This printing process is similar to the SLA process. However, the material used in this process is in powder form. Powders are stored in a tank placed below/near to the printing bed which moves down during the process to construct the geometry layer by layer [5]. The basic structure of a SLS machine can be found in Figure 3, below.

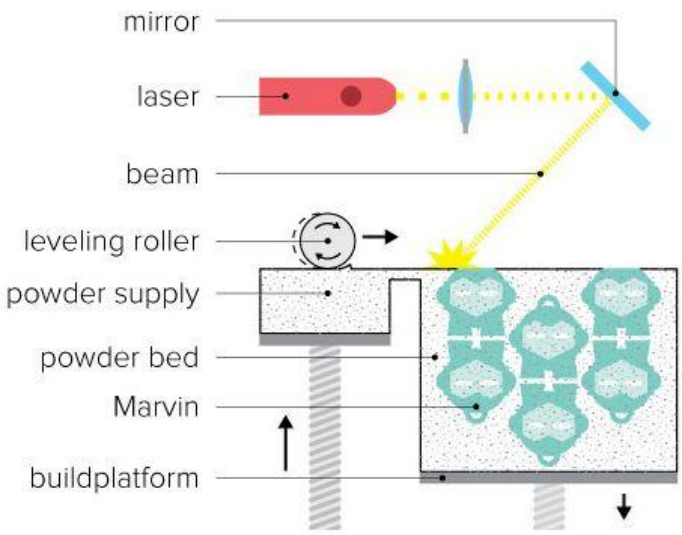


Figure 3: Structure of a SLS machine [6]

Unlike SLA, this method is flexible in terms of the material. In other words, both plastics such as nylon and polystyrene and as well as metals like steel, titanium and others can be used in the SLS process [5]. SLA uses liquid materials, but SLS works with powder materials [6]. The cost of powder materials is less the cost of photopolymers.

This method is slower than SLA. It is mostly used for low volume production for small parts whose precision is important [5]. SLA manufacturing method results in better tolerance values than SLS. SLS requires some post processing like sanding to increase the surface quality and dimensional accuracy [7].

### 2.1.3 Fused Filament Fabrication (FFF)

Another name of FFF is Fused Deposition Modeling (FDM). It is a manufacturing technique where the sequential addition of molten material at high

temperatures. The material used is mostly plastic which is stored in a filament spool as filaments. The material is led to the heated nozzle and material is extruded through the nozzle to where it is needed on a flat building. After a layer deposited, the next layer is constructed over the previously completed layer. Fundamental components of an FFF printer are shown in Figure 4.

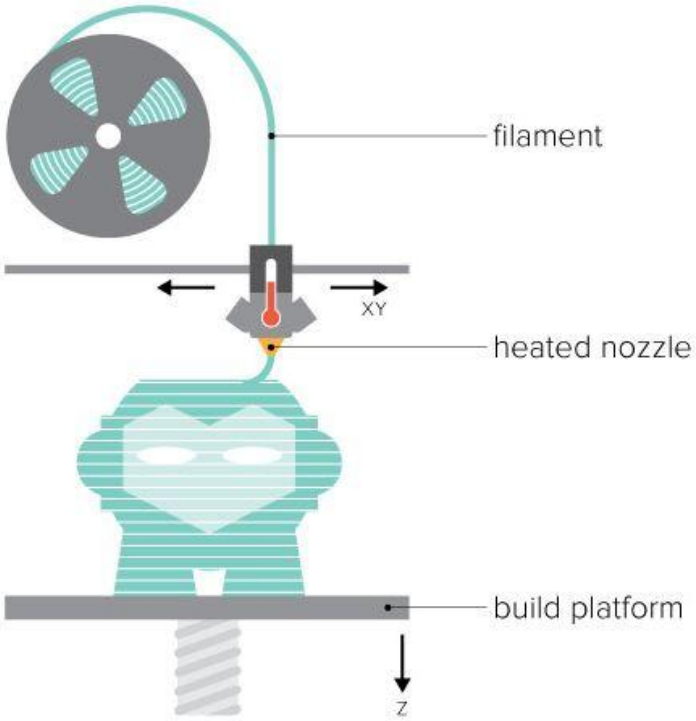


Figure 4: Structure of a FFF 3D printer [6]

In FFF method, infill percentage is one of the most important parameters. This gives flexibility to designers to adjust the strength, weight, etc. of the artifacts. FFF method is an affordable and faster 3D printing method for larger objects. Because of these advantages for manufacturing with standard tolerances, FFF method is preferred more among other AM methods [5].

One significant characteristic of  is that the 3D printers which use FFF method can be manufactured as small enough to be desktop 3D printers [1]. This characteristic gives advantages as being cheap, fabricating more compact products, etc. The method has insignificant waste generation when it is compared with the other traditional manufacturing methods. Because of all these advantages, FFF 3D

printers are used in broad numbers of engineering and science areas these days. Within FFF technology, plastic materials are usually used such as ABS, PLA, Nylon, etc. [1].

As stated above, FFF 3D printers are used in broad number of areas. This growing interest about 3D printing is stimulating new research topics for the researchers to improve the characteristic properties of the 3D printed parts. Because of the structure and the methodology of the FFF 3D printers, there are many parameters which affect the characteristic of the manufactured parts. These parameters can be considered within three subtopics; surface quality, dimensional accuracy and mechanical behavior. However, it can be stated that the most studied topics for the FFF type of 3D printing technology are characterizing and improving the mechanical behavior, i.e., durability of the manufactured parts.

## 2.2 3D Printing and Surface Quality

Surface quality is an important phenomenon for AM. Regarding surface quality, Boschetto et al. [8] worked on a development of a mathematical surface profile used to predict the roughness of the surfaces. They modeled a mathematical surface, used this model as a function of process parameters and tried to characterize all the parameters related with roughness by using a profilometric analysis. Moreover, Krolczyk et al. [9] studied on the analysis of the roughness and texture of the surfaces of the machined parts manufactured via FDM method. They tried to observe the surface integrity of these parts. They used infinite surface integrity machine for the surface integrity analyses. They concluded that while FDM surface had steep gradients, the smooth gradients existed on the surface after turning. Furthermore, Kuo and Su [10] studied on the usage of aluminum added epoxy resin to develop a method to improve the surface quality of a wax injection tool, which was manufactured by FDM technology. They achieved a surface roughness improvement up to 80% by using their proposed technique. Aditya et al. [11] worked on a vapor smoothing technique to improve the surface quality of ABS prints. They used acetone vapor to increase the smoothing of the surfaces by removing the ruins

due to printing process. They benefited from solubility of the ABS material in acetone vapor. This approach is highly utilized by the 3D printing community. Lucknow et al. [12] also studied on the surface roughness issue by considering the effects of the powder size on it. They used contact infiltration treatments cycle in 3D printing process. They concluded that the greatest improvement can be achieved about the surface roughness than a process where standard filtering processes were used by using non-reactive highly polished surfaces as contact place for the printed face. Takagishi et al. [13] developed a new technique to improve the surface quality of 3D printed resin products. They studied on a new 3D Chemical Melting Process (3D-CMF). In this technique, they applied solvent by using pen tips to certain sides of the printed part. They proposed that more precise shaping with less solvent can be achieved by using this technique. Wang et al. [14] studied on the surface quality improvement of the 3D printed parts via optimizing the printing direction. They developed an algorithm which provides a segmentation of a part into some patches whose surfaces normal are aligned perpendicularly to the printing direction. In other words, the parts were divided into some patches such that each of them was printed in an orientation where the surfaces normal were separated from the printing direction. They proposed that the stairway effects on the surfaces of the 3D printed parts can be removed by using this method. Lanzetta and Sachs [15] studied on bimodal powder distribution to improve the surface quality of 3D printed. They studied the interaction of binder and powder which is the key interaction for 3D printing process. They concluded that by using bimodal powders, the surface finish can be improved due to the improved binding quality of the building blocks, i.e., individual printing lines. Zhao et al. [16] studied on a new method to fill the interior of the parts. They examined the continuous Fermat Spirals for infill. In their work, the infill patterns were constructed as a one continuous line by connecting the Fermat Spirals. They concluded that this method gives better surface quality for the interior structures and the exterior of the parts. Furthermore, this new kind of space filling method gives possibilities to prevent the curves from being locked in pockets, gives possibilities to select the start and end points and makes the toolpath planning easier for production.

## 2.3 3D printing and Dimensional Accuracy

Dimensional accuracy is another important topic for 3D printing. Considering dimensional accuracy, Fodran et al. [17] worked on the dimensional and mechanical characterization of FDM building styles. They evaluated different bonding agents and flow rates. Furthermore, Sahu et al. [18] optimized the process parameters such as layer thickness, orientation, air gap, etc. Sudin et al. [19] studied on the effects of four main features of the parts on the dimensional accuracy. They considered different sizes of the holes, cylinders, slots and spheres by using the part manufactured with ABS material. As a conclusion, they obtained results stating that the features such as spheres and cylinders cannot be manufactured accurately by using the FDM methodology. However, the FDM machines can produce the square-shaped parts such as slots with high accuracy. Besides, Samatha S. [20] worked on circle precision by considering effects of poly count on it. Poly count is the number of triangles in .stl file of the geometry. She tried to observe the effects of the increase in the number of triangles on geometry, i.e. poly count. She concluded that the accuracy of the circular toolpath can be improved by increasing the poly count which results on the increased cost of data for motion control. She stated that when the poly count is great enough, the printed circular geometry is accurate with reasonable data cost. She also studied on the effects of the perimeter order on the dimensional accuracy. She concluded if the perimeter order is greater than 1 and if the printing is started from the outer perimeter path, the dimensional accuracy is improved. Simsek et al. [21] also studied about the dimensional accuracy of the parts with holes manufactured with FFF desktop 3D printer. They worked on the shrinkage of the holes by focusing on the interior structures of the parts near the holes. The interior of the structures was constructed by using different patterns such as linear lines in different densities, sun shape infill patterns, etc. They concluded that when the interior structures around the hole feature are constructed by using linear lines as stretching elements, the dimensional error due to the shrinkage of the filaments can be decreased by 80%. Ingavale P. et al. [22] studied on the dimensional accuracy by considering the shrinkage on parts such as Geneva mechanism, Wankel engine

housing and spur gears. They considered the printing parameters like scale, fill density, print speed, solid layer number etc. as the factors that affect the dimensional accuracy of the 3D printed parts. In their study, the parameters as layer height, fill pattern and perimeter were kept unchanged to eliminate their effects on shrinkage of the 3D printed parts. They concluded that geometric shapes directly affect the shrinkage. They also said that the reduction on the scale of the parts increases the shrinkage amount and there is no significant effect of the solid layer number on the shrinkage. They obtained that the most amount of shrinkage obtained in Geneva mechanism. Kitakis et al. [23] worked on low cost 3D printing in medicine and dimensional accuracy. They utilized FFF technique 3D printers and focused on the effects of the printing material, infill rate, number of shells and the layer height on dimensional accuracy. Then, they evaluated whether the FFF 3D printers can be used in medicine or not. They concluded that the FFF 3D printers can be used for medicine by optimizing the 3D printing process parameters. Islam et al. [24] considered also the dimensional accuracy and repeatability of 3D printed parts manufactured by using Z450 3D printer model. They focused on the accuracy errors on linear dimensions and diameters of the holes. They produced the same parts and compared them using CMM. They concluded that plane dimensions in the 3D printer base plane are always undersized however the dimensions in the height direction are always oversized for the parts manufactured by using Z450. Besides the hole diameters are always oversized is another conclusion of this work. Kechagias J. et al. [25] studied on the effects of the parameters of the Polyjet Direct 3D printing process on dimensional accuracy. They considered the layer thickness, build style and model scale as process parameters. They analyzed the parameters by using the Analysis of Means (ANOM) and Analysis of Variances (ANOVA) methods. They tried to reach the optimum level for each parameter. They concluded that the build style and the layer thickness affect the dimensional accuracy of the external dimensions, while the layer thickness and the model scale affect the internals. Mendricky R. [26] studied on the dimensional accuracy of the Rapid Prototyping technology. He analyzed the dimensional and the shape accuracy of the parts manufactured by 3D printing and he

compared the analyses results with the accuracy data given by the 3D printer manufacturers. He considered different 3D printers using FDM methodology.

### 2.4 3D Printing and Mechanical Behavior

There are several studies in the literature about the mechanical behaviors of the AM fabricated parts. As a recent work, Vicente et al. [1] examined the effects of the two controllable parameters such as infill pattern and infill density on strength of the 3D printed parts by using ABS material. In their work, they used standard infill patterns like honeycomb, rectilinear, etc. They also compared the behaviors of the parts which are produced by using the 20%, 50% and 100% densities for each infill types on a loading condition. They concluded that the dominant effect is due to the density variations. According to their work, although the infill pattern changes the strength less than 5%, the density changes the strength more than infill pattern. They came up with the result that the rectilinear infill pattern with 100% density has the highest tensile strength. Moreover, Johansson [2], in his master thesis, argued that the most common failure scenario of a part produced with FFF 3D printer is the layer bonding. He worked on the parameters which affect the layer bonding and mechanical behavior. He considered the software settings and the material as the fabrication parameters. He used polyethylene terephthalate, ABS and PLA materials. He also considered the printing orientation, temperature, flow rate, layer height and printing speed as parameters. He concluded that the ABS has the highest tensile strength and the major factors which affect the layer bonding are extruder temperature, printing speed and layer height. He stated that the parts manufactured with an extruder temperature of 250 $^{o}$C are seven times stronger than the ones fabricated with 190 $^{o}$C. He further added that manufacturing the part with 0.1 mm layer height increases the load capacity by 91% when compared with the 0.4 mm layer height. The parts fabricated with a printing speed of 10 mm/sec has 95% better layer bonding performance than the parts with 130 mm/sec printing speed. Lu et al. [27] worked on a method to reduce the material cost and weight while keeping the parts as durable as possible. They proposed a hollowing optimization algorithm

based on honeycomb shaped cell structures. They used Voronoi patterns to construct the interior structure. As a result of their work, they reached an easily controllable, adaptive optimization methodology. They suggested their method creates light-weight parts while keeping their durability under the same loading conditions by using a density function defined by a stress analysis result. Similarly, Stauben et al. [4] worked on improving the strength of the 3D printed parts using the results of a stress analysis as a function of modification of interior structure. They introduced a new implicit slicing methodology. The developed algorithm, which uses data from FEA software as an input, constructs the tool-path for the interior structure according to the stress values. In this work, the infill patterns are not standard patterns. The constructed pattern can be considered as a kind of random pattern which depends on the stress field. The stress field data was examined by considering the mathematical curves to get the infill pattern. As a result of their work, they reached an improvement on tensile strength about 45%. They also manufactured a part whose elastic modulus was increased by 57% when the developed algorithm was employed. Adams and Turner [28] worked on the improvement of the strength of the parts by eliminating voids and gaps by modifying the interior structure. They tried to develop an implicit slicing algorithm. They considered an infill structure constructed by considering the finite element analysis results and mathematical curves modifying the FEA results as mentioned in Stauben's work. They considered the same infill structures. However, they examine the effects of this infill structures on gaps and voids. They used standard dog-bone shape specimens for their tensile testing performance. They compared the test results of the specimens with modified interior structures with the ones which have diagonal, eggcrate, honeycomb and Hilbert shape lines as interior structure. They obtained these interior structure types from the mathematical equations. They concluded that the appropriate selection of the modified infill structures allows the designer to modify the strength, stiffness, yielding behavior, and the failure behavior of 3D printed parts. Tam and Muller [29] studied also on the structural performance of the parts manufactured by AM. They considered the issue in two cases: 2D planar parts manufactured by using traditional 3-axis 3D printers and 2.5D surface geometries manufactured by using a multi-axis

robot arm enabled manufacturing method. In 2D case, they considered the topology and toolpath planning. They also studied the effects of the printing orientation. They used FEA to obtain the stress lines which were used to construct the infill structure of the parts. They tried to optimize the interior structure by considering the volume/mass ratio. They concluded that the method which uses stress lines resulting from the FEA produces more durable parts. They also concluded that the strength of the part is higher where the parts are oriented to preserve the continuity of the infill lines. In 2.5D case, they used a multi-axis robot arm to preserve the continuity of the stress lines result from the finite element analysis on curvatures. They concluded that the parts manufactured by using the multi-axis robot arm shows higher strength characteristics due to the continuous infill lines derived from stress results. Baikerikar and Turner [30] studied on the effects of the different infill structures on the strengths of the specimens. They also performed FEA and compared the results of analyses with experimental tensile tests. They used standard dog-bone shaped specimens with hexagonal and circular infill structures. They modified only the infill structure of specified region on gage section. They constructed infill structures by using the hexagonal and circular shapes. Besides, for comparison, they construct specimens with fully filled interior. However, for specimens with fully filled interior, the thickness of the specified region was decreased to provide the same weight for comparison. They concluded that the FEA results are not always reliable means of predicting FDM part behaviors.

While there exist some works in literature which uses the FEA results for interior structure modification, all these studies have manual methods to construct the internal structures. No automatic method which directly uses the FEA results exits. Besides, the studies exist in the literature use the well-known FEA software whose licenses are expensive to be bought. In this study, an implicit slicing method is developed to fill the interior of the structure by using the FEA results and to obtain the G-code file automatically, which provides strength improvement. Throughout the work, Karamba3D® is used as FEA software which is embedded to Rhinoceros3D®. Moreover, this study provides cheaper solution for strength improvement of 3D

printed parts because of that the software used throughout the study is cheaper than other well-known ones.

In the following chapter, the method developed throughout this thesis work is described.

# CHAPTER 3

# FINITE ELEMENT ANALYSIS BASED METHODOLOGY

In this chapter, the developed methodology is explained. First of all, the design process of the test parts is described. For the sake of reliability, the standard test part used during the design stage is addressed. The CAD software used for the part design is also referred. Then, the FEA method is described by explaining the used finite element software and the details of the analysis set-ups throughout the study. Besides, the post processing of the results from the quasi-static FEA and the utilized tools for the post processing are expressed. Moreover, the method to obtain a stronger part, which gives the G-code file for the open source 3D printer, is described. Finally, the developed algorithm is concluded with a brief conclusion including the pseudo-code of the developed algorithm.

## 3.1 Introduction

Throughout this study, the main aim is to improve the strength of the parts manufactured by an open source FFF 3D printer utilizing PLA material. The method provides a pipeline starting from the design and ending with the fabrication of the artifacts. During the development of the method, several software packages are used to construct the complete algorithm. The reliability of the method is proved by performing structural tensile tests.

As a first step, 2D geometries are considered to develop the method in details. Then, 2.5D geometries constructed by the proposed method are manufactured and tested to assert the reliability of the developed method. All the manufactured geometries are tested according to a test standard by considering the related loading conditions to prove the applicability of the method by comparing them with standard parts.

In the following subsections, the pipeline of the development process can be found from design to manufacturing stages. It can be said that the method consists of the design, quasi-static FEA performed under the desired loading conditions, and G-code generation for manufacturing steps. Then the tests are performed for the method to be accepted as prospering.

## 3.2 Design of the Test Parts

The proposed method starts from the design stage as mentioned before. At the design stage, initial geometry is constructed by using CAD software. In this study, Rhinoceros3D® is used as the CAD software to model the geometries.

### 3.2.1 CAD Software: Rhinoceros3D®

Rhinoceros3D® is standard CAD software which is used generally by designers and architects. It provides tools like accurate modeling, documentation of designs, rendering, animation, drafting, engineering, analysis and manufacturing. By using Rhinoceros3D®, Non-Uniform Rational B-Spline (NURBS) curves, surfaces, and solids can be created, edited, analyzed, documented, rendered, animated, and translated without complexity problems on degree or size. Rhinoceros3D® also allows working with polygon meshes and point clouds.

The created geometry in Rhinoceros3D® can be converted other related formats to be manufactured with laser cutters, milling machines or 3D printers. These flexibilities are what make Rhinoceros3D® different from general 3D modeling tools. Rhinoceros3D® has an open architecture. Resulting from its open architecture, Rhinoceros3D® can be used as a development platform. It provides possibility to be used by programmers of any level of expertise.

It has several plug-ins for nesting, terrain creation, parametric architecture, rendering, animation, CAM, subdivision modeling, jewelry, mold design, etc. [31].

As a first step of the study, the test specimen is modeled in 2D. In other words, a 2D planar cross-sectional geometry of the test parts is drawn in

Rhinoceros3D®, since the same cross-section is used for all the layers. It is drawn according to a standard named as ASTM D638. The details about this standard can be found in the following subtopic.

### 3.2.2 Used Standard for Design of the Parts: ASTM-D638

For useful and qualitative characterization, reliable data is required for the research and development studies. A standard should be considered to obtain precise comparative results. Thus, in the first step of the design stage and the testing stage, ASTM-D638 standard [32] is used for the sake of reliability, which is technically equivalent with ISO-527 test standard. ASTM-D638 is a standard test method for the plastics in the form of standard dumbbell-shaped test specimens. This standard defines the test conditions like pretreatment, temperature, humidity and the test speed for different test specimens which are up to 14 mm thickness.

In ASTM D638, there are several specimen types available to be used for the rigid and semi-rigid plastics, non-rigid plastics, reinforced composites and rigid tubes. For rigid or semi-rigid plastics, if the specimen has sufficient material and its thickness is 7mm or less, the Type I specimen is the preferred specimen. If it is expected that the specimen does not break in the narrow section of the Type I specimen, the Type II specimen should be used. The Type V specimen has a thickness of 4 mm with limited material. It is mostly used for thermal or environmental stability tests. To compare the rigid and semi-rigid materials, the Type IV specimen should be selected. Between the thicknesses of 7mm and 14mm, the Type III specimens should be used. In case of non-rigid plastic materials, the Type IV specimen can be used for the specimens with 4 mm thickness or less. If the thickness of the specimen is between the 7mm and 14mm, the Type III specimen should be used for the design and the test. For reinforced composites which includes highly orthotropic laminates, the Type I specimen shall be used.

Throughout the first stage of this thesis work, the detailed shape and the dimensions of the test specimens are taken from this standard. ASTM D-638 Type-1 specimen is selected, since it is more suitable for the molded or extruded semi-rigid

plastic materials. The geometry of the specimen is provided in Figure 5 and the related dimensions are provided in Table 1.

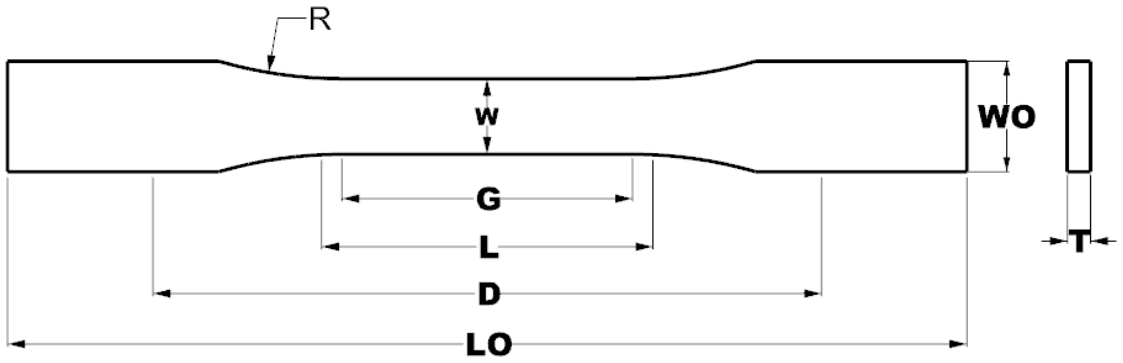


Figure 5: ASTM-D638 Type-1 test specimen [32]

Table 1: ASTM-D638 Type-1 specimen dimensions [32]

| **Dimensions** | **[mm]** | **Dimensions** | **[mm]** |
|---|---|---|---|
| W–Width of narrow section | 13 | G–Gage length | 50 |
| L–Length of narrow section | 57 | D–Distance between grips | 115 |
| WO–Width overall (min) | 19 | R–Radius of fillet | 76 |
| LO–Length overall (min) | 165 | T–Thickness | 4 |

In this test method, it is suggested to test the specimens by fixing them from the one end and pulling from the other end. However, the alignment of the grips is one of the most important issues. The specimens should be aligned as perfectly as possible with the direction of the puller so that no rotary motion that may induce slippage will occur in the grips. Thus, self-aligning grips should be used or it should be certain that there is no misalignment between the grips.

There are also different test speeds suggested according to the types of the specimen and the strain rates. The test speeds for the specimens are provided in Table 2, provided below.

Table 2: ASTM-D638 standard testing speeds [32]

| **Classification** | **Specimen Type** | **Speed of testing [mm/min]** | **Nominal Strain Rate [mm/mm.min]** |
|---|---|---|---|
| Rigid and Semi-rigid | I, II and III | 5 ± 25%<br>50 ± 10%<br>500 ± 10% | 0.1<br>1<br>10 |
| | IV | 5 ± 25%<br>50 ± 10%<br>500 ± 10% | 0.15<br>1.5<br>15 |
| | V | 1 ± 25%<br>10 ± 25%<br>100 ± 25% | 0.1<br>1<br>10 |
| Non-rigid | III | 50 ± 10%<br>500 ± 10% | 1<br>10 |
| | IV | 50 ± 10%<br>500 ± 10% | 1.5<br>15 |

In proposed method, the FEA process comes after the design stage. The details of the FEA method can be found in the following topic.

### 3.3 Algorithm Development and Finite Element Analyses of the Designed Parts

In this work, the goal is to obtain more durable parts, manufactured by FFF 3D printer, by considering the mechanical behavior of it under a tensile loading condition. In other words, it is proposed that the parts have higher strength values when they are informed about their structural behavior under desired loads. So, quasi-static FEAs are performed to obtain the mechanical behavior of the 3D printed parts under tensile loading conditions to inform the parts about their structural properties between the design and the manufacturing steps.

The FEA part can be divided into three sub-topics. In the first topic, the quasi-static FEA is performed by using Abaqus®, which is widely accepted FEA software by the engineering society. In other topics, the FEAs are done by using software, named as Millipede® and Karamba3D®, directly embedded to Grasshopper3D®. Grasshopper3D® is an algorithmic design tool for Rhinoceros3D®. These plug-ins used as FEA software have their own solvers based on the finite element methods. In the following topics, the details of the FEA performed can be found.

Throughout the algorithm development, the basic software used is Grasshopper3D® and it is described in the following subsection.

#### 3.3.1 Grasshopper3D®

Grasshopper3D® is an algorithmic design tool for Rhinoceros3D® CAD software. It is generally used by designers and architects. There is no need to have high programming skills unlike Rhino-Script. Without the knowledge of scripting, Grasshopper3D® allows designers to construct form generators [33].

Grasshopper3D® can be used in a diverse range of fields which include product design, engineering, architecture, etc. It gives opportunity to control the designed models parametrically. Workflows can also be generated in Grasshopper3D® interface. Besides, it can be considered as a platform for programming with a graphical interface [34].

As a summary, Grasshopper3D® is a graphical algorithmic modeling tool based on block diagrams. The example pipelines for algorithms consist of blocks including specific functions can be seen in the following subsections.

### 3.3.2 Finite Element Analyses

The base of the proposed algorithm is to use the structural information of the parts under tensile loadings. In other words, the aim is to manufacture structurally informed parts under tensile loading cases to increase durability. For this reason, to get the structural information, quasi-static FEAs are performed by considering the functionality of the parts.

For the initial studies, Abaqus® FEA software is used because of the fact that it is highly popular in engineering society. Then, Millipede® and Karamba3D® software which work on Grasshopper3D® are used to construct faster and automated method. In the following topics, the details about the FEAs performed by Abaqus®, Millipede® and Karamba3D® can be found.

#### 3.3.2.1 Finite Element Analysis Performed by Abaqus®

##### 3.3.2.1.1 Abaqus®

Abaqus®/CAE is an analysis environment which uses finite element method to perform the analysis. It gives possibility to use an interface for creating, submitting, monitoring, and evaluating the results from Abaqus®-Standard and Abaqus®-Explicit simulations.

The structure of the Abaqus® software consists of modules which are used throughout the analysis process such as, geometry definition, material property definition, mesh generation, etc. In other words, by using each module moving from one to other, model is built in Abaqus®/CAE to get an input file for simulations performed by using Abaqus®-Standard or Abaqus®-Explicit solvers. There is also a model tree inside the Abaqus® which gives possibility to switch one module to

another. A basic graphical user interface of the Abaqus® can be seen in the below figure.

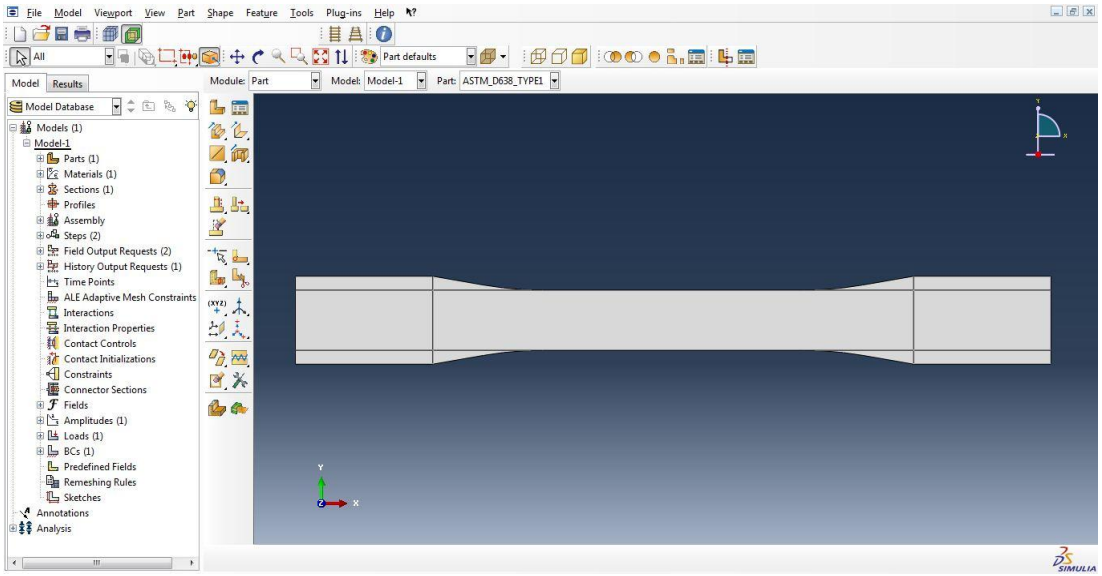


Figure 6: Graphical user interface of Abaqus®/CAE

As a post-process of the results from the modules which include solvers, visualization module of Abaqus®/CAE is used. This module uses the output database of the solver modules to view the result of the specified FEA [35]. The module provides graphical representation of finite element models and the analysis results. It also provides an opportunity to animate the FEA case and its result.

Abaqus® is finite element software which does not have a standard unit system. In other words, it is a unitless finite element program. The units of the used quantities should be defined by the user according to standard unit systems. Throughout the thesis study, SI (mm) unit system is used for FEA performed in Abaqus®. The units in this system are as length [mm], force [N], mass [tonne ($10^3$ kg)], time [s], stress [MPa ($N/mm^2$)], energy [mJ ($10^{-3}$ J)] and density [$tonne/mm^3$].

### 3.3.2.1.2 Analysis Details in Abaqus®

In this study, the test specimens are analyzed under the tensile loading conditions via FEA software. For this case, the 2D geometry constructed in

Rhinoceros3D® is transferred to the Finite Element Method (FEM) software in step file format. The loading case through the quasi-static FEA can be considered as a plane stress case where one of the dimensions of the part is very small when compared with the other two axes. Regarding z-axis, which is perpendicular to the printing plane, stress values in this direction are considered to be negligible, which is an assumption in plane stress case according to the elasticity theory [36].

After the part is designed in Rhinoceros3D® and transferred to the Abaqus®, material should be defined to perform the analysis. Actually, because of the fact that the stress fields due to the applied load are only considered, the material definition is not significant for this step. The stress values which define the stress regions in stress field results are not important for this step In other words, one of the materials from the material library can be used for the analysis to obtain only the stress field results. The only important case for the material selection is being isotropic. Isotropic material means that the material has same mechanical properties in all directions. So, aluminum material is defined manually. The Young's modulus is used as 70000 MPa and the Poisson's Ratio is used as 0.33.

Then, boundary conditions should be defined in the analysis settings. In FEM software, the part is fixed from the left end and the loading is applied from the other end. Boundary conditions can be seen in Figure 7, where the shapes with orange color define the fix boundary and the arrows with purple like color defines the loading condition.

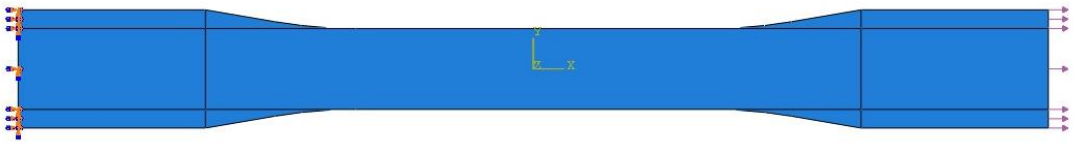

Figure 7: Boundary conditions

In FEA, the specimen is meshed by using the quad type meshes as suggested in the Abaqus® manual. To construct the meshes in more homogenous structure, the part is sliced in 11 sub-parts as seen in Figure 7. The constructed mesh is provided in Figure 8.

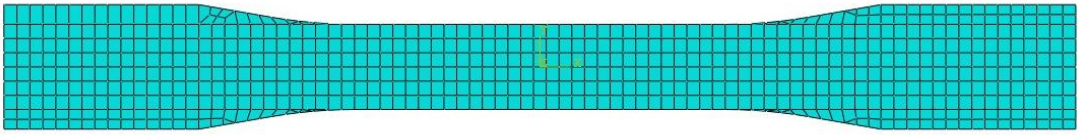

Figure 8: Constructed mesh structure

The PLA material utilized by the 3D printer used throughout the study is a ductile and isotropic thermoplastic material. So, the Von Mises theory, which is also named as Maximum Distortion Energy theory, is considered, which are generally used for ductile materials. In this theory, yielding occurs when at any point in the body; the distortion energy per unit volume becomes equal to that associated with yielding in simple tension test [37]. The distortion energy for the general case can be defined in terms of the principal stresses as;

$$U_d = \frac{1+\gamma}{6E}[(\sigma_1-\sigma_2)^2+(\sigma_2-\sigma_3)^2+(\sigma_3-\sigma_1)^2]$$

For simple tensile test, the principal stresses of $\sigma_2$ and $\sigma_3$ are equals to zero. Yielding occurs when $\sigma_1 = \sigma_y$ where $\sigma_y$ is yield strength. So, these give distortion energy equation at the yield point as;

$$(U_d)_y = \frac{1+\gamma}{3E}\sigma_y^2$$

From these equations for yielding under a single, uniaxial state of stress, the equivalent stress for yielding, which is known as Von Mises stress, can be written as

$$\sigma_{vm} = \sqrt{0.5[(\sigma_1-\sigma_2)^2+(\sigma_2-\sigma_3)^2+(\sigma_3-\sigma_1)^2]}$$

Therefore, for a single, uniaxial loading of a ductile part, failure occurs when the Von Mises stress, which is equal to the first principal stress, is equal to the yield strength according to the Maximum Distortion Energy theory [37]. This yielding criterion can be given as

$$\sigma_{vm} = \sigma_1 = \sigma_y$$

The load is applied as 1 kN which is the same loading with Stauben's work [4]. 1 kN loading is applied as distributed load. As a result of the FEA under the tensile loading condition, obtained stress field can be seen in Figure 9. For this study, only the stress field regions are important. Thus, it is enough to prevent yielding in quasi-static FEA, i.e., it is enough to be in the elastic region. By using the loading as 1kN, only about 19.2 MPa maximum stress occurs for this standard specimen. So, it can be obviously said that the part does not yield under 1kN loading since the yield strength of the aluminum material is about 276 MPa. For PLA material utilized in this study, the tensile yield strength is about 49.5 MPa. Since 19.2 MPa stress is still lower than the 49.5 MPa, it is obvious that the yielding does not occur for 1kN loading. For PLA material, 2.57kN loading is also used to obtain the stress field results just before the yield point. By trial and error, 2.52 kN loading creates 49.45MPa maximum stress which can be considered as a point just before the yielding starts. The stress field results related with this loading can also be seen in Figure 9. Since there is no significant difference between the stress fields results, the stress field resulting from 1kN loading can be used for these specimens. The stress field regions and the first principal stress direction vectors are enough to be used to modify the interior structure in this method. Hence, the stress values which define the stress regions in the stress field results are not significant.

This method can be used for brittle materials where the proper elasticity theories defined for these materials such as maximum principal stress theory. By changing the results visualization settings and selecting the maximum principal stresses, the method can also be used for brittle materials.

Because of the fact that the stress field results are used to construct the stress modified infill, they are shown on un-deformed part to manufacture the part in original dimensions. The red field corresponds to the section where the stress values are the highest. In other words, the red fields are the most critical regions for the specimen under tensile loading because of the highest stress values. Besides, the blue fields correspond to the sections where the smallest stress values exist, i.e., the

least critical regions. The spectrum which starts from red and continues to dark blue color shows the stress values from the highest values to the lowest ones, respectively.


a)


b)

Figure 9: Stress field results under a) 1kN tensile loading and b) 2.52kN tensile loading obtained in Abaqus® FEA software

Since this method is a kind of manual one for the first trials, the FEA results should be transferred to the Rhinoceros3D® manually to be used in Grasshopper3D® for constructing the interior. Thus, the colored mesh which is the result of the quasi-static FEA is exported from the Abaqus® in *wrl* file format. This file format can also be mentioned as *vrml* format. The imported colored mesh file to the Rhinoceros3D® can be seen in Figure 10below.

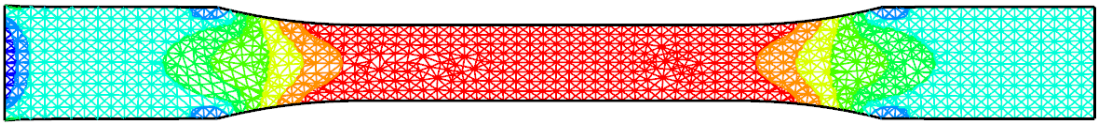

Figure 10: Colored mesh imported to Rhinoceros3D®

The Virtual Reality Modeling Language (VRML) file format, with an extension of *wrl*, is a standard file format to represent 3D interactive vector graphics. It is a text file format which includes vertices and edges with surface colors, image mapped textures, transparency, etc. The VRML files are commonly called as

"worlds". Many 3D modeling software can export the data in VRML file format [38].

By considering the computational work, the color scale obtained from the Abaqus® FEA is decreased to obtain a faster method. This can be considered as a kind of optimization. The final Von Misses stress field results used for the method development case can be seen in Figure 23 given in section 3.3.3.

As mentioned above, this method used for transferring of the results of FEA in VRML file format is a kind of manual method. So, it is required to automatize the method to construct the more automatic, logical and useful algorithm and to decrease the computational work. So, some other FEA tools named as Millipede® and Karamba3D® are used to perform the DEA inside the algorithmic pipeline, which is constructed in the Grasshopper3D®. In this manner, the algorithm is more automated to obtain the required G-code file to fabricate the parts with stress modified infill. In the following subtopics, the details about the FEA using Millipede® and Karamba3D® are mentioned, respectively.

#### 3.3.2.2 Finite Element Analysis Performed by Millipede®

To obtain a faster method than the case where the Abaqus® is used as FEA software and to decrease the computational work, it is required to construct an automated method. Here, an automated means that the user gives only the geometry to the proposed algorithm and the method itself evaluates the parameters used through the algorithm (stress fields' boundaries, infill density, etc.) and generates the G-code file belonging to the object whose infill is modified according to the stress field information from the FEA. For such an automatization, it is required to decrease the tools used throughout the method. In other words, the method should perform all the tasks required to obtain the G-code file on its own. In this way, the FEA can be performed inside the block based pipeline constructed by using Grasshopper3D® and its plug-ins.

Two different plug-in can be used to perform the FEA work to obtain the stress fields under the desired tensile loading throughout this thesis study. Firstly, Millipede® is used for stress analysis. So, the details of Millipede® are provided in

the upcoming subsection. In later topics, the second case, where Karamba3D® is used for the FEA, is described. The case where the Karamba3D® is used as FEA software is the current case used through this thesis study.

#### 3.3.2.2.1 Millipede®

Millipede® is an analysis tool designed to work on Grasshopper3D®, which performs structural analysis and optimization [39]. It can be used for the solution of numerical and geometric problems [40]. In Millipede® frame and shell elements can be used in 3D linear elastic analysis for higher performance. Moreover, 3D volumetric elements can also be used. Besides, 2D plate elements can be used to construct the analysis scenario for in plane forces.

Millipede® has also built-in topology optimization methods. All systems can be optimized using them. For that matter, due to its speed, it can be used for form finding problems by collaborating with Galapagos add-on. In addition, some geometric tasks can be performed by using Millipede®. Iso-surface meshes from scalar fields can be extracted from Millipede®. Besides, curved contours can be extracted over any mesh structure. Furthermore, some numerical analysis tools exist in Millipede®. For example, Fast Fourier Transform can be performed in 1D and also in 2D. It has sparse linear system solver and eigenvalue calculation for large matrices [39].

Surface re-parameterization module exists in Millipede®. This module enables vector field aligned patterns generation over any mesh structure. This function can be used to create grid shells or reinforcement patterns which can be aligned according to the principal stresses and their direction vectors [39].

#### 3.3.2.2.2 Analysis Details in Millipede®

In this thesis study, for constructing an automated method, Millipede® add-on is used for the quasi-static FEA for first trials for automatization. By using Millipede®, there is no need to export the geometry from Rhinoceros3D® to different

software. The geometry is defined in Grasshopper3D®, which is mentioned in the following topics.

In Millipede®, first of all, the boundaries of the geometry should be defined. Then, the mesh structure can be constructed. For example in 2D, the mesh numbers in the direction of x and y axes are defined on xy-plane. Besides, extra geometries should be defined to represent the required boundary conditions. For this study, extra rectangular shapes are drawn for two edges. At one side the part is fixed and on the other side the loading is applied. In Figure 11, the constructed part geometry and the geometries for the boundary conditions can be seen. The left gray rectangle is used to fix the part and the right gray rectangle is used to apply the tensile load. The applied load is 1 kN distributed load as in the work of Steuben et al. [4].

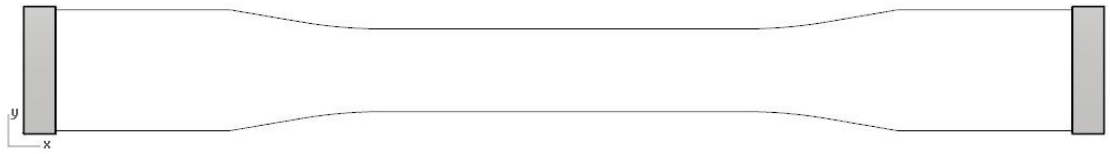


Figure 11: Constructed part and geometries for boundary conditions

As a next step, a finite element mesh network should be constructed. To construct this mesh system; meshed geometry, material and the thickness are required. For this part, 150 mesh elements are constructed in x-axis and 50 mesh elements are constructed in y-axis. These numbers are not referenced number, they are just random. Besides, the steel material defined in Millipede®'s library is used for the analysis because of that only the stress field regions are required which results from the applied loading for this automated method. Thickness of the part is defined as 1 unit. Since Millipede® has no units; user should construct the unit system properly. These parameters are enough to construct a finite element mesh system in Millipede®. The block diagram of the constructed mesh system can be seen in Figure 12. In this analysis, the mesh system is constructed by using shell elements because of in-plane loading.

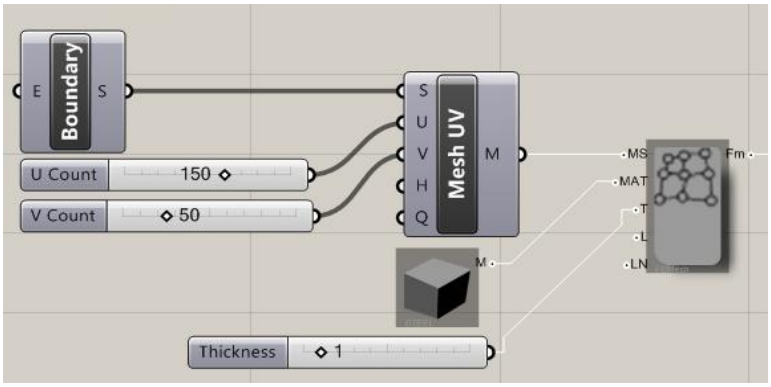


Figure 12: Finite element mesh network construction

After the mesh network is constructed, FEA system should be defined in Millipede®. To define this system; finite element mesh system, support type region and load region information are required. For the analysis, support region is defined as fixed from the gray rectangle existing on the left edge of the part as can be seen in Figure 13. Load region is also defined as distributed tensile 1kN from the gray rectangle existing on the right edge can be seen in the same figure. The block diagram of the constructed FEA system can be seen in Figure 13.

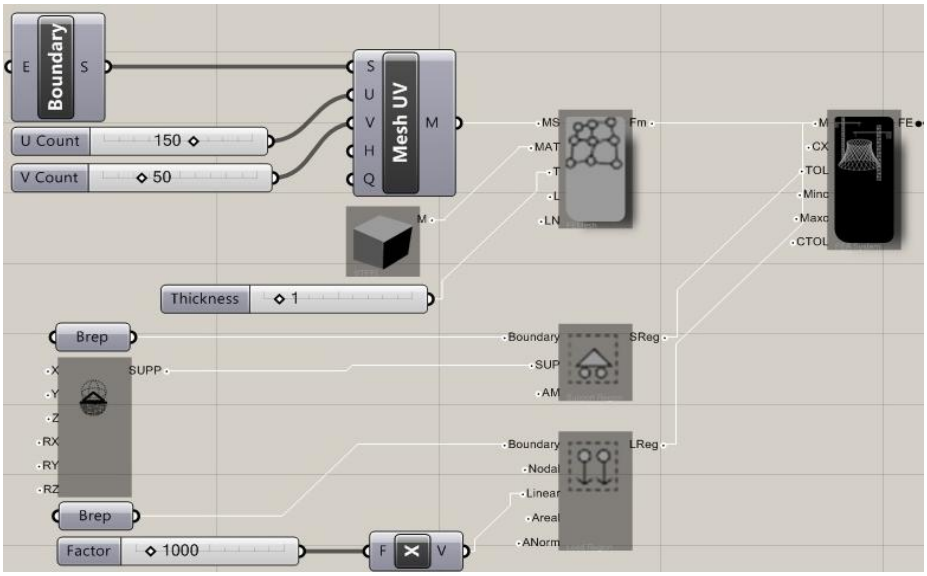


Figure 13: FEA system in Millipede®

The last step is to assign the FEA system to the solver of Millipede®. After this assignment is performed, the solver performs FEA.

The mesh can be visualized as a colored mesh according to stress fields in Millipede®. For this purpose, mesh visualization block can be used. The principal stress lines can also be figured out by using the stress lines block. Besides, the positions for the points where the principal stress lines cross can be defined to the stress line block. In this way, the principal stress lines belonging to the specified regions can be obtained. The block diagram of the solver and the post-processor can be seen in Figure 14.

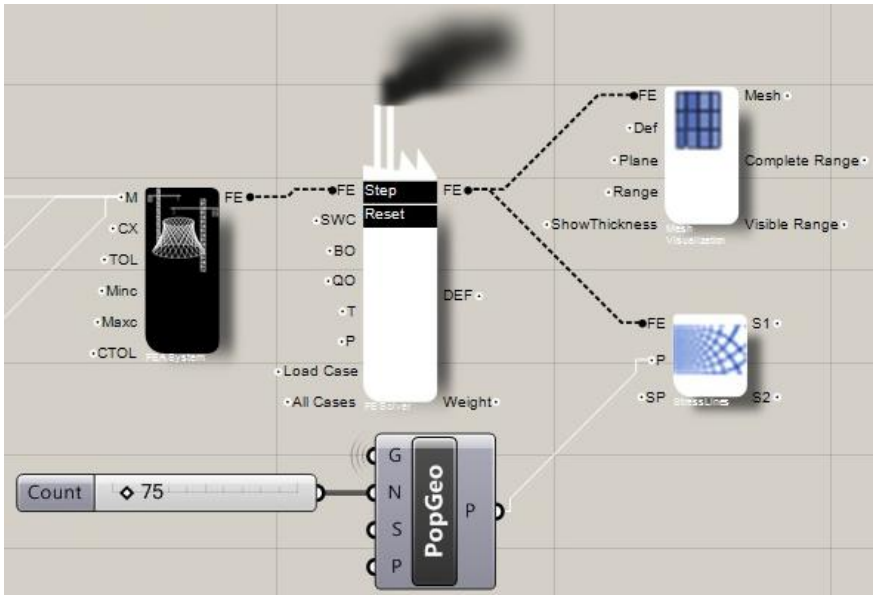


Figure 14: Block diagram of the solver and the post-processor in Millipede®

The resulting lines connect the first principal stress direction vectors of the quasi-static FEA performed by Millipede® can be seen in Figure 15.

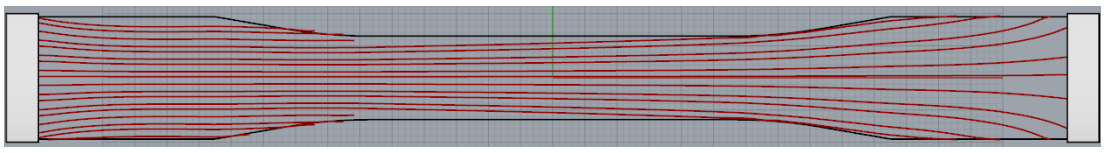

Figure 15: Lines connect the first principal stress direction vectors obtained in Millipede®

#### 3.3.2.3 Finite Element Analysis Performed by Karamba3D®

Secondly, Karamba3D® is used for quasi-static FEA inside the constructed algorithm since it has a user interface which is easier to deal with than one for Millipede®. Moreover, useful tools exist for the post processing of the analysis results in Karamba3D®. Another reason is that there exists more documentation available for Karamba3D® than Millipede® which helps to user for the FEAs performed.

##### 3.3.2.3.1 Karamba3D®

Karamba3D® is another finite element add-on used through this thesis study. It has some significant advantages over the others in different aspects. First of all, it can be used by non-expert users easily. It is FEA software tailored for the needs of engineers and architects for design purposes. Its computational cost is less than the other finite element software [41]. Besides, the documentation available for Karamba3D® is more than the ones for Millipede® which makes easier to be used by the user.

Karamba3D® is fully integrated into the Grasshopper3D® environment where parametric procedures are the base. In other words, it can be considered as an add-on of Grasshopper3D® which is also an add-on of the 3D modeling tool Rhinoceros3D®. In this way, it is easy to parameterize the modeling and the FEA phases in the same software environment. These early phases can also be combined easily with the optimization algorithms constructed for the Grasshopper3D® [41].

Karamba3D® is finite element software for static analysis. To construct a static analysis in Karamba3D®, there exist 6 basic steps. These steps are briefly considered in Figure 16.

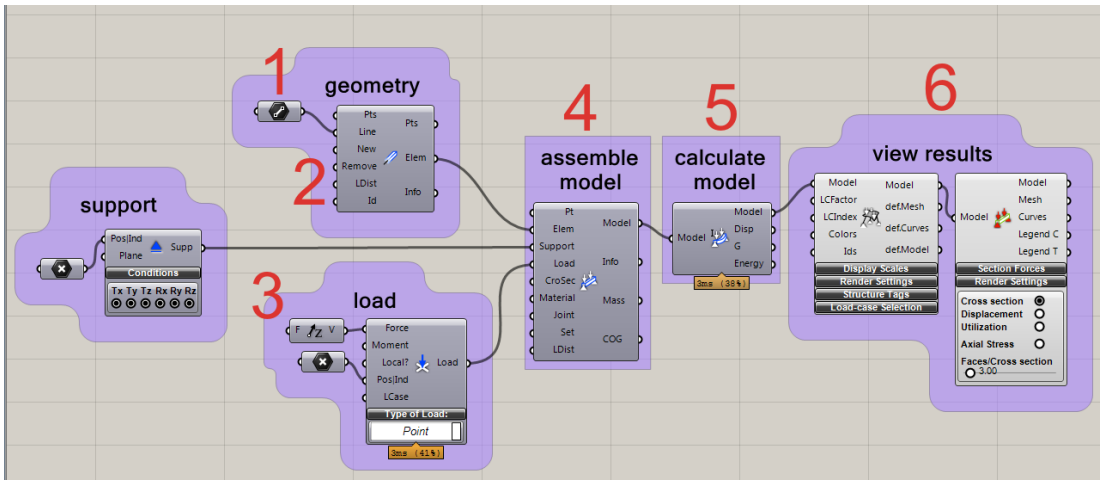


Figure 16: Basic steps for static analysis in Karamba3D® [41]

First of all, geometry of a finite element mesh structure is needed for the analysis. The user can create a wireframe or a point based geometry. A mesh structure can also be utilized. Then, the constructed wireframe or point geometry should be converted to Karamba3D® beams. The constructed mesh structure should be converted to shell structure. As a third step, the boundary conditions should be defined. The points which are supports and places where the loads are applied should be defined clearly. After all these definitions are completed, the structural model should be assembled, which consists of the geometry, supports and loads. The material can be assigned to the geometry from the library of the Karamba3D® or it can be defined by the user. Custom cross section geometries can also be assigned for the wireframe structures, which exist in Karamba3D® library. When Karamba3D® structural model is ready; it can be analyzed [41].

After the analysis is finished, the results can be visualized by using Karamba3D®'s ModelView component. This component has abilities to scale the deflections, to show the multiple load cases together or separately, etc. BeamView and ShellView components also exist in Karamba3D® to generate the mesh representations. By using these components, stress, strain and deflection data can be visualized easily. The important structural data such as the lines created by using first principal stress direction vectors can be obtained and visualized by using these view components [41].

#### 3.3.2.3.2 Analysis Details in Karamba3D®

As well as FEA performed by using Millipede®, Karamba3D® is also used to construct an automated method which includes the stage from the design phase to pre-manufacturing. In other words, design and FEA steps are performed in the same pipeline to obtain the G-code file of the strengthened part for the fabrication by using an open-source 3D printer.

Karamba3D® is more useful add-on of Grasshopper3D® than Millipede® in terms of being user friendly and proficient. Moreover, it has more ability to perform a real-like analysis than Millipede®. Beside, visualization and the post processing of the results are easier and more suitable for the thesis study. Although it is very similar to the FEA case with Millipede®, the process steps followed for the analysis with Karamba3D® is explained below.

Like previous trials performed using Millipede®, using Karamba3D® as the FEA software gives an automated algorithm for the thesis. In this pipeline, there is no need to export the geometry from the Rhinoceros3D® to external FEA software which prevents the mismatches between the file formats and reduces the computational work.

Before doing quasi-static FEA using Karamba3D®, geometry is constructed via Rhinoceros3D® and defined in Grasshopper3D® as in the previous cases. At the beginning of the analysis, the geometry should be meshed. In Karamba3D®, geometry can be meshed by using Mesh Surface block via providing the mesh numbers through x and y axis. Since this component takes surfaces as input, the defined geometry should be converted to a boundary representation. After the mesh structure is constructed, it should be converted a shell structure to assemble the whole system for FEA. The structure from the boundary definition to mesh-to-shell conversion can be seen in Figure 17.

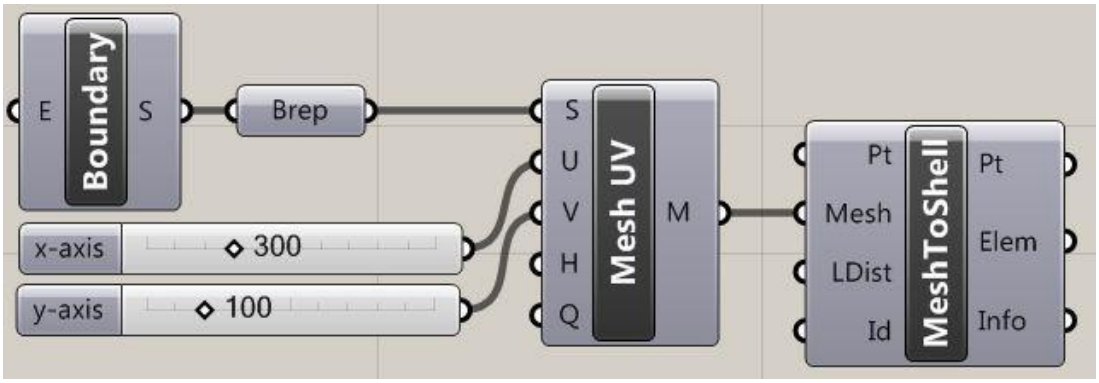


Figure 17: Pipeline starts from boundary definition to shell conversion

Moreover, the boundary conditions and the loading cases should be defined before the analysis. In Karamba3D®, fixed support function needs points as input. So, the points on the left side of the boundary are used as inputs to the support box. Point load function is also available to use for the loading case in Karamba3D®. Thus, the points on the right side of the boundary are used as inputs for the load region function. From these points, 1 kN distributed axial load through the positive x-axis is applied to the geometry as in Stauben's work [4]. The pipeline of the support and load region definition can be found in Figure 18.

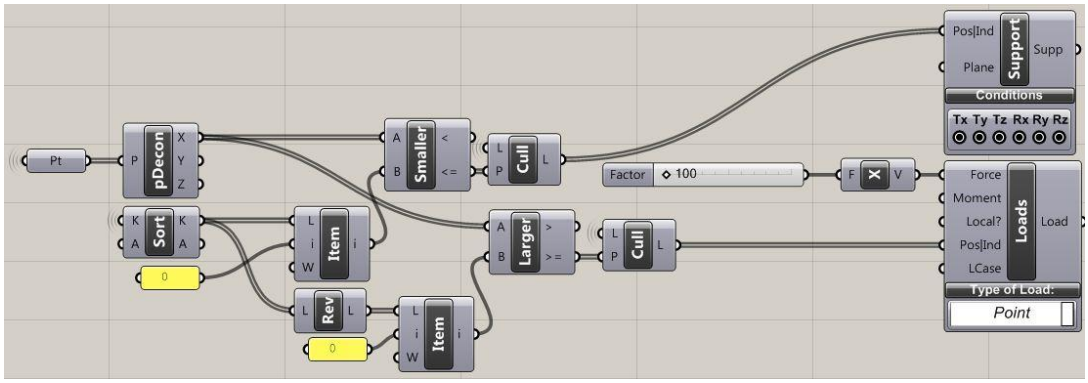


Figure 18: Pipeline for support and load region definition in Karamba3D®

For the next step, all these boundaries, supports, loads, etc. should be assembled to construct the finite element model for the solver. Assemble model function can be used to construct this model. This function takes inputs as points, elements, supports, loads, cross sections, materials, joints, sets and some limit

distances. For the present FEA only the elements, supports and loads are given as inputs. After the finite element model is constructed, the analysis is started by using AnalyzeThl function of Karamba3D®, which calculates deflections of a given model using the first order theory for small deflections. The output of this analysis is a finite element model with deflections, stress & strain values, etc. The ModelView function takes the output of the AnalyzeThl function. The structure of the described assembling and analysis tasks can be seen in Figure 19.

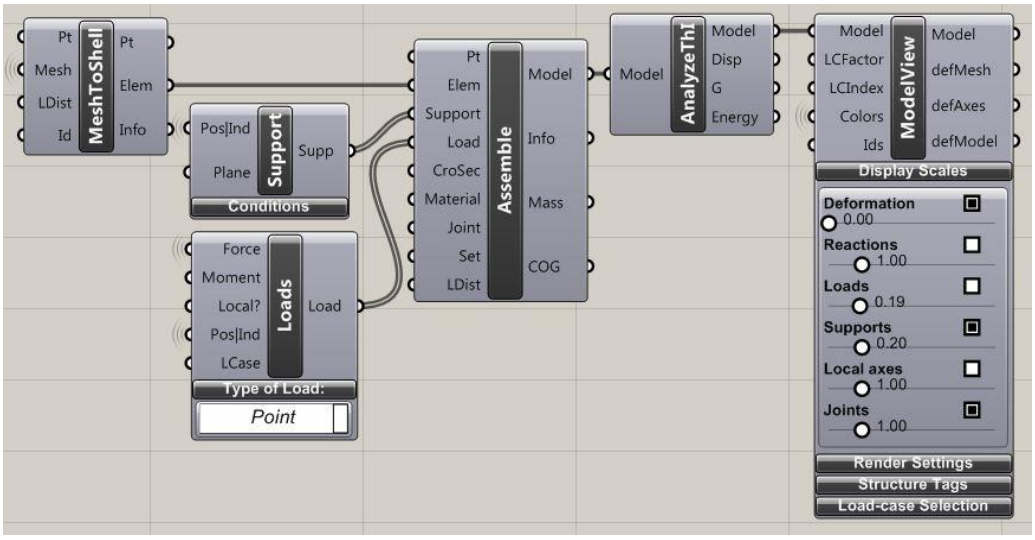


Figure 19: Structure of the analysis in Karamba3D®

Visualization of the results is simpler than Millipede®. By using ShellView function box, displacement, principal stresses and Von Misses stress results which are considered for ductile materials can be visualized. The pipeline for the visualization of the results can be seen in Figure 20.

Throughout the methodology development, Von Misses stress field results from the FEA are used. Thus, the stress field results are visualized by using the ShellView component, which can be seen in Figure 21.

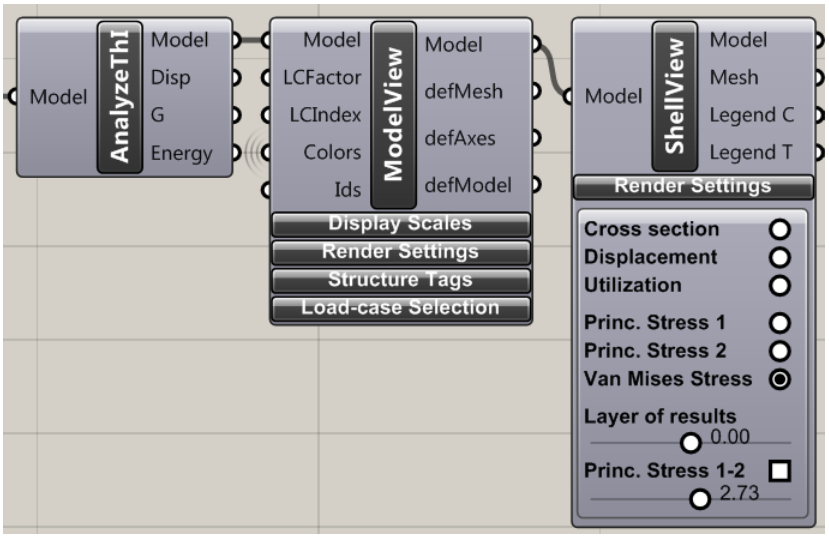


Figure 20: Visualization in Karamba3D®

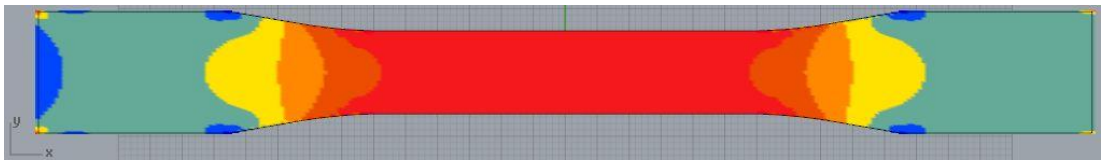

Figure 21: Stress field results in Karamba3D®

The color range is constructed by the user to visualize the stress fields as common engineering approach. In the default mode, the red field implies the region which has the least stress values and the blue field implies the field with the highest stress. However, in our method, the stress ranges from lowest to the highest value visualized in a color range from blue to red. This Von Misses stress field results and the stress related colored regions are used to develop the methodology, whose details can be found in the next topics.

For FEA performed in Karamba3D®, number of colors used to construct the color spectrum can be adjusted. For this study, the number of 10, 8 and 6 colors range are used. The stress field result obtained by using 10 colors range can be seen in Figure 21. The obtained stress field results with 8 and 6 colors range in Karamba3D® can be seen in the following figure.

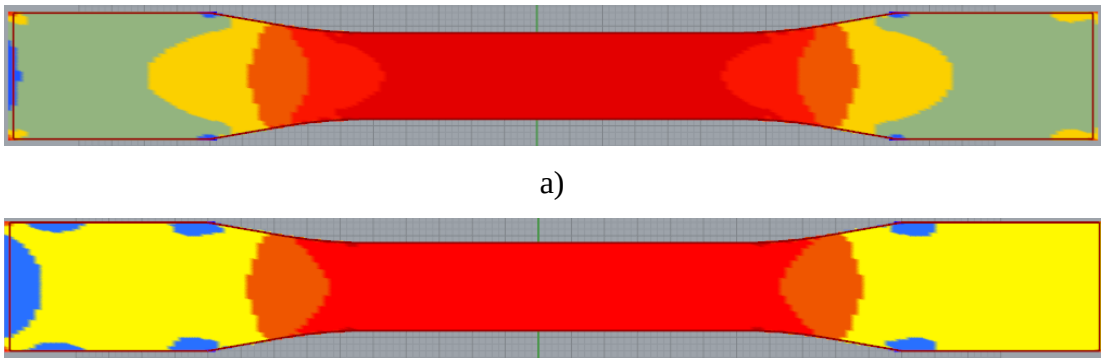

a)

b)

Figure 22: The stress field results for a) 8 colors range and b) 6 colors range

When all these results are compared, it can be seen that there is no significant differences between them. So the 6 colors range is used throughout the study by considering the computational work.

### 3.3.3 Developed Algorithm by Using Grasshopper3D® from the Results of Abaqus® FEA

The developed method is based on the results of quasi-static FEA. These analyses are performed to obtain the stress fields under tensile loading condition to strengthen the specimens by modifying the infill structure, informing the part about its mechanical behavior under the loading. So, throughout the method, the infill structure is modified according to obtained results from FEA.

As mentioned before, the first trials are performed by using the FEA software Abaqus®. The method constructed upon the stress results from the Abaqus® is a kind of manual method. In other words, the transfer of the stress field results from the Abaqus® and the boundary definition of the colored mesh fields to Grasshopper3D® are manual. The regions are also filled manually whose densities are specified according to the color of it, i.e., stress values inside the region.

As mentioned in Section 3.3.2.1.2, a colored mesh is obtained as a result of the quasi-static FEA. The mesh colors are constructed according to the stress field results under the tensile loading of the specimen in Abaqus®. As a next step, the obtained mesh structure is transferred to Rhinoceros3D® to be used to construct the

method in Grasshopper3D®. The mesh structure is exported as a document in .wrl format to be imported into Rhinoceros3D®. The imported mesh structure into Rhinoceros3D® can be seen in Figure 23.

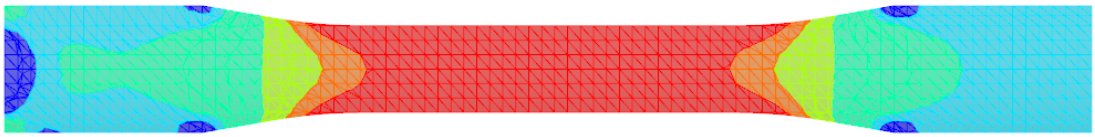

Figure 23: Colored mesh structure imported into Rhinoceros3D®

After the mesh structure is exported from the Abaqus® and imported into Rhinoceros3D®, the outer boundaries of the stress regions, from red to blue color, are acquired. These outer boundaries are used to fill the regions with the specified pattern with respect to their stress values. Since the red regions show the fields where the highest stress values exist, these regions should be filled with the highest density infill. After all of the boundaries for the specimen and the stress fields are obtained, they should be defined in Grasshopper3D® in which the algorithm providing infill density, infill pattern and G-code files are constructed. It is enough to define the boundaries as curves in Grasshopper3D® to use the algorithm properly. The obtained boundaries can be seen in Figure 24.

Figure 24: Stress field region boundaries

After these definitions are done, the constructed algorithm fills the regions with the stress-modified patterns. The densities of these fields transferred from the FEA software are determined with respect to the stress values of the corresponding regions. The method fills the regions via using linear lines whose densities are determined by considering the stress values. For example, the regions with the lowest stress values are filled with the linear lines whose spacing is 2 mm. For the region

with the second lowest stress values, the constructed linear structure with 2 mm spacing is shifted with a distance of 0.4 mm, which is equal to the nozzle diameter. The interior structure is constructed by offsetting the linear structure from blue to red regions. Actually, during the filling of the regions, the density is defined by considering the colors of the regions. In other words, the red fields have the highest density infill and the dark blue fields have the lowest. By using this technique, the regions with the highest stress values have the interior with the highest density. The specimen with 70% stress-modified infill density which is used for the tensile testing is constructed using the proposed method. Here, having 70% infill density is not an important case. 70% is a random density value chosen for the first trials performed to construct the method. The specimen for the first trials can be seen in Figure 25.

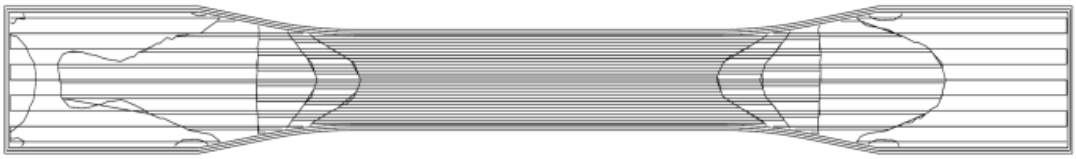

Figure 25: Constructed specimen with 70% infill density

The specimen mentioned above is used to obtain the G-code file to be manufactured and to perform the tests which are mentioned in the following topics. The pipeline for the constructed method can be seen in Figure 26 below.

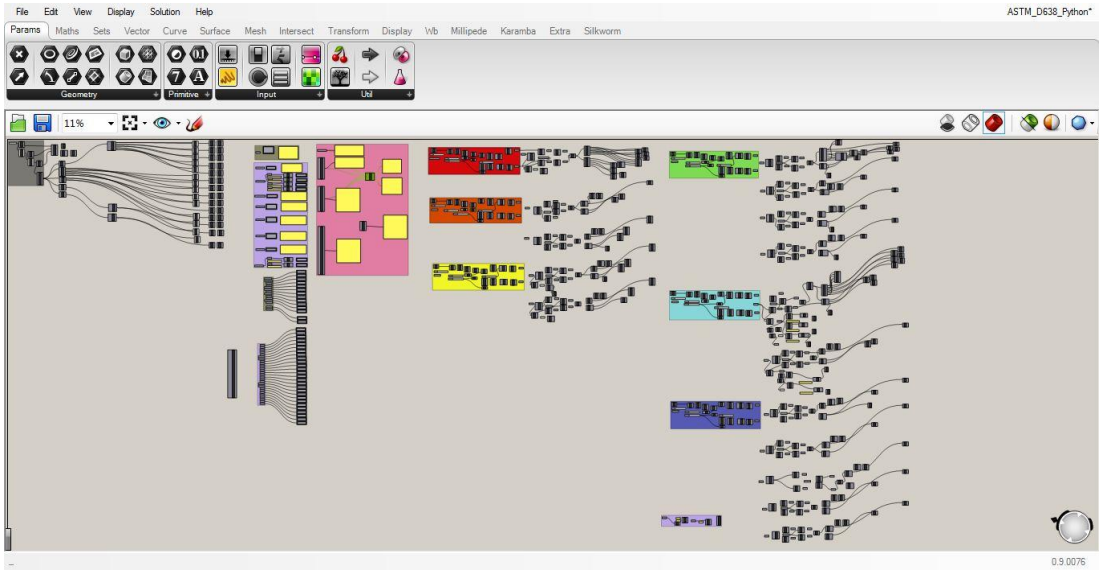


Figure 26: Pipeline for the method developed using Abaqus® FEA software

### 3.3.4 Developed Algorithm by Using Grasshopper3D® from the Results of Millipede® and Karamba3D®

The method developed by using the stress field results from the FEA performed in Abaqus® FEA software is a kind of a manual method. This means that the transfer of the results from the FEA and the boundary definitions for the stress regions with different colors are performed manually. There is a need to construct more automatic method to decrease the computational work and to increase the speed of the method. Thus, the FEAs are performed with Millipede® and Karamba3D® plug-ins of Grasshopper3D®, as mentioned before. The method is mentioned for the case where Karamba3D® is used for the quasi-static FEA since the methods of the cases with Millipede® and the Karamba3D® are similar. This makes it easier to integrate the analysis into the pipeline of the constructed method which provides automation of the method. For the present method, it is enough to define the geometry, boundary conditions and the loading conditions. Because of the fact that the constructed method can only be used with the plane stress case, it is enough to define the outer boundary and the details of the interior geometry such as holes, etc. The boundary definition can be done using the boundary block seen in Figure 27.

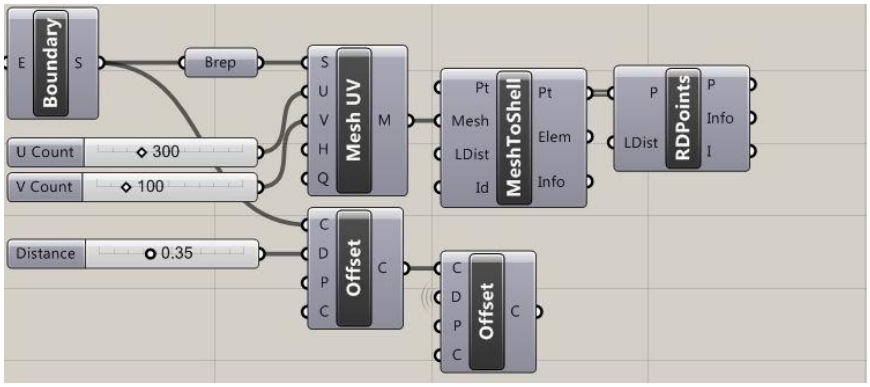


Figure 27: Boundary definition in Grasshopper3D®

For this constructed method, the boundary condition and the loading condition definitions are performed using the points existing on the mesh corners. To define all these conditions, the points on the edges of the boundary are used. The points on the left side of the boundary are used to define the fixed boundary and the points on the right side of the boundary are used to define the 1 kN distributed loading condition. The pipeline for these definitions and the selected points for these conditions can be seen in Figure 28 and Figure 29.

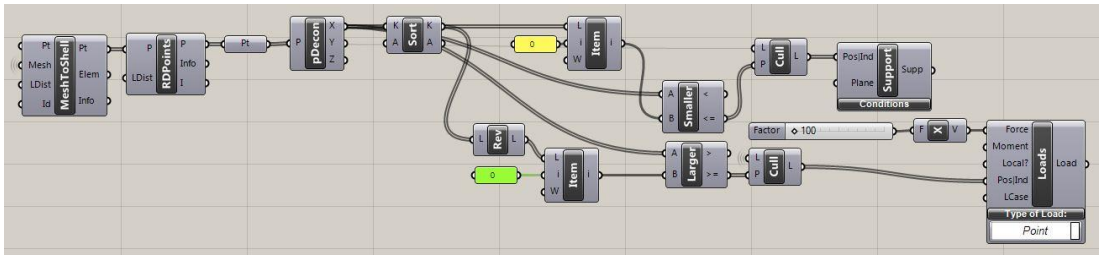


Figure 28: Pipeline for boundary condition and loading condition definitions

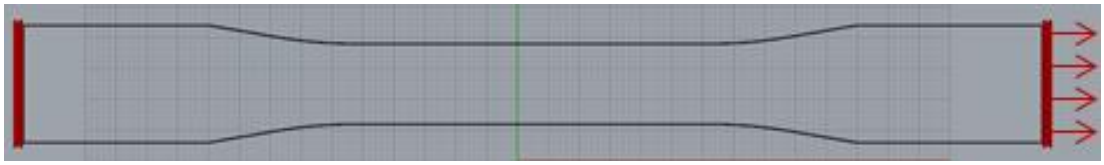

Figure 29: The boundary and the loading conditions locations

These definitions are enough to use the method. After these, FEA is performed by Karamba3D® to obtain the stress field results and to extract the

boundaries of the stress regions with different colors according to stress values. The obtained stress field results for 6 colors range and the obtained boundaries from the stress regions can be seen in Figure 30 and **Error! Reference source not found.**, respectively.

Figure 30: Stress field result from the FEA with Karamba3D® (top) and boundaries of the stress field regions (bottom)

After the boundaries are obtained, the method constructs the interior structure by using the first principal stress directions. To verify the reliability of the Karamba3D®, the first principal stress vectors are obtained in Abaqus® first. The obtained vectors can be seen in Figure 31 given below. These results are again obtained by considering the 6 colors spectrum in Abaqus® FEA.,

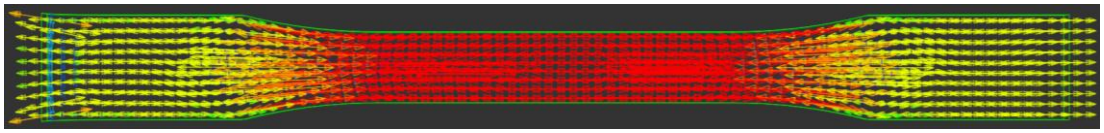

Figure 31: First principal stress direction vectors in Abaqus®

The lines which connects the first principal stress direction vectors are obtained from the FEA performed in Karamba3D®, which can be seen in below figure.

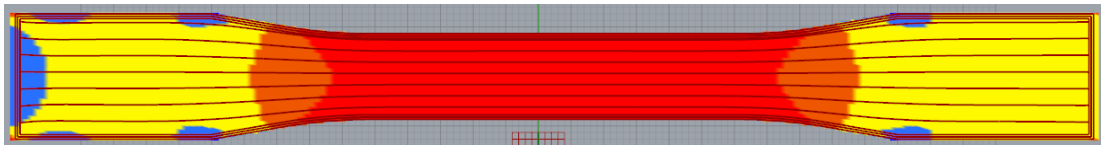

Figure 32: The lines which connect the first principal stress direction vectors

When these two figures are compared, it can be clearly said that the obtained lines which connects the first principal stress vectors in Karamba3D® are reliable and they can be used for the proposed method.

Automatically in the method, the internal structure of the geometry is constructed by offsetting and trimming these lines with respect to stress field region boundaries. The constructed final interior structure for this geometry can be seen in Figure 33.

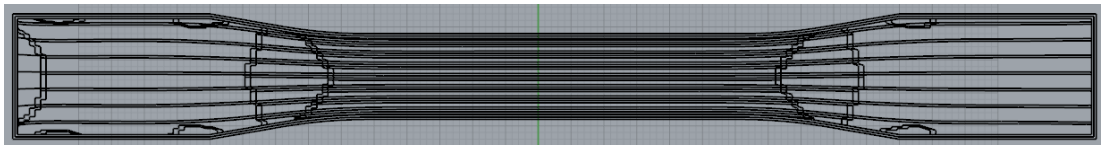

Figure 33: Constructed internal structure

### 3.4 G-Code Generation

The final step in Grasshopper3D® is to obtain the G-code files for the open source FFF 3D printer to manufacture the models using the generated tool paths with the help of the other blocks in Grasshopper3D®. G-code file is generated by using a customized block written in Python programming language. Throughout the algorithm, the interior structure is constructed by using FEA results. Then, the structure is divided into points to be input as point lists in rearranged branches. These point lists are supplied to the G-code generator Python script block as inputs. A pseudocode provided below can be examined to understand the post-processor.

*01. Open a G-code file*
*02. Initialize parameters*
*03. Write start G-codes to the file*
*04. For layer in layers*
*05. For outer boundaries*
*06. Write appropriate G-codes to the file*
*07. For stress region boundaries*

*08. Write appropriate G-codes to the file*

*09. For stress flow lines*

*10. Write appropriate G-codes to the file*

*11. Write end G-codes to the file*

*12. Close the file*

### 3.5 Discussion and Conclusion

In this chapter, the FEA based developed method is expressed. In the first steps of this developed method, Abaqus® FEA software is used to construct the artifacts with modified interior structure. The results from the FEA are used for modification. The interior structures of the artifacts are constructed manually by using the results of the FEA. The pipeline for the first version of the proposed method can be seen in Figure 34.

In this version, the geometry is required to be designed and to be transferred to Abaqus®. The FEA is performed via Abaqus® for the supplied geometry under tensile loading. From the FEA, the Von Misses stress field results are obtained which is suitable for ductile materials. The method can also be used for brittle materials by changing the visualized results as ones obtained by considering the maximum principal stress theory. The stress field results are transferred back to Grasshopper3D® to be used for interior structure modification, as colored meshes. Only the stress region boundaries are used for modification. After interior structure modification is completed, a G-code file is generated to be supplied to an open source 3D printer.

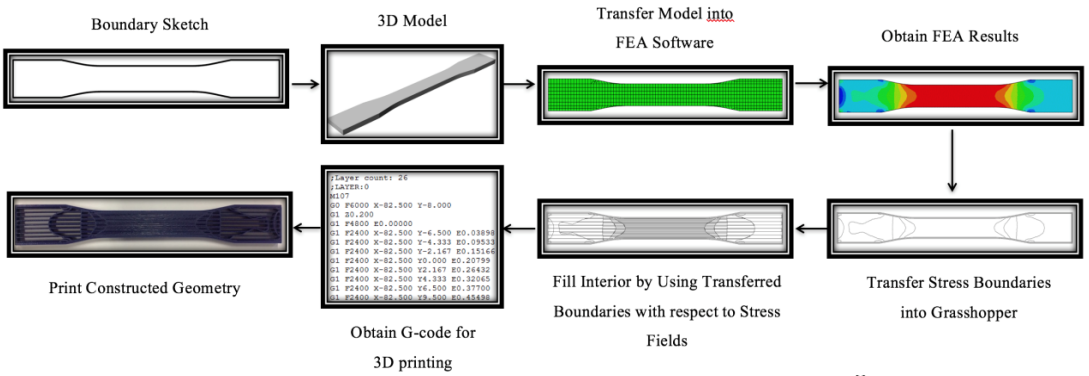


Figure 34: Flowchart of the manual methodology by using Abaqus® as FEA software

Afterwards, an automated method is developed. Automatization means that the user only gives the designed geometry and obtains the G-code file for the artifact with modified infill structure from the algorithm. Throughout the development of this method, Karamba3D® is used for FEA, which is an embedded plug-in of Grasshopper3D®. By using Karamba3D®, the FEA, which is performed externally in scope of manual method, is performed directly inside the algorithm developed in Grasshopper3D®. The interior of the artifacts is modified by using not only the stress field boundaries obtained from the FEA results but also using the lines which connect the first principal stress vector directions. The fundamental steps of the proposed methodology are provided below. The algorithm constructed via Grasshopper3D® can be summarized as below and can be seen in Figure 35.

*01. Draw the outer boundaries and inner details like holes, gaps, etc. in 2D plane and offset them twice by 0.35mm*

*02. Convert the drawn boundaries to a surface for meshing.*

*03. Mesh the surface with specified mesh number in x and y axes.*

*04. Choose the points where the boundary conditions and loading applied and set he types of them*

*05. Assemble all the meshes, boundary conditions and loadings*

*06. Run the solver under specified conditions*

*07. Obtain the Von Misses stress field results*

*08. Obtain the boundaries of the stress field regions by using VB scripting and the lines connect the first principal stress direction vectors*

09. *Offset the lines with 0.35 mm several times and trim them by using stress field regions*
10. *Divide the outer boundaries and their offsets, stress field region boundaries and obtained lines and their offsets to get the required point list*
11. *Rearrange the branch numbers of each lists belong to each curve*
12. *Supply the point lists with ordered branch numbers to a python script which creates the G-code file*

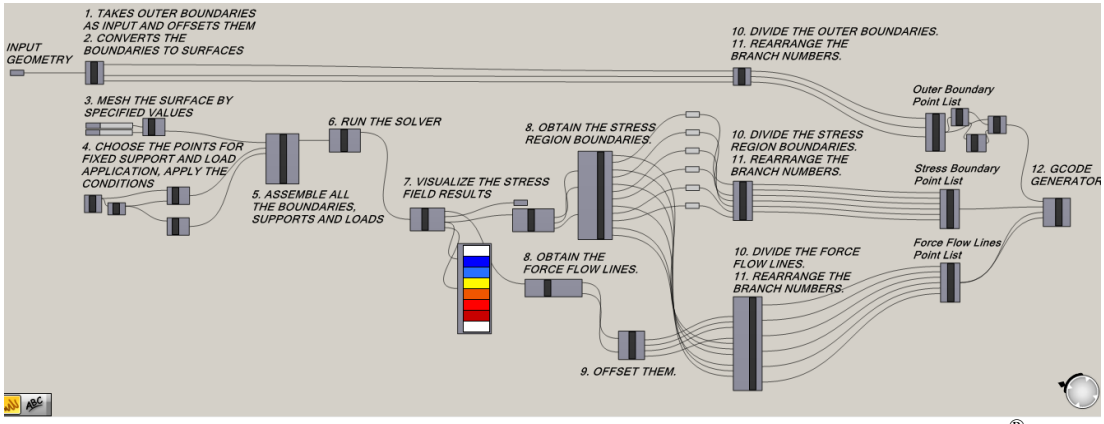

Figure 35: Constructed automatized algorithm in Grasshopper3D®

In further topics, the proposed methods are verified by the tensile loading tests.

# CHAPTER 4

# TENSILE TESTING FOR METHOD DEVELOPMENT: ASTM D638

## 4.1 Introduction

Throughout the study, an automated method is developed to manufacture the parts with improved strength characteristics for AM technology. For previous stages of the developed method, ASTM-D638 Type 1 specimen is used. As stated in the previous chapters, the geometries are manufactured by using an FFF type open source 3D printer. The load carrying capacities of the parts are tried to be increased by modifying their interior structures using the Von Misses stress field results and the lines connect the first principal stress direction vectors obtained from FEA software Karamba3D®.

For detailed characterization and to prove the validity of the method, tensile testing is performed through the thesis study. In other words, the method is enhanced by using the results of the tensile tests, consistently. For example, the parameters such as number of stress field regions, densities of the infill structures within these regions, etc. are modified consistently to reach the optimum values in tensile testing results.

In further topics of this chapter, information about the equipment used through the testing, details about the tensile testing of ASTM D638 Type 1 specimens manufactured by using an open source desktop 3D printer, etc. are explained in a detailed manner. In related topics, the results of the tests are also discussed.

## 4.2 Effects of Infill Types and Densities on Mechanical Behavior

A detailed algorithm runs behind AM processes, called slicer as stated in the previous topics. When a part is manufactured by using 3D printing technology, only the outer boundaries of the geometries are to be considered as significant. However, the slicer algorithms of traditional 3D printers perform important tasks to fill the interior of the geometries. Algorithms can construct the interior with the specified infill types and densities. As stated in the previous topics, slicing algorithm takes the geometry in triangular mesh form and slices it into specified number of layers. Then, it fills the interior of the outer boundaries with standard infill structures according to the specified densities for each layer.

Infill type is one of the most important parameter which affects the mechanical behavior of a part under specified loading conditions. When a part is exposed to load, it is mostly carried by the interior structure of the part. The resulting stress from the applied load flows through the interior structures of the parts along a path. By setting the infill type properly, a part can show mechanical behaviors as desired under the specified loading condition. It can be stronger, more ductile or more brittle under the specified loadings, which results from the selected or modified infill structures. The interiors of the geometries are constructed by using standard infill structures defined in the CAM software of the 3D printers. In traditional CAM software of 3D printing technologies, the infill structures such as rectilinear, concentric, honeycomb, Hilbert's curve, etc. are used to fill the geometry's interior [42]. Some examples of these structures can be seen in Figure 36.

.

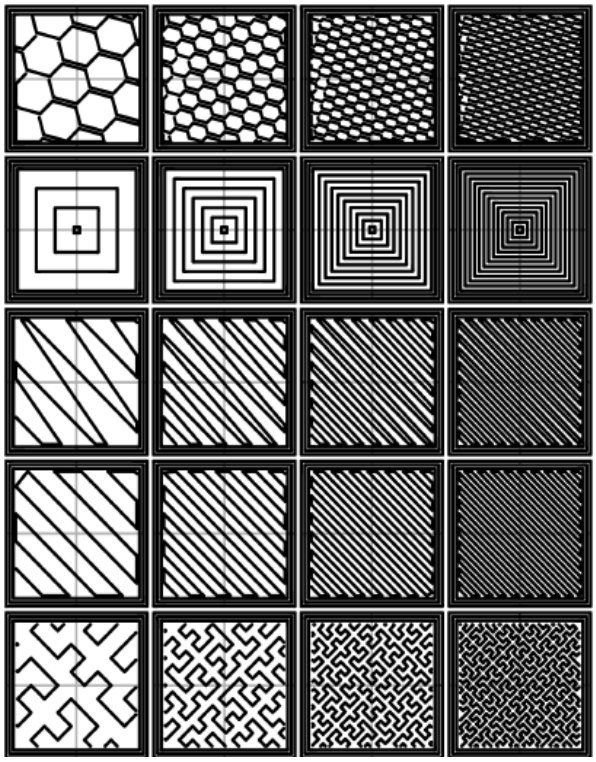

Figure 36: Infill Patterns. Top to bottom: Honeycomb, Concentric, Line, Rectilinear, and Hilbert Curve. Left to Right: 20%, 40%, 60%, 80% Infill Densities [42]

Moreover, the infill densities of the parts can also be set up as desired. The density can be set in the range from 0% to 100%. While 0% infill density means that the geometry is hollow, 100% infill density means that the geometry is manufactured with fully filled interior.

Easy adjustment of infill type and infill density through 3D printing process motivates the researchers to work in this area. In literature, most of the works performed are related with the effects of infill types and densities beyond topology optimization on mechanical behavior of the 3D printed parts.

Steuben et al. [4] worked on the direct effect of the infill types on mechanical behaviors of the specimens under specified loadings, which is also closely related with this proposed method. They proposed an implicit slicing methodology which provides a way to increase the strength of the 3D printed parts. They used standard infill structures of traditional CAM software of 3D printers and physics based field defined over the geometry, obtained from FEA, to modify and construct an interior

structure. They obtained FEA results from the COMSOL FEA software. Then, they used these stress field results to modify the standard infill structures for each layer of the part which is to be manufactured via a desktop 3D printer. In their work, linear infill patterns tilted by -45$^{o}$ and 45$^{o}$, for odd and even numbered layers respectively, was used for the experimental works. The linear infill pattern was modified for each layer by using stress field results obtained from the COMSOL by considering all the axis for the first specimen and by considering only the x-axis for the second specimen [5]. For the odd layers, the linear infill patterns tilted with -45$^{o}$ was modified by using the stress field results. Similarly, for even layers, the linear infill with 45$^{o}$ tilt angle is used to be modified by the stress field results obtained from the FEA. The constructed toolpath and the manufactured parts can be seen in Figure 37.

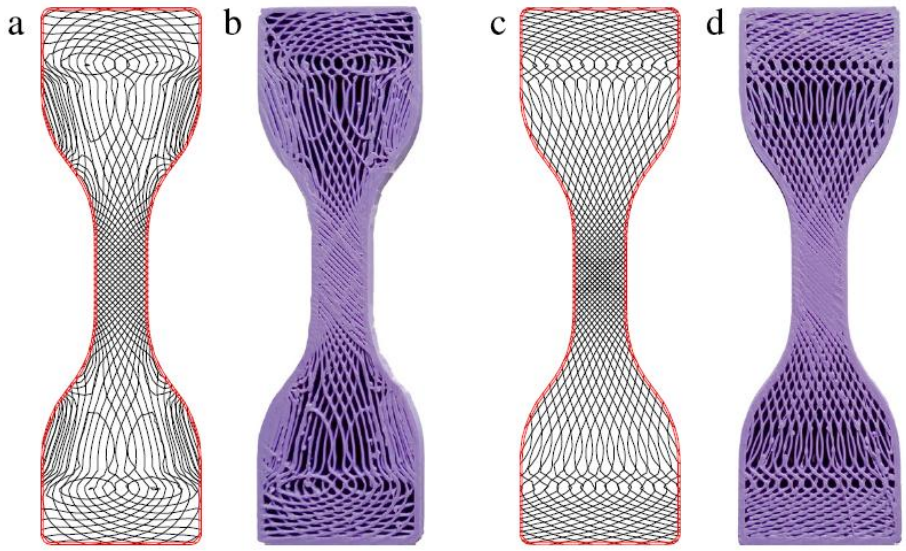


Figure 37: a) Toolpath and b) corresponding manufactured specimen for linear infill modified by using stress field results in x, y and z axis, c) Toolpath and d) corresponding manufactured specimen for linear infill modified by using stress field results consider [4]

The specimens for which the stress field results in all 3-axes are used for infill modification are named as *Stress A* and the specimens for which the stress field results only in x-axis are used to modify the infill are named as *Stress B*. The results they obtained are summarized in Table 3.

Table 3: Results of Steuben's work

| | **Linear** | **Stress A** | **Stress B** |
|---|---|---|---|
| Ultimate Stress [MPa] | 13.7 | 19.4 | 19.8 |
| Elastic Modulus [GPa] | 0.79 | 1.24 | 1.71 |
| Specimen Mass [g] | 6.97 | 6.99 | 6.99 |
| Filament Length [mm] | 1011.5 | 1012.7 | 1012.5 |
| Print Time [s] | 1263 | 1403 | 1329 |

As a result of their work, they obtained about 43% ultimate stress improvement when the results compared with the ones for the specimens with only linear infill structures are utilized.

Like Steuben's work, Baikerikar et al. [30] also worked on the effect of infill types and their densities on mechanical behavior of 3D printed parts under tensile loadings. They also used standard infill patterns existing in the traditional CAM software of the 3D printers. They used hexagonal and circular infill patterns. They manufactured their specimens with a specified region in gage section of the specimen with indicated infill patterns. To evaluate the results, they used continuous specimens which mean that the interior of the specimens is fully filled. However, the thickness of the specified central region of the specimens was decreased to satisfy the same infill density with the corresponding specimen having standard infill pattern. The specimens used for this study can be seen in Figure 38.

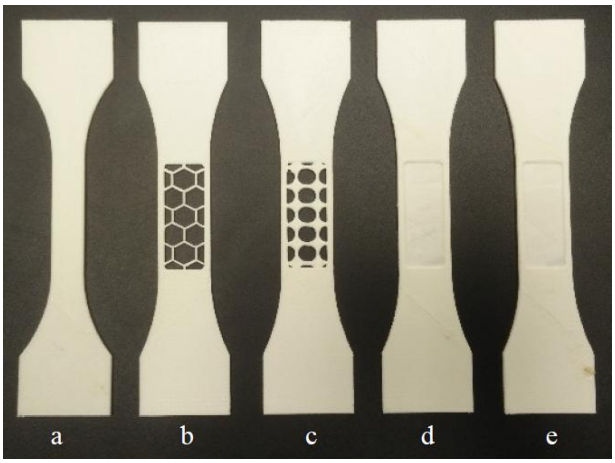


Figure 38: Printed specimens: a) continuous, b) hexagonal c) circular, d) circular continuous e) hexagonal continuous [30]

In Figure 38, hexagonal continuous specimen means that the thickness of the specified central section of the specimen is decreased to satisfy the same infill density with the specimen having hexagonal infill structure. Similar consideration exists for the specimen having circular infill. The test results of these specimens can be seen in Table 4.

Table 4: Results of Baereikar's work

| | **Max. Load Applied [N]** | **Ultimate Strength [MPa]** | **Ultimate Strain** | **Effective Modulus [GPa]** |
|---|---|---|---|---|
| Continuous | 724 | 27 | 0.06 | 1 |
| Hexagonal | 301 | 28.1 | 0.045 | 1.26 |
| Hexagonal Continuous | 285 | 16.7 | 0.0726 | 1 |
| Circular | 426 | 24.9 | 0.027 | 1.6 |
| Circular Continuous | 407 | 16.9 | 0.027 | 0.99 |

They concluded that the specimens with circular and hexagonal infill structures have better strength values than the specimens with circular continuous and hexagonal continuous infill structures.

In this proposed method, the infill structure is constructed by direct usage of the stress field results obtained from Karamba3D®, an FEA plug-in of Grasshopper3D®. The stress flow lines are obtained from the FEA and modified by considering the stress field regions according to stress values existing in the stress regions. Actually, the colors of the stress field regions are used throughout the algorithm. The mesh structure is colored according to their stress values under the tensile loading in Karamba3D®. The RGB values are used to get the stress field region boundaries. After the modification of the stress flow lines by using the stress field regions, the related G-code file is generated to be conveyed to an open source 3D printer for fabrication process. To prove the validity of the method, only the tensile tests are performed during the study. Tensile test performances are considered in next topic of this chapter.

### 4.3 Tensile Test Performance

Tests are performed to observe whether the developed method increases the strength of the 3D printed parts or not. Tensile tests are conducted to obtain mechanical properties of the specimen such as strength, maximum load carrying capacity, etc. under tensile loading. Instron 8802 Servohydraulic Fatigue Testing Machine located in the Material and Processing Laboratory (M&P) of the Turkish Aerospace Industries (TAI) is used to perform tensile tests. This machine can be used for static tensile testing and dynamic testing, i. e., fatigue testing.

The tensile test machines in the M&P laboratory of TAI are set to be used with ASTM-D638 standard which is technically equivalent to the ISO 527-1 standard used in the literature [32]. Therefore, the specimen should be tested by using 5 mm/min test speed when the strain rate is up to 0.1 mm/mm·min. When the strain rate is between 0.1 mm/mm·min and 1 mm/mm·min, the testing speed should be 50 mm/min. The recommended test speeds for different test specimens can be seen in

Table 5. Another important point is that the specimen should be fixed from one side and loaded from the other side [32]. Throughout all the tests, these criteria are considered.

Table 5: Recommended test speeds in ASTM D638 [32]

| **Classification** | **Specimen Type** | **Speed of Testing mm/min (in/min)** | **Nominal Strain Rate at Start of Test mm/mm·min (in/in·min)** |
|---|---|---|---|
| Rigid and Semi-rigid | 1, 2, 3, rods and tubes | 5 (0.2) +/- 25%<br>50 (2) +/- 10%<br>500 (20) +/- 10% | 0.1<br>1<br>10 |
| | 4 | 5 (0.2) +/- 25%<br>50 (2) +/- 10%<br>500 (20) +/- 10% | 0.15<br>1.5<br>15 |
| | 5 | 1 (0.05) +/- 25%<br>10 (0.5) +/- 25%<br>100 (5) +/- 25% | 0.1<br>1<br>10 |
| Non-rigid | 3 | 50 (2) +/- 10%<br>500 (20) +/- 10% | 1<br>10 |
| | 4 | 50 (2) +/- 10%<br>500 (20) +/- 10% | 1.5<br>15 |

### 4.3.1 Instron 8802 Servohydraulic Fatigue Testing Machine

All of the tensile tests are performed by using the Instron 8802 Servohydraulic Fatigue testing machine. ASTM-D638 tensile testing standard for plastic materials are used for the tests since all the testing machines in M&P laboratory of the TAI are set to be used with this standard as stated in previous topics. The hardware used to control these machines is also set to be used according to criteria defined in ASTM-D638 tensile testing standard.

Instron 8802 testing machine is a servo-hydraulic fatigue testing machine which can also be used for static tensile tests up to 100kN loads. It has two grips, one is fixed located below and the other is moving grip located on a moving crosshead, above the fixed grip. The testing machine can be seen in Figure 39.

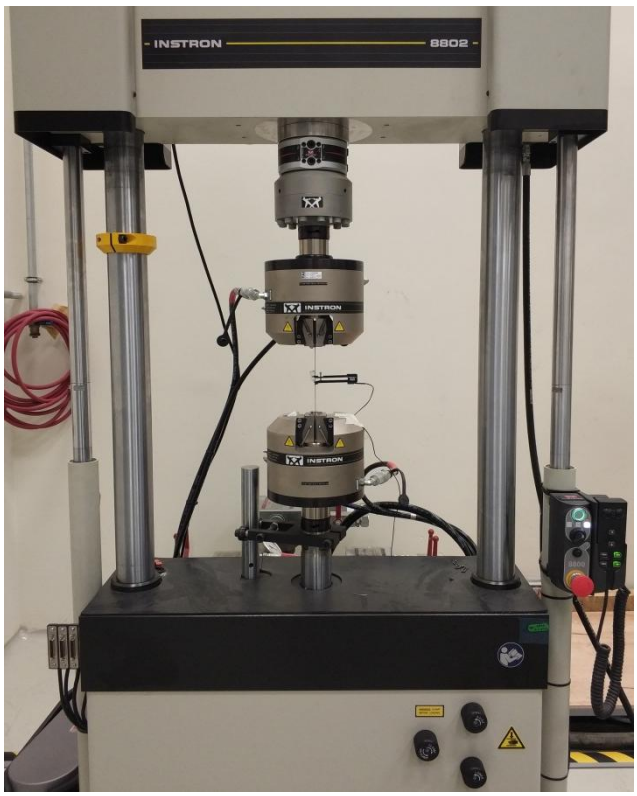


Figure 39: Instron 8802 Servohydraulic fatigue testing machine

Forces used to grip the test specimen are provided by hydraulic pressure. The pressure values are in the range of 0 to 250 bars. During the tensile tests performed

throughout this thesis study, 20 bars grip pressure is used, which can be considered as very low pressure value for these grips. This grip pressure value is chosen to provide squeezing pressure on the grip regions of the test specimens.

The specifications of the tensile testing machine, Instron 8802, can be summarized as below.

- Axial stroke capability is +/- 75 mm and 150 mm in total.
- Actuator of the machine is equipped with anti-rotation fixture.
- Loading sensitivity of the machine is 1%.
- Noise level of the system does not exceed 80 dB.
- Load capacity is +/- 100 kN.
- Load-cell read out meets 1% sensitivity between 1 kN and 100 kN.
- Testing machine includes alignment fixture.
- Grip pressure ranges from 0 to 250 bars.

### 4.3.2 Tensile Tests Performed for ASTM-D638 Type 1

In the scope of this study, the specimens which are manufactured by considering the ASTM-D638 tensile testing standard are tested under tensile loading. Only the tensile testing results are considered for the method development. In other words, there is no FEA performed for the final product with modified interior structures. Thus, the tensile tests are very significant for this thesis study.

Tensile tests are performed first to observe the effect of infill types and infill densities on the mechanical behaviors of the 3D printed specimens under specified tensile loading conditions. For further works, the tests are used to develop the proposed method and to verify the validity of the method on the strength improvement by comparing the results with the ones in literature.

The test cases can be divided into two sub-cases;

i. Initial tests where the tensile load capacities and tensile strength values are obtained to evaluate the validity of the results by comparing them.

ii. Further tests where the load carrying capacity versus weight ratio is also considered to verify that the proposed method can also be used for more complicated geometries.

First of all, some ASTM D638 type 1 specimens are used for tensile testing. For these specimens, standard infill structures available in the CAM software of the 3D printer are chosen. Linear and diagonal infill types are used for early considerations. 20% and 40% infill densities are employed for the first tensile testing cases. These initial tests are performed to be able to observe the effects of infill types and densities on the mechanical behavior of the parts under specified tensile loading. The specimens with linear and diagonal infill structures can be seen in Figure 40 given below. Regarding the further tensile tests, 70% and 100% infill densities are used for the same specimens to be sure about the validity of the obtained test results in the initial tests.

All the test specimens are manufactured by using PLA material which is biodegradable thermoplastic. Thus, the tests are performed by considering the conditions defined in ASTM-D638 testing standard for plastics. One of the test configurations of these specimens can be seen in Figure 41 given below. Additionally, an extensometer is used to measure the strain from the gage section of the ASTM D638 type 1 specimens, which can also be seen in the same figure.

Specimens with 20% and 40% linear and diagonal infill structures can be considered as the first specimen set which are exposed to tensile testing to compare the testing results with some related studies in the literature. This set includes four test specimens, two with 20% density linear and diagonal infill structures and other two with 40% density linear and diagonal infill which can be seen in Figure 40.

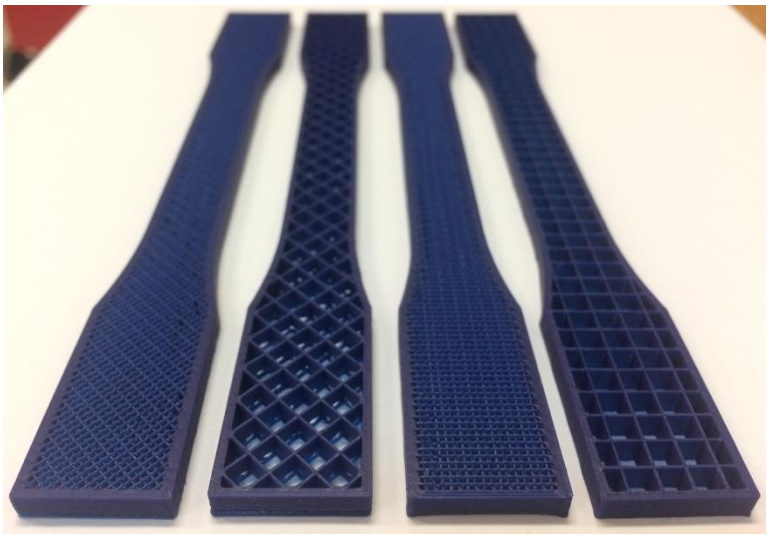

Figure 40: ASTM D638 Type 1 test specimens with infill structures left to right: 40% diagonal, 20% diagonal, 40% linear and 20% linear

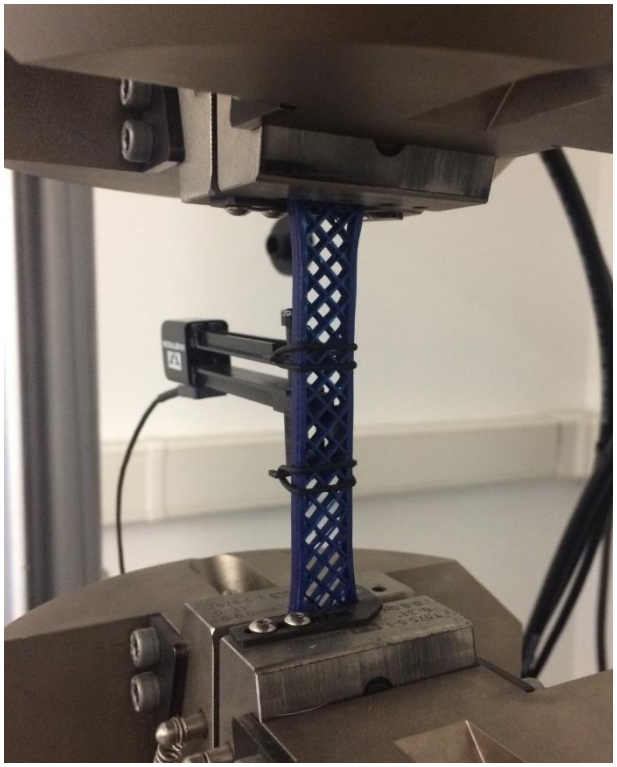

Figure 41: Test configuration of specimen with 20% diagonal infill structure

Test results for the first set of specimens can be seen in Table 6 given below. When the obtained results are examined, it can be stated that the results are

reasonable by considering the works in the literature and the theoretical knowledge in the theory of linear elasticity. They are also reasonable when the experience in the testing field is considered. It is obvious that the tensile strength and the maximum load values are higher for the linear type infill than the diagonal infill for the same density values. These results are also rational, since the interior structure is constructed along the loading directions which increase the maximum load that can be carried by the specimen. In other words, the material used for the secondary direction which has no effects on the tensile strength directly is used in the tensile direction. This situation means that larger amount of material carry the tensile load which gives possibility to increase the tensile strength. Furthermore, when the extension values are considered, it can be said that the extension values for the diagonal infill patterns are more than the ones for linear infill patterns with the same infill density, which is also a reasonable result based on the theory of elasticity [36]. Since there is an angle between the primary and secondary lines of diagonal infill types, the lines of the infill can rotate as the specimen is loaded. This lets the specimens extend more in the loading direction.

Table 6: Tensile test results for linear and diagonal infill structures

| **Specimen #** | **Ultimate Load [N]** | **Ultimate Tensile Strength [MPa]** | **Extension at Ultimate Load [mm]** | **Infill Structure** |
|---|---|---|---|---|
| 1 | 403.4 | 7.72 | 1.052 | 20% Linear |
| 2 | 342.8 | 6.63 | 1.72 | 20% Diagonal |
| 3 | 791.3 | 15.0 | 1.71 | 40% Linear |
| 4 | 652.4 | 12.4 | 1.87 | 40% Diagonal |

Here, tensile strength values are obtained directly from the test execution software of Instron tensile testing machine. The idea behind calculation is very basic. In elasticity theory, the stress value which is represented by $\sigma$ can be defined as

$$\sigma = \frac{F}{A}$$

where;

F: Applied load

A: Cross sectional area

In the test results, the tensile strength values are calculated by considering the above formula directly in the software. For example, for the first specimen whose results can be seen in Table 6, the cross sectional area is calculated nearly by using 13mm width and 4mm thickness values which are given in ASTM D638 tensile testing standard. By using these reference values, the cross sectional area is calculated as 52mm$^2$. From the results, the maximum load value is 403.4N. By considering the above formula, the tensile strength value can be calculated as;

$$\sigma_u = \frac{F_{max}}{A_0} = \frac{403.4\ N}{52mm^2} = 7.76\ MPa$$

where;

$\sigma_u$: Ultimate tensile strength

$F_{max}$: Maximum (ultimate) load applied

$A_o$: Original cross sectional area of the gage section

It can be seen in Table 6, the tensile strength value is calculated as 7.72 MPa. The difference results from the manufacturing tolerances of the specimen. For the first specimen, the width is 12.97mm while the thickness is 4.03mm. So, the cross sectional area is 52.26 mm$^2$ for real case which results in 7.72 MPa tensile strength value.

For the ultimate tensile strength value calculations, the complete cross sectional area of the gage section is used. The net cross sectional area usage, which is smaller due to the infill density and infill structure than the complete cross section, requires more calculation works. First of all, it is enough to compare the maximum load carrying capacity for this method. So, no detailed calculations for net sections are needed. These calculations are really hard to be performed since the failure section of the specimen cannot be predicted before the test to calculate the original net section

area used in ultimate stress formula. So, the net section calculation from the software cannot be performed due to the uncertainty of the failure section. The area cannot be measured from the tested specimen's failure section since original cross sectional area should be used for the stress formula given above. So, the complete sectional area of the gage section is used throughout the tensile strength calculations for the ASTM D638 type 1 specimens.

The load vs. extension graphs for these four specimens can be seen below.

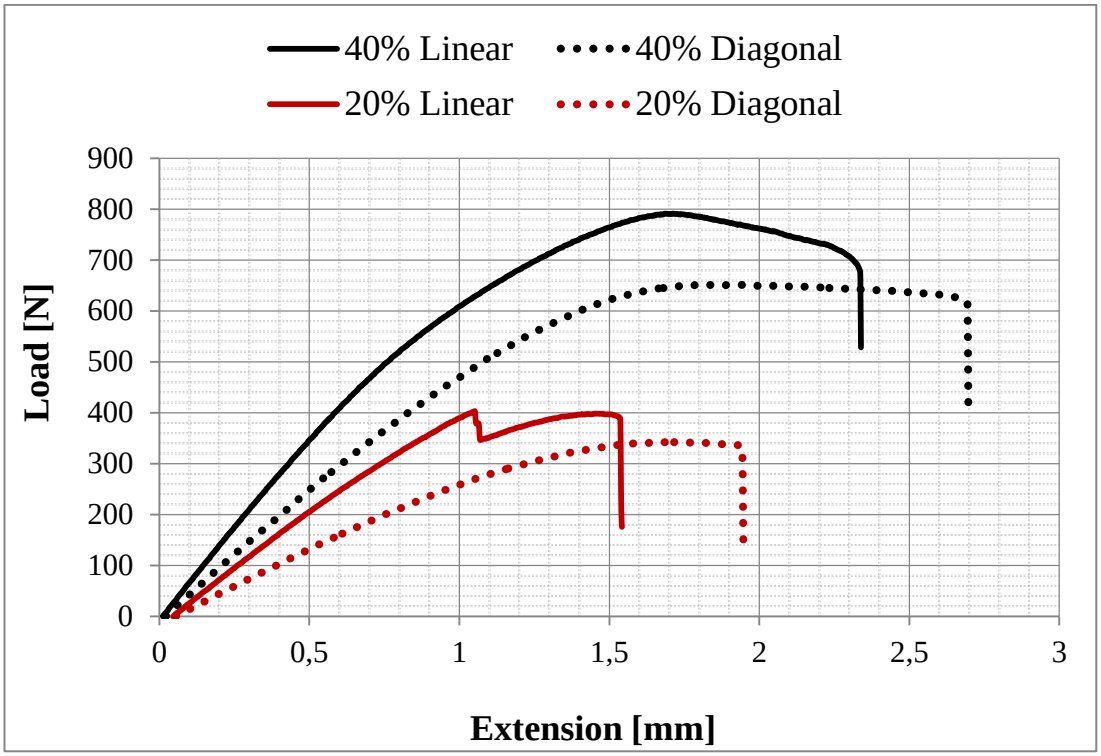


Figure 42: Load vs. extension graph for geometries with 20% and 40% infill density of linear and diagonal infill structures

When the load vs. extension curves are considered, it can be said that the PLA material behaves like a ductile material for these specimens.

Specimens which have 40% infill density have strength values nearly two times the ones for specimens with 20% infill densities. The load capacities are almost double for the specimens with 40% infill density. It can be clearly said that these results are also reasonable when the linear theory of elasticity is considered.

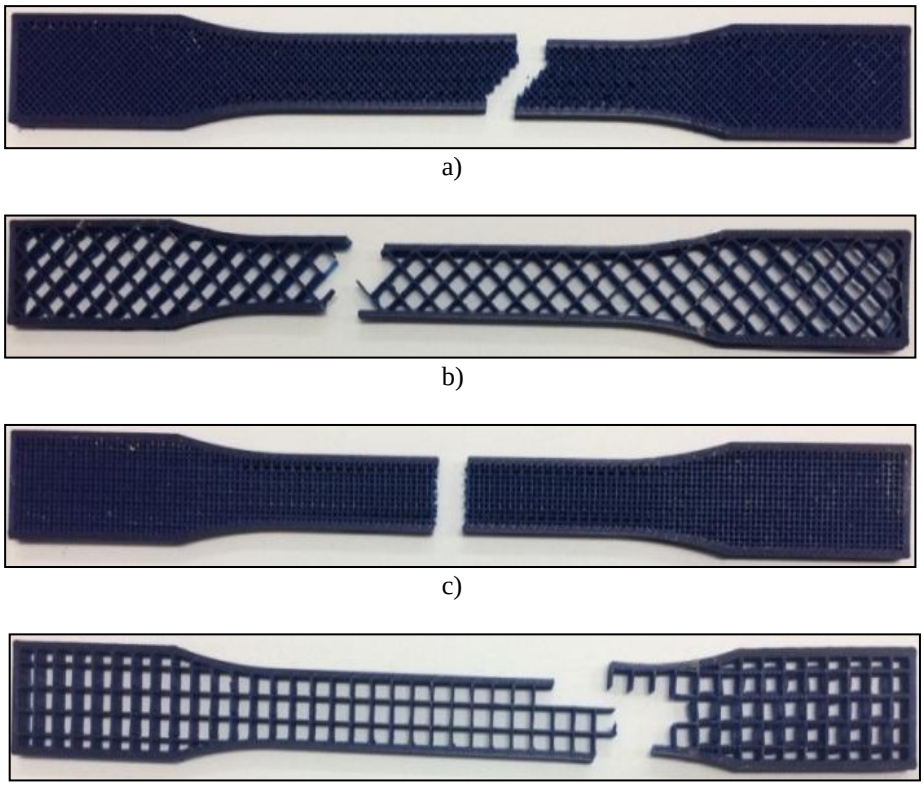

Figure 43: Failure modes for specimens of (a) 40% diagonal infill (b) 20% diagonal infill (c) 40% linear infill and (d) 20% linear infill

When the failure sections are examined, it can be observed that the failure occurs on the surface which is completely transverse to the loading direction i.e., pure tension failure occurs for the specimens with linear infill patterns. However, for the diagonal infill patterns, failure occurs on the surface with an angle about $45^{o}$ with the loading direction i.e., pure shear failure occurs for 40% density [36]. The failure modes of these specimens can be seen in Figure 43 given above.

Regarding the further test cases, specimens with 70% infill density are considered. In this set, two specimens are exposed to tensile testing. While one of the specimens has 70% density of linear infill, other has 70% density of diagonal infill type. This set is again used to verify the tests results by comparing them with the ones obtained from the previous tests. The specimens can be seen in Figure 44 given below.

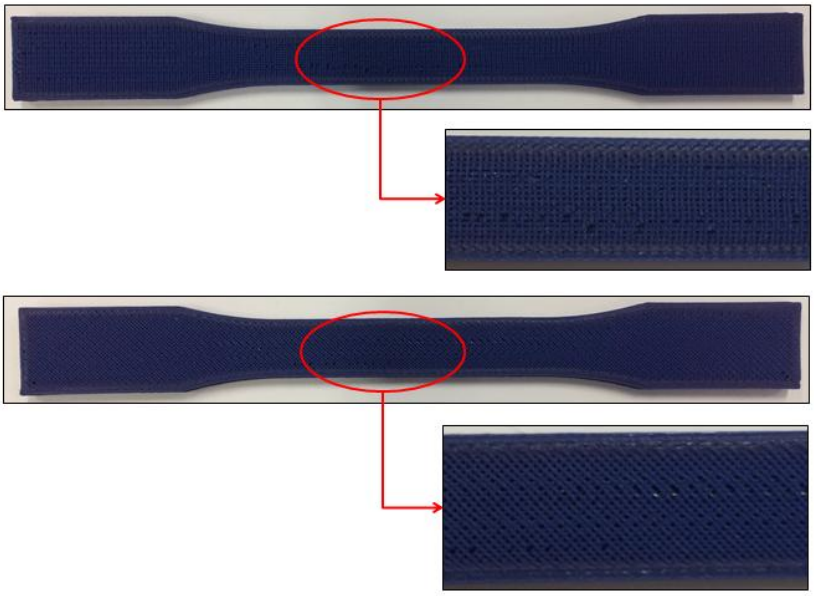

Figure 44: Test specimens; one with 70% linear infill density (top) and the other with 70% diagonal density (bottom)

Test configurations for all the specimens belong to this set are the similar. One of the test configurations can be seen in Figure 45.

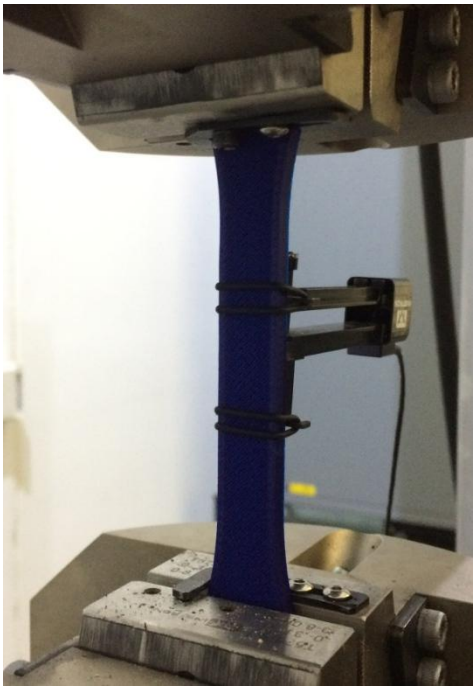

Figure 45: Test configuration for the specimen with 70% diagonal infill

The results of the tensile tests of the specimens with 70% density infill can be seen in Table 7 given below.

Table 7**:** Tensile test results for 70% density with linear and diagonal infill structures

| **Specimen #** | **Ultimate Load [N]** | **Ultimate Tensile Strength [MPa]** | **Extension at Ultimate Load [mm]** | **Infill Structure** |
|---|---|---|---|---|
| 1 | 1006 | 18.9 | 2.215 | 70% Diagonal |
| 2 | 1146 | 21.3 | 1.893 | 70% Linear |

The load extension graphs of geometries with 70% density diagonal and linear infill structures can be seen in the following figure.

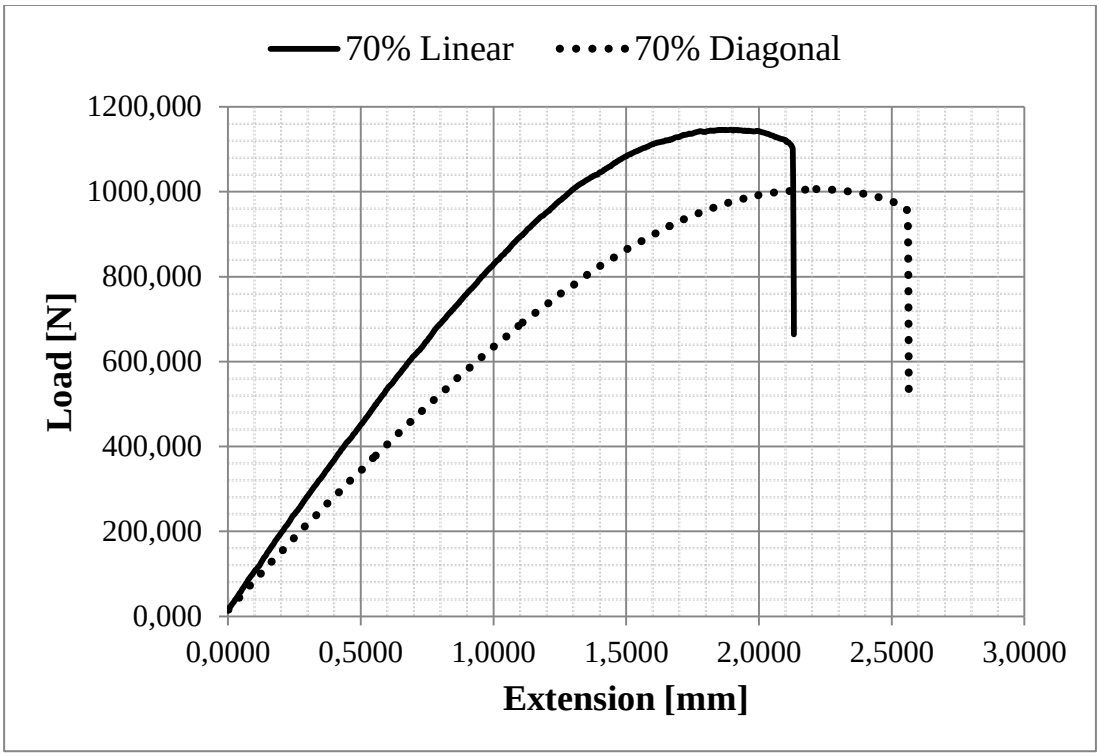


Figure 46: Load vs. extension graph for geometries with 70% infill density of linear and diagonal infill structures

When the load vs. extension plot is examined, it can be observed that the material has neither ductile nor brittle characteristic for this case. By considering the results, it can be obviously said that these results are also reasonable when compared with the test results of the previous sets. For specimens with 70% infill density of diagonal infill, the maximum carried load is smaller than the one with 70% infill density of linear infill, as expected. This situation results from the same reason explained for the 20% and 40% density specimens. Moreover, the specimen with 70% diagonal infill has larger extension values because of the diagonal infill type. The 70% linear infill specimen has larger maximum load and strength values when compared with the one with diagonal infill. These results are also expected when the previous test results and the theory of elasticity are considered.

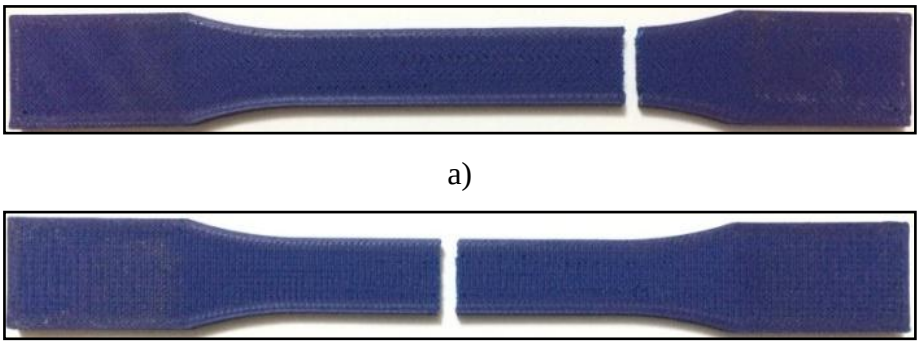

a)

b)

Figure 47: Failure modes of specimens; a) 70% diagonal infill and b) 70% linear infill

When the failure sections of these specimens examined, it can be seen that the failure section places on the region between the grips, i.e., gage section. In this case, the failure mode of the specimen with 70% diagonal infill is pure tension in contrast with the results of the one with 40% diagonal infill. Theoretically, for diagonal infill structures, the failure mode is pure shear as can be seen in Figure 43. As similar with 40% infill density case, the failure mode for the specimen with 70% linear infill is also pure tension which is reasonable when the previous test results and the elasticity theory are considered.

As a further test set, the specimens with 100% infill density, which means the specimens are fully filled, are considered. Three specimens exposed to tensile testing exist for this set. All of the specimens have linear infill pattern. These specimens are used through tensile tests to obtain the maximum load carrying capacity and the tensile strength values for the fully filled ASTM D638 Type 1 specimens. One example of these specimens can be seen in Figure 48.

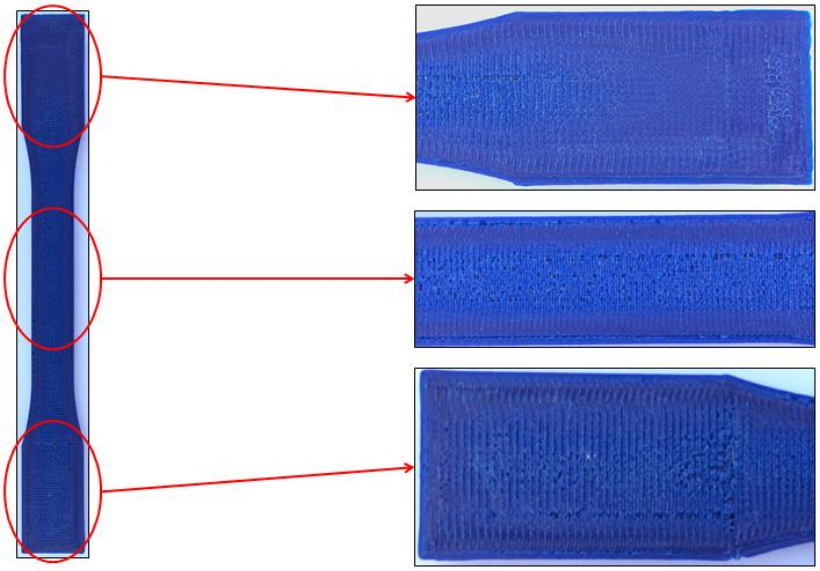

Figure 48: Test specimen with 100% linear infill

All the test specimens for this set have an appearance as they have porous interior structure. This situation results from the nozzle speed of the 3D printer mainly. The tensile test configurations for the specimens with 100% infill are also the same. One of them can be seen in Figure 49.

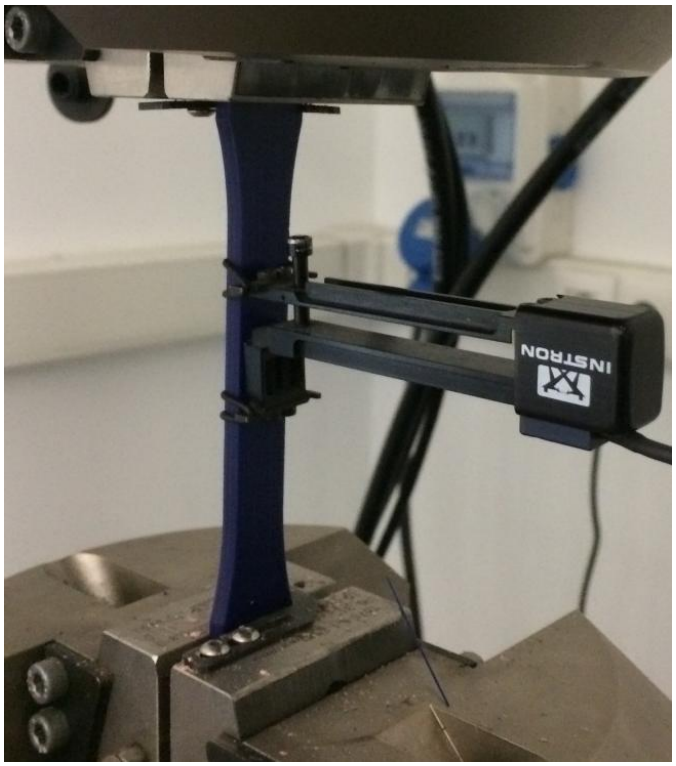


Figure 49: Test configuration for the specimens with 100% infill

The obtained results of the tensile tests of the specimens with 100% infill can be seen in the Table 8.

Table 8: Tensile test results for 100% density linear infill structures

| **Specimen #** | **Ultimate Load [N]** | **Ultimate Tensile Strength [MPa]** | **Extension at Ultimate Load [mm]** | **Infill Structure** |
|---|---|---|---|---|
| 1 | 1496 | 26.9 | 1.999 | 100% Linear |
| 2 | 1630 | 30.5 | 2.094 | 100% Linear |
| 3 | 1663 | 30.4 | 2.04 | 100% Linear |

The load vs extension curves for these specimens can be seen in Figure 50.

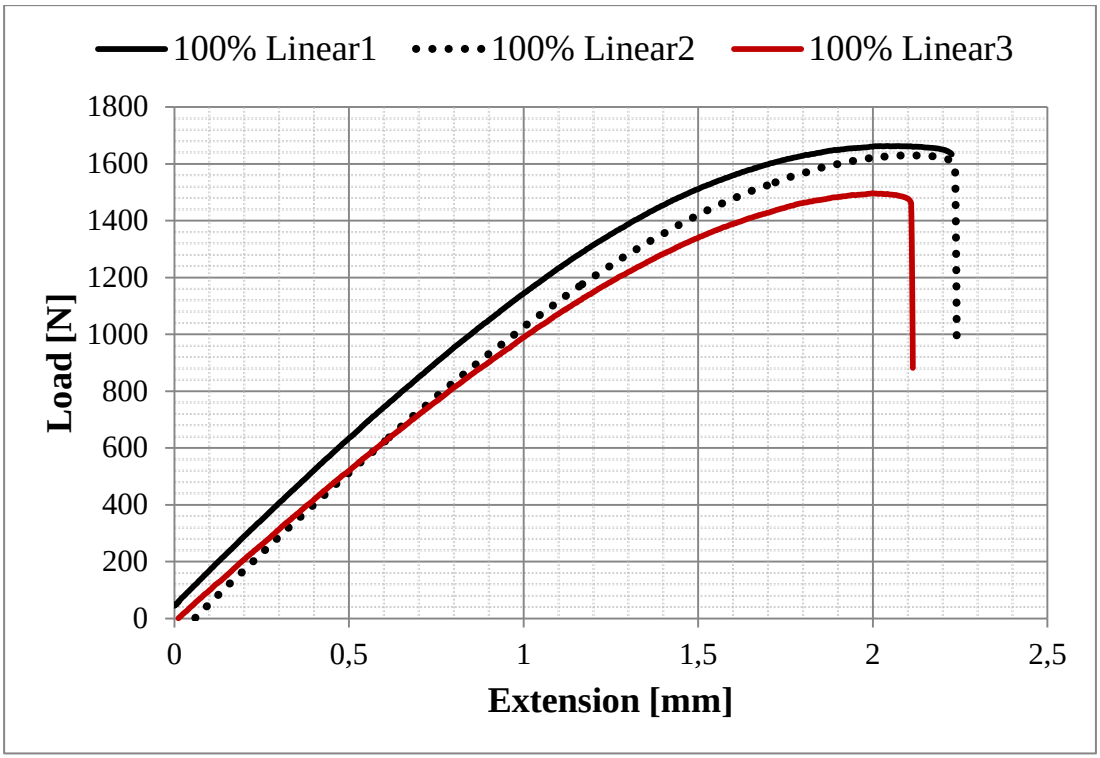


Figure 50: Load vs. extension graph for geometries with 100% infill density

When the load vs. extension plot is considered, it can be said that the material has a beharior like brittle material. These results are also reasonable when compared with the results of previous tests. For this case, although specimen 2 has lower maximum load carrying capacity, it has larger tensile strength value than specimen 3. This situation results from the dimensions of the specimens. Even if the design of the specimens is the same, the real dimensions of the manufactured parts are a bit different due to the manufacturing process on the 3D printer. The gage thickness of the second specimen is 4.05mm while the gage width is 13.18mm, which results in 53.28 $mm^2$ cross section area for the gage section. However, for the third specimen, thickness is 4.15mm and the width is 13.19 mm, which results in 54.74 $mm^2$ area of cross section. When the maximum load values for these specimens are divided by the related cross section area values, the results are as given in Table 9. All observations made for the tested specimens up to now are also valid for this set of specimens. The first specimen has the lowest maximum load value. This is due to the printing quality of it. It has more porosity than the others.

Figure 51: Failure modes of the specimens with 100% infill

When the failure modes of these specimens are considered, they are also rational. All of the specimens with 100% linear infill structure have the failure type of pure tension as expected. However, due to printing quality, failure occurred near the grip regions in gage section. Since the failures occur between the grip sections, they can be considered as valid for this study.

All results obtained for the specimens with standard infill types at different density percentages are summarized in Table 9.

Table 9: Tensile test results for 100% density with linear and diagonal infill structures

| Specimen # | Ultimate Load [N] | Ultimate Tensile Strength [MPa] | Extension at Ultimate Load [mm] | Infill Structure |
|---|---|---|---|---|
| 1 | 403.4 | 7.72 | 1.052 | 20% Linear |
| 2 | 342.8 | 6.63 | 1.72 | 20% Diagonal |
| 3 | 791.3 | 15.0 | 1.71 | 40% Linear |
| 4 | 652.4 | 12.4 | 1.87 | 40% Diagonal |
| 5 | 1146 | 21.3 | 2.215 | 70% Linear |
| 6 | 1006 | 18.9 | 1.893 | 70% Diagonal |
| 7 | 1630 | 30.5 | 1.999 | 100% Linear |
| 8 | 1663 | 30.4 | 2.094 | 100% Linear |
| 9 | 1496 | 26.9 | 2.04 | 100% Diagonal |

The load vs. extension plots for these all specimens can be seen in figure given below.

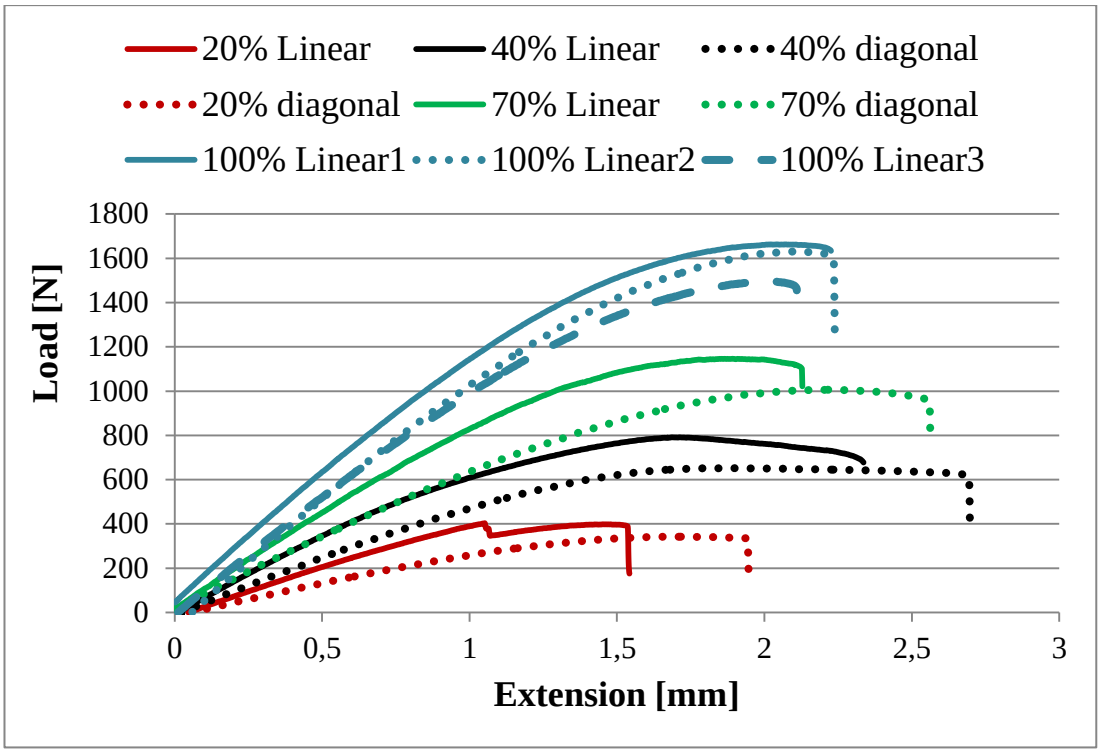


Figure 52: Load vs. extension graph for all geometries with standard infill structure

When all the results are examined, it is obvious that the tensile testing method used through this study is valid for further developments. While the infill density of the specimens increase, the maximum load capacities increases. Moreover, for all the specimens, the specimens with linear infill structures have larger maximum load carrying capacities. The specimens with diagonal infill have larger extension values. In other words, these specimens are more ductile than the ones with linear infill structures. Furthermore, the maximum load carrying capacity increases with an increase in the density.

For the method development, the specimens with 70% infill density are chosen to be exposed to tensile testing to reach an optimum method developed by using Abaqus®, manual method, and specimens with 66.5% infill density are chosen to verify the effectiveness of the automated method developed by using Karamba3D®, automated method. Test specimens have infill structures constructed by using the developed methods.

There are seven specimens used for tensile testing work of the set where the specimens are constructed by using the manual method. The specimens

manufactured with 70% infill density and having stress modified structure can be seen in Figure 53.


Figure 53: Test specimens with 70% infill density with stress modified infill

All these specimens are manufactured by using PLA material with blue and black colored filaments used in the 3D printer. Test configurations for all these specimens are the same. They are fixed from the bottom ends and loaded from the upper ends as defined in ASTM D638. Test configuration for one of the specimens can be seen in Figure 54 given below.

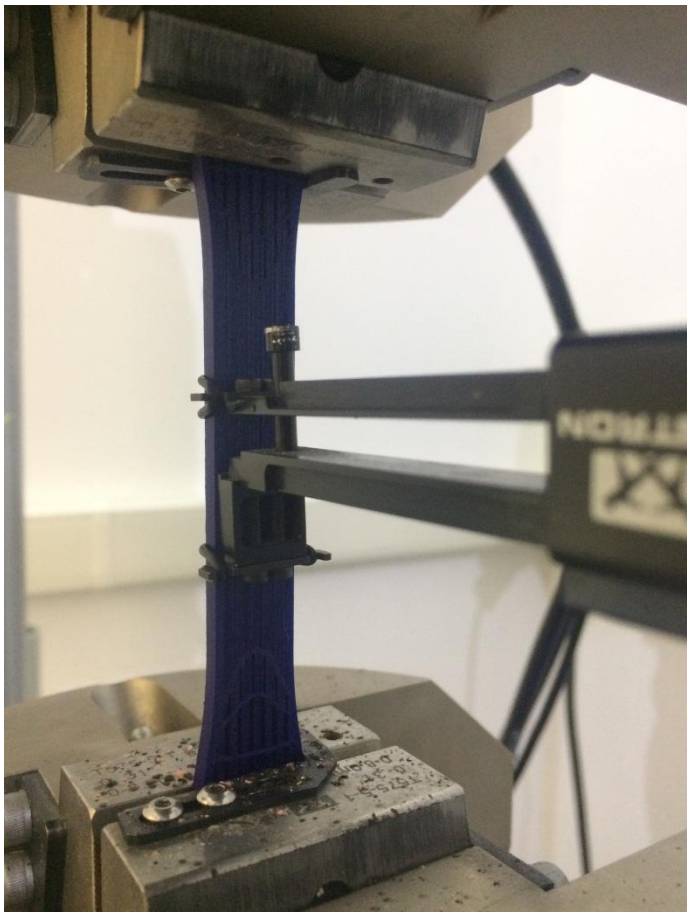

Figure 54: Tensile test configuration of one of the specimens with 70% stress modified infill

The test results are used for further improvement of the method. Obtained results of the tensile tests performed for specimens with 70% stress modified infill structures are summarized in Table 10.

Table 10: Tensile test results of the specimens with 70% stress modified infill structure

| **Specimen #** | **Ultimate Load [N]** | **Ultimate Tensile Strength [MPa]** | **Extension at Ultimate Load [mm]** | **Infill Structure** |
|---|---|---|---|---|
| 1 | 1302 | 24.7 | 1.06 | 70% stress modified |
| 2 | 1394 | 26.2 | 1.55 | 70% stress modified |
| 3 | 1416 | 27.0 | 1.52 | 70% stress modified |
| 4 | 1462 | 27.7 | 1.44 | 70% stress modified |
| 5 | 1377 | 25.8 | 1.25 | 70% stress modified |
| 6 | 1708 | 32.5 | 1.64 | 70% stress modified |
| 7 | 1629 | 30.9 | 1.48 | 70% stress modified |
| Ave | 1469.71 | 27.0 | 1.42 | 70% stress modified |

The load vs. extension curves for this specimen can be found in Figure 55.

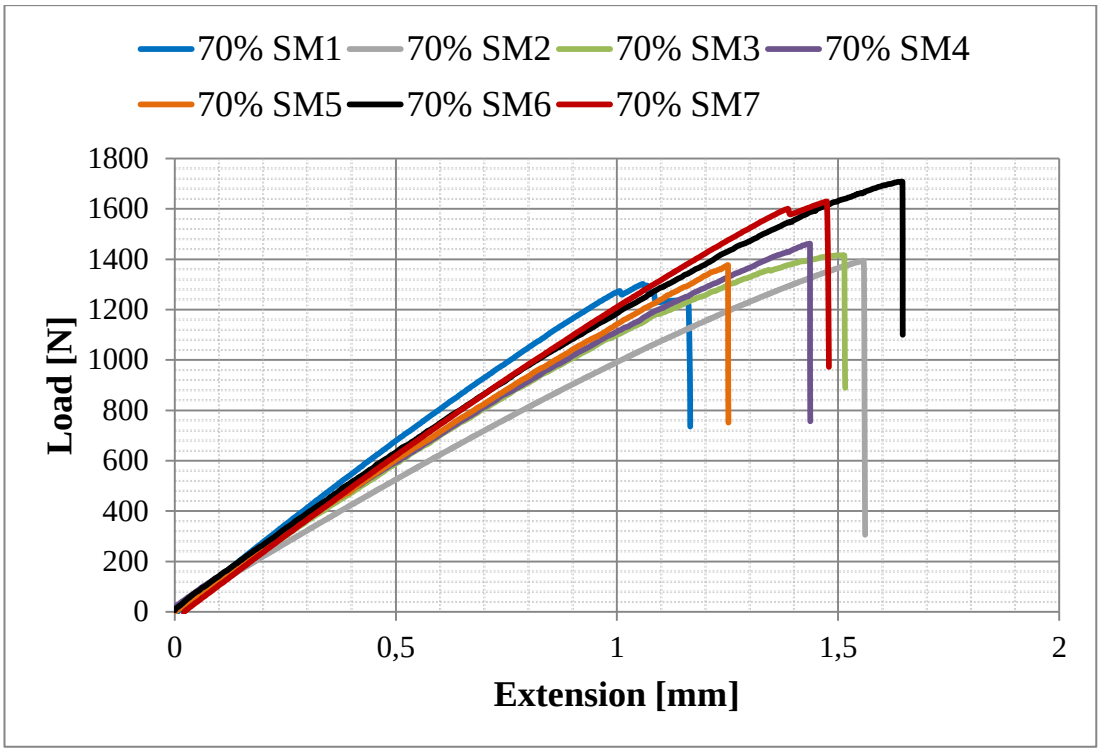


Figure 55: Load vs. extension plots of specimens with 70% density stress-modified infill structure

When the tests results are examined, it is clear that the material behaves as brittle, although the Von Mises stress field results are considered to construct the interior stress modified structure. The usage of the theories developed for brittle material failures such as maximum principal stress theory can be used as a future work for this study.

It is also obvious that the proposed manual method improves the mechanical behaviors of the specimens under tensile loading. If all the test results are analyzed, it can be inferred that the method is enhanced step by step. The details of the method are given in Chapter 3. For comparison with 70% linear infill density specimen, the average values of the maximum load capacities, tensile strength values and the extensions for all these specimens can be taken in consideration. For the average values, it is obvious that the specimen with 70% stress modified infill structure has 28.2% better maximum load carrying capacity. It has also 26.8% larger tensile strength value than the one with 70% linear infill structure. It can be observed that the Specimen 6 has 49% larger maximum load carrying capacity. Moreover, it has

52.6% larger tensile strength value. When the extensions of the specimens are compared, it can be said that the proposed method decreases the ductility of the specimens. For consideration of average values for this specimen set, the extension value for the one with 70% stress modified infill is 33.3% less than the specimen with 70% linear infill. If the specimen with maximum values is considered, the extension value is 20% less.

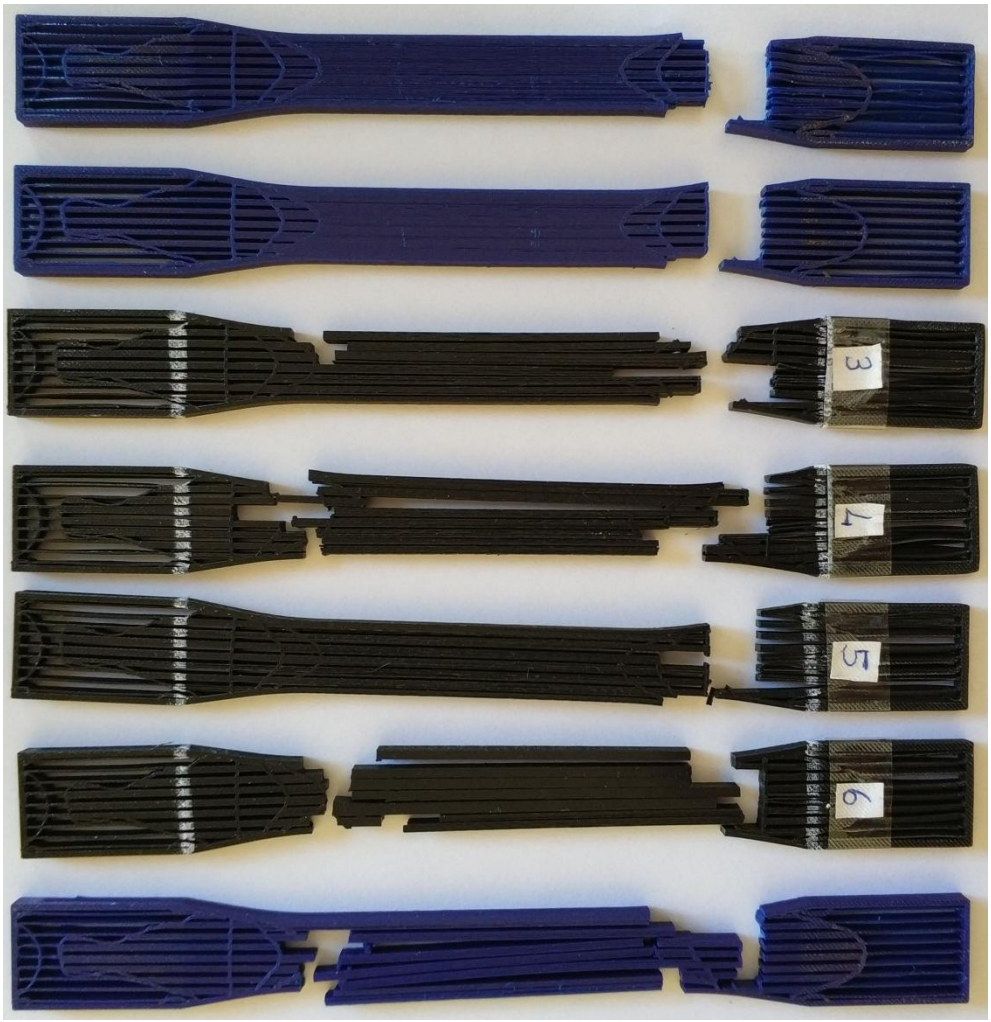


Figure 56: Failure modes of specimens with 70% stress modified infill density

When the failure modes are considered, it can be said that the results are rational and the proposed method can be used to strengthen the parts to be fabricated on open source 3D printers. Regarding the first trials of the method, Specimens 1 and 2 are constructed using the method and manufactured via a 3D printer. In the case of

these specimens, the regions where the maximum stress values exist, i.e., gage sections of the specimens, under tensile loading are fully filled as can be seen in Figure 56. That's why the failure occurs near the grip regions. Due to the fully filled interior, the gage sections are not the weakest regions for these specimens. After these observations are done, specimens are manufactured by removing one the last offset lines of the stress flow lines in the maximum stress regions. The specimens constructed with the updated method can be seen in the Figure 56, Specimens 3, 4, 5, 6 and 7. For this set, only the result of Specimen 5 is not good. The maximum load carrying capacity of this specimen is less than the others. The failure mode of it is not a good mode for tensile testing. However, it can be considered as valid because of the fact that the failure region is in between the grips. When the failure modes of the Specimens 3, 4, 6 and 7 are considered, it can be observed that the failure occurs on the gage sections as expected. From these results, it can be clearly said that the proposed manual method provides a strength improvement in the consideration of the linear elasticity theory.

The specimen set whose interior structures are constructed by using the automated method where the FEA step is embedded to the algorithm by using the Karamba3D®. 66.5% infill density is used for this set of specimens. There exist six specimens, one of these specimens has diagonal infill structure and the others have stress modified interior structure constructed by the automated method. The specimens in this set can be seen in below figure.

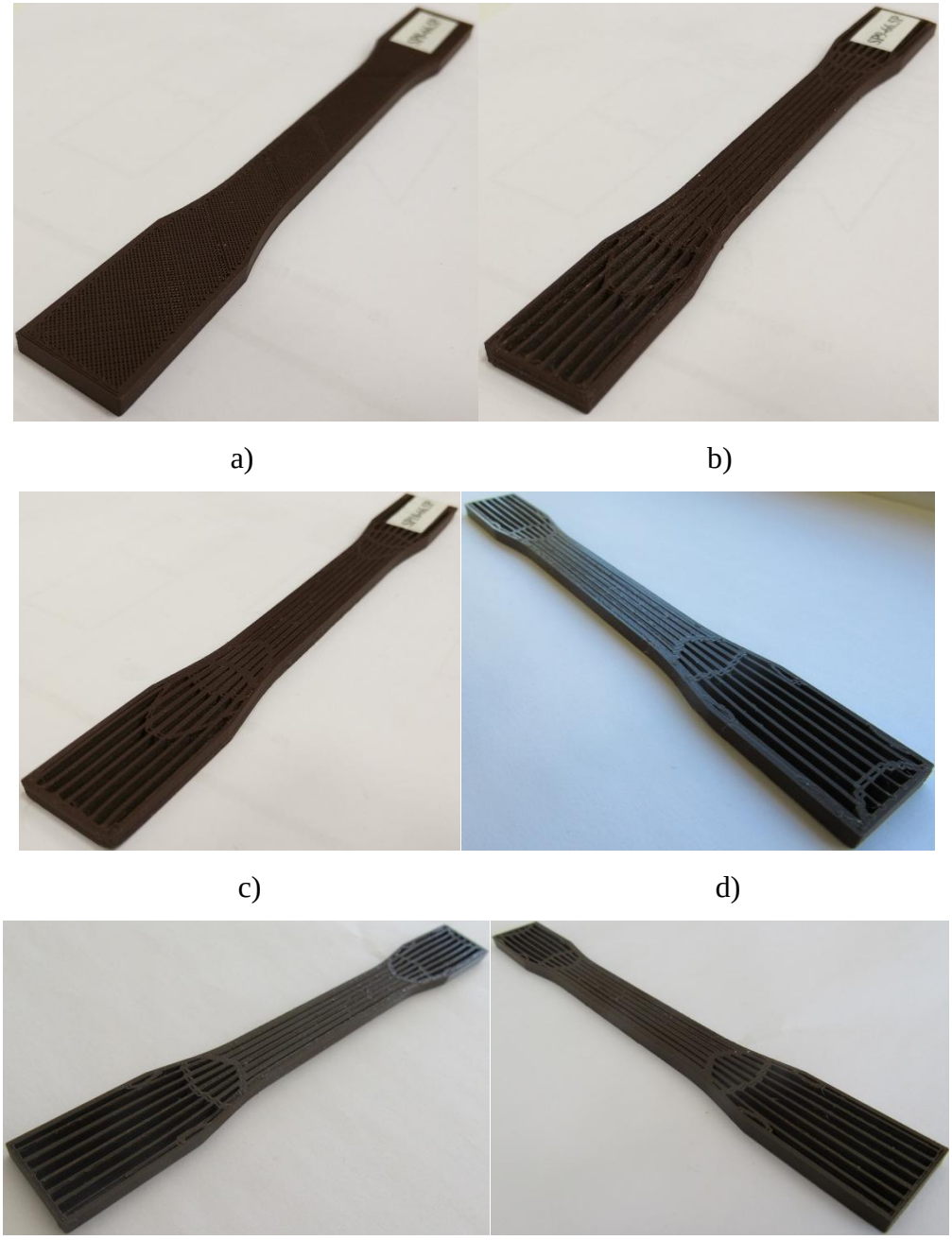

a) b)

c) d)

e) f)

Figure 57: ASTM D638 Type 1 specimens with 66% infill density a) diagonal infill structure b), c), d), e) and f) stress modified infill structure

The tensile test configuration for this specimen set is similar with the previous specimen sets. The tensile test results of these specimens can be seen in the table given below.

Table 11: Tensile tests results of the specimens whose interior structure is constructed by proposed automated method

| **Specimen #** | **Ultimate Load [N]** | **Ultimate Tensile Strength [MPa]** | **Extension at Ultimate Load [mm]** | **Infill Structure** |
|---|---|---|---|---|
| 1 | 737 | 14.20 | 5.003 | 66.5% Diagonal |
| 2 | 1008 | 19.00 | 1.329 | 66.5% stress modified |
| 3 | 1321 | 25.00 | 1.430 | 66.5% stress modified |
| 4 | 1011 | 18.90 | 1.200 | 66.5% stress modified |
| 5 | 1078 | 20.73 | 1.318 | 66.5% stress modified |
| 6 | 1080 | 20.77 | 2.887 | 66.5% stress modified |

The load vs. extension curves for these specimens can be seen in figure given below.

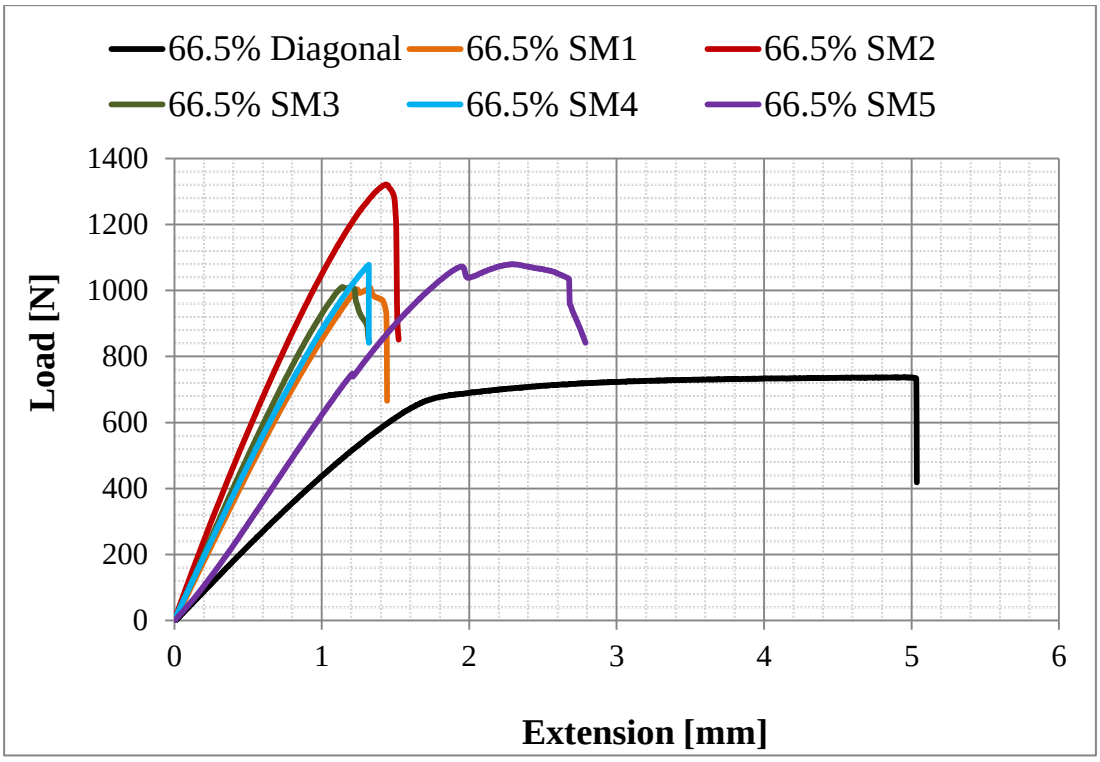


Figure 58: Load vs. extension plots of the specimens with 66.5% infill density stress-modified infill structure

When the load vs. extension curves are considered, the material behaves as ductile material only for the geometry with 66.5% diagonal infill structure. For other geometries with stress modified infill structures, it behaves as a brittle material. Similar with the geometries with stress modified infill structures constructed by using the manual method; these geometries have brittle material behavior. So, the methods like maximum principal stress theory can be used to further development of the method proposed in this thesis work.

From the tensile test results, it can be said that the maximum load carrying capacity for the stress modified structures is about 1100 N, which is 737 N for the specimen with diagonal infill structure. By using the stress modified infill structure constructed by the proposed automated method, 49.3% increase is obtained in the load carrying capacities of the ASTM D638 specimens. Besides, the average ultimate tensile strength is 21 MPa for the specimens with stress modified infill structures, which means 47.9% improvement in average for ultimate tensile strength values.

From the results, it can be said that the improvement in tensile load carrying capacity for maximum case is about 79% while it is 76% for ultimate strength values.

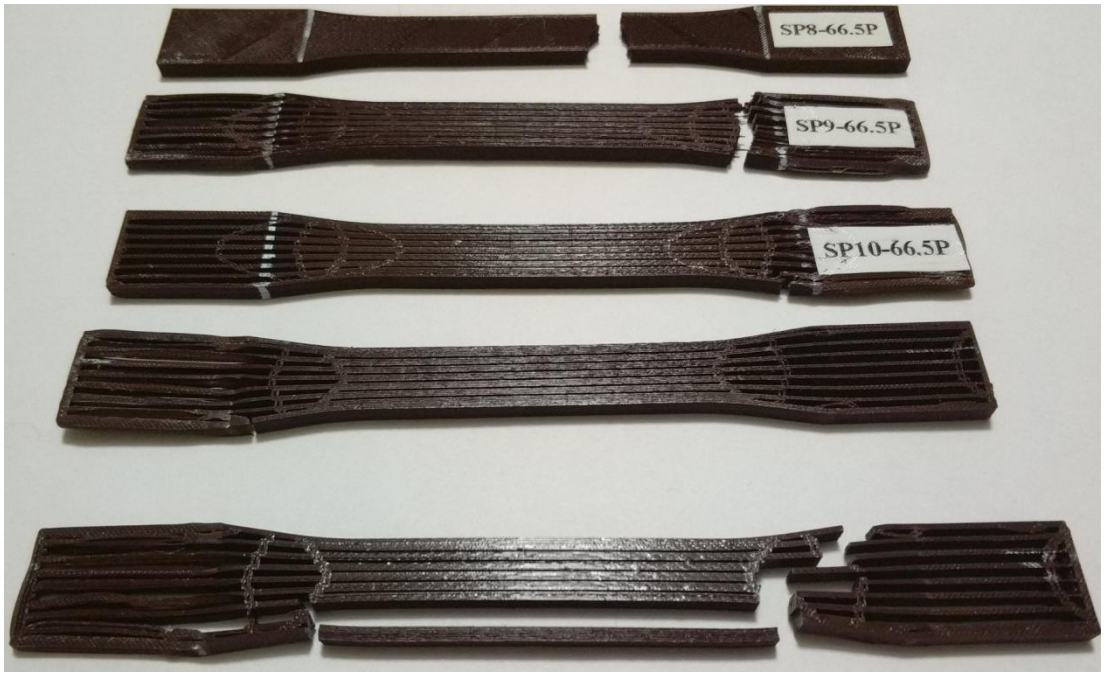


Figure 59: Failure modes of ASTM D638 Type 1 specimens with 66.5% stress modified infill structures constructed by using automated method

There are some issues observed from the failure modes of these specimens. Some of the specimens with stress modified infill structures have failures from the regions near the grip regions. These failure regions are valid but not preferable. However, it can be said that a significant improvement on load carrying capacity along with the ultimate tensile strength is obtained even by considering these results.

### 4.4 Discussion and Conclusion

In this chapter, all the tests performed for the development of the method and the effects of the proposed method on mechanical behaviors of the parts manufactured by using an open source 3D printer are considered. The sixteen specimens, which are fabricated by considering the ASTM D638 tensile testing standard for plastic materials, are exposed to tensile testing for the purpose of the

method development and verification. Because of the fact that it is defined for the molten and extruded plastic materials, the Type 1 specimen defined in the related test standards is used for the test cases.

Throughout the method development, the specimens with 20%, 40%, 70% and 100% infill densities and having linear and diagonal infill structures are considered. First of all, four specimens with 20% and 40% infill density with linear and diagonal infill structures are used to understand the effects of infill types and the densities on the mechanical behaviors of the specimens under tensile loading. These specimens are also used to be sure about the testing method. When the results of these specimens are considered, it is observed that the specimens with 40% density infill structures have greater strength value than the ones with 20% density infill as discussed in the literature. Besides, the specimens which have linear type infill structure carry more loads than the ones with diagonal infill. However, the diagonal infill structures have larger extension values than the linear infill type. In other words, the specimens with diagonal infill structures are more ductile than the ones with linear infill structures. There exist two specimens with 70% infill density. One of them has linear infill structure while the other has diagonal one. All the observations made for the tensile test results of the previous specimen set are valid for these two specimens. While the specimen with 70% linear infill structure carries higher loads, the one with 70% diagonal infill structure is more ductile. The specimens with 100% density infill are used to get the maximum load which can be carried by the specimens with standard homogeneous infill structures. Since the linear infill structure carries more loads than the diagonal one (observed from the results of the previous tensile tests and the results obtained in the literature), all the specimens with 100% infill density are manufactured by using linear infill type. There exist three specimens for 100% infill density case. When the results of the tensile tests of these specimens are considered, it can be clearly said that the load carried by the specimen is directly proportional with the specimen density.

70% infill density is used for the method development and verification of the ASTM D638 Type 1 specimens. There exist seven specimens fabricated using the method. First two specimens have an infill structure where the maximum stress

regions are fully filled. For other specimens, one of the offsets of the lines which connect the first principal stress direction vectors is removed on these regions. Because of the fully filled interior in the maximum stress regions, the specimen failure occurs near the grip regions. These results are not good for tensile tests. However, they are valid due to the failure occurs in the region between the grips. For other five specimens, failure occurs on the gage section directly. When the results of these specimens are considered, it can be clearly said that the maximum load capacities of the specimens constructed by the help of the proposed method are 28.2% larger than the ones with standard infill, in average. For the maximum cases, the load carrying capacity is increased by 49% for the specimens whose interior structures are constructed by using the proposed method. For the tensile strength values, the increase is about 26.8% in average and 52.6% in maximum cases. In other words, the specimens with 70% stress modified infill structures have larger tensile strengths than the ones with 70% linear infill.

When the load vs. extension curves are considered, it can be observed that the material behaves as a ductile material for some specimens with standard infill structures. However, it behaves like a brittle material for the geometries whose interior structure is constructed by using the proposed manual and automated methods. Actually, for failures of the brittle materials, other failure theories than Von Mises theory, such as Maximum Principle Stress Theory or Coulomb-Mohr theory should be used. For ASTM D638 type 1 geometries the stress field regions by considering Von Misses theory and the Maximum Principle Stress theory can be seen in below figure. These stress field regions were obtained by using Abaqus® FEA software.

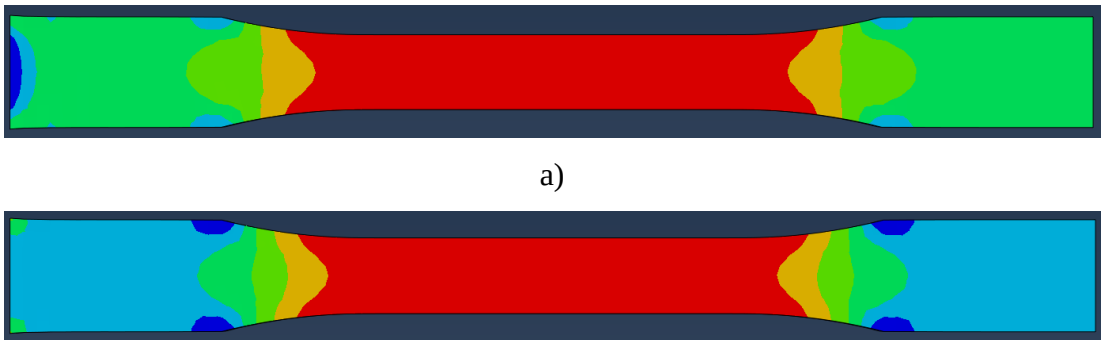

a)

b)

Figure 60: The stress field results obtained in Abaqus® FEA software by considering a) Von Mises theory and b) Maximum Principal Stress theory

When the above figure is examined, it can be said that the stress fields are similar visually. Also, because of the fact that the method is developed only for the tensile loadings, the stress values defined in the stress fields in same colors are also similar for these two methods. Thus, the developed method can be used for the geometries under tensile loading because, the loading considered is only tensile and the stress field results from the different theories are similar. Besides, this thesis study considers only the tensile loading of the specimens which makes the first principal stresses more effective. So, for these simple geometries, the obtained stress field results by considering the Von Mises theory and the Maximum Principle stress theory are very similar to each other. The obtained stress field results by considering these two failure theories in Karamba3D® can be seen in the below figure. In Karamba3D®, these fields are almost the same which can be observed in the given figure. So, the method can still be used for strength improvement issues. Moreover, in Karamba3D®, it is very easy to switch the failure theory considered to obtain the stress field results. So, this method can also be used for brittle materials. The switch option between the visualized stress field results can be seen in following figure.

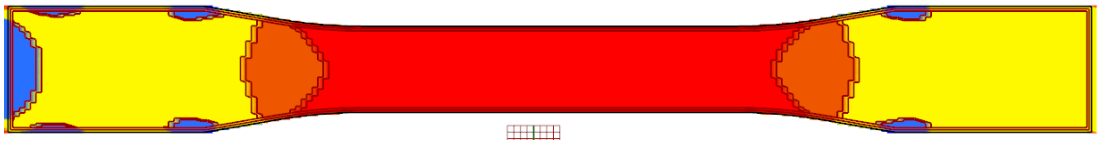

a)

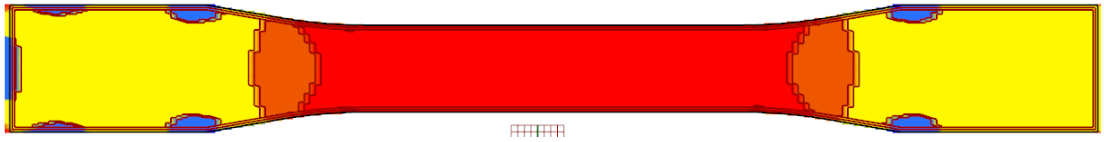

b)

Figure 61: The stress field results obtained by using a) Von Mises stresses and b) maximum principal stresses

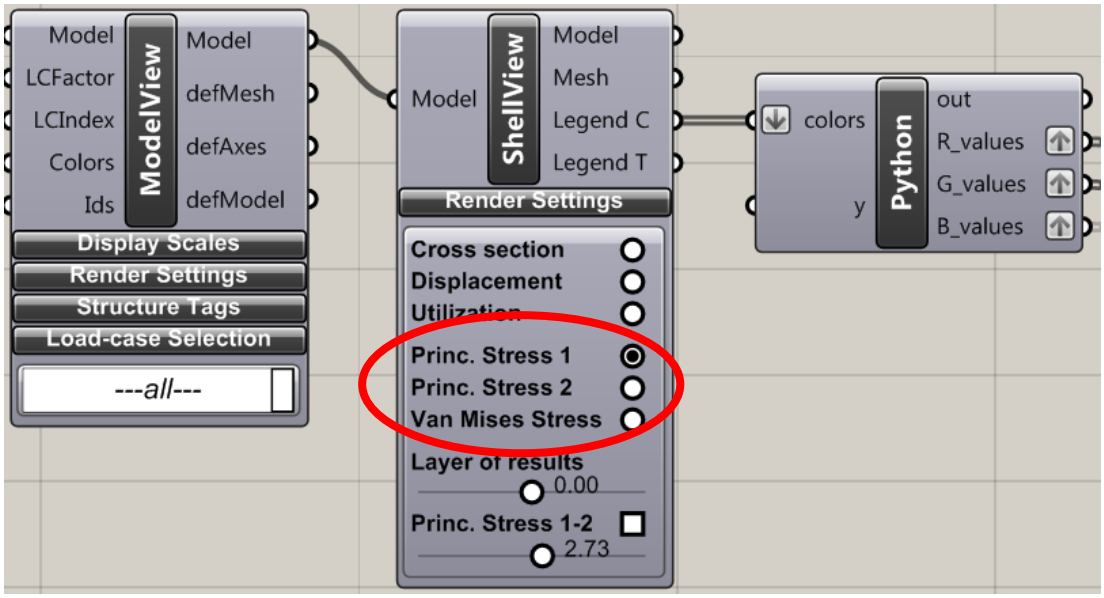


Figure 62: Switch option between the Von Mises stresses and the maximum principal stresses for stress field visualization

In conclusion, this thesis proposes a method which gives possibility to improve the mechanical behaviors of the specimens under tensile loading. By the help of the proposed method, more durable parts having same amount of material can be obtained. Besides, the method can be used for geometries constructed by using either ductile or brittle materials by changing the theory behind the visualized stress field results. In the following chapter, the applicability of this method to more complex geometries will be examined.

# CHAPTER 5

# APPLICATION OF THE METHOD TO DIFFERENT GEOMETRIES

## 5.1 Introduction

Up to now, the method which gives possibility to improve the durability of 3D printed parts is developed and verified by using the ASTM D638 Type 1 specimens. It can be obviously said that the proposed method can be used to improve the mechanical behavior of 3D printed parts.

In this chapter, the developed method is used for different types of 2.5D geometries. By applying the method to more complex geometries, it is aimed to show that the method is also valid for different geometries.

Throughout the chapter, the geometries are firstly defined. Then, application of the method to these geometries is explained in details. Later, the resultant geometries with stress modified infill structures are addressed. After all these steps are done, the tensile tests performed by using these specimens are explained. Finally, a brief conclusion is made about the contribution of the method to the strength of the specimens.

## 5.2 Application of the method to different geometries

For the method development case, the specimens designed by considering the ASTM D638 tensile test standard defined for plastics are used. The interiors of these specimens are modified by using the proposed method. Then, the resultant specimens are manufactured with an open source 3D printer. To develop and verify the validity of the method, tensile tests are performed according to the related standard explained in details in Chapter 3 and Chapter 4.

In this chapter, three types of specimens having more complex geometries than ASTM D638 Type 1 geometry are chosen to show the validity of the proposed method. The used geometries are named as rectangle with necks, rectangle with slot and s-shaped. These geometries can be considered as sets in their own.

As a first set, a custom part having necks on both sides is designed. The details of this geometry can be seen in Figure 63. Its sizes are adjusted according to the building area of the 3D printer.

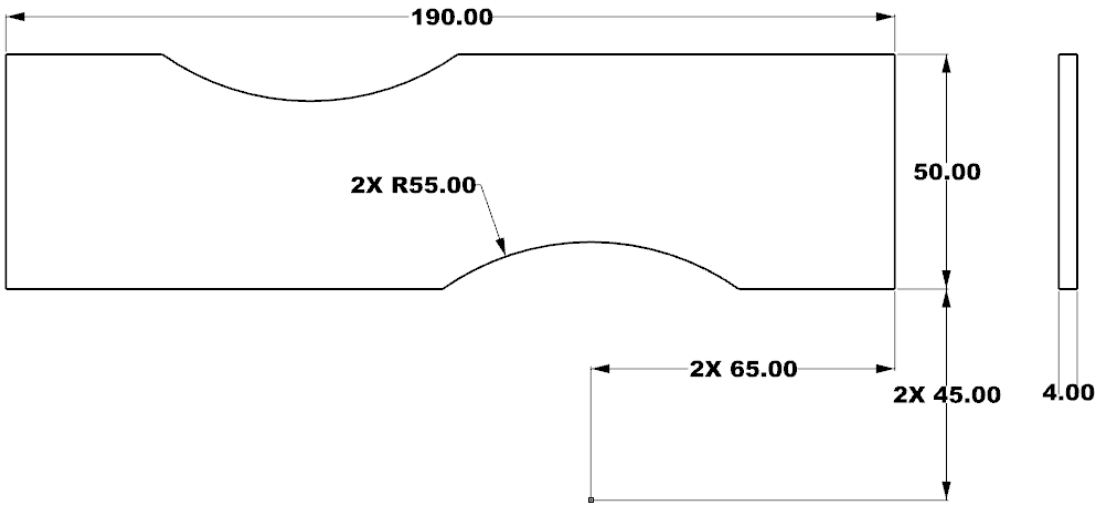


Figure 63: Details of the rectangle with necks geometry (All dimensions are in mm)

The geometry is the only input for the method. The support points are detected by the method automatically. The left most edge is used to apply the fixed boundary and the right-most edge is the boundary for the load application. Since only the stress field regions and the stress flow lines are important for the method, the applied load value is set to 1000 N. The stress field results and the geometry with stress modified infill structure can be seen in Figure 64.

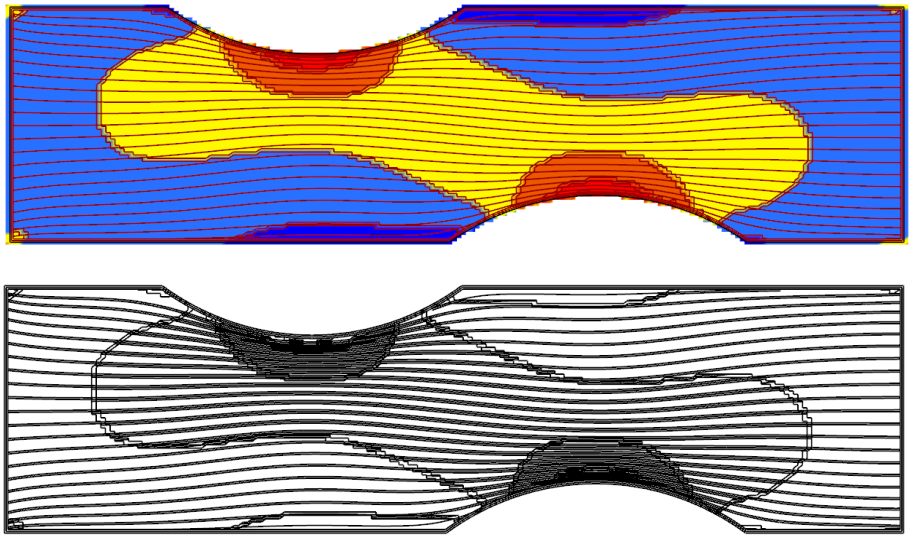

Figure 64: Stress field results obtained in Karamba3D® (Top) and stress modified infill structure (Bottom)

After geometry design and the FEA steps are done, the G-code file obtained from the method is supplied to the 3D printer to manufacture the constructed geometry. There exist five geometries manufactured for this set. First two geometries have linear and diagonal infill structures constructed by using the standard infill in the CAM software. Since the infill density of the geometry constructed by using the method is 58%, all the geometries are manufactured by using the same infill density for this set. The other specimens of this set have stress modified infill structures. The manufactured specimens which are exposed to the tensile tests can be seen in Figure 65.


Figure 65: Specimens used for tensile tests. From top to bottom; 58% linear infill, 58% diagonal infill and specimens with 58% stress modified infill structures

As a second set, rectangle geometry with a slot located in the center of the geometry is used. This geometry is used to observe the performance of the method for the geometries with holes or slots. The specimens are named as rectangle with slot. The dimensions of the geometry are determined again randomly. The details of the geometry can be seen in Figure 66.

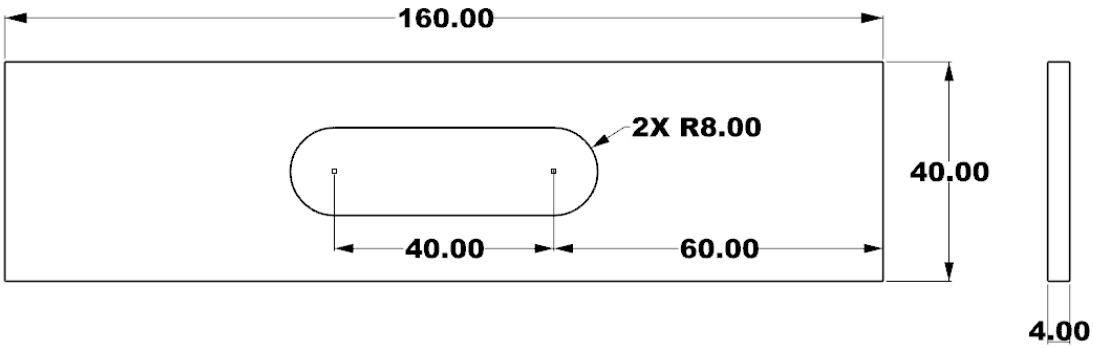


Figure 66: Details of the rectangle with slot specimen (All dimensions are in mm)

For this set, the geometry defined above is given as input to the method to obtain the geometry with stress modified infill structure. The density of the infill for this specimen is also 58%. The obtained stress field region results and the interior structure modified by using these results can be seen in Figure 67.

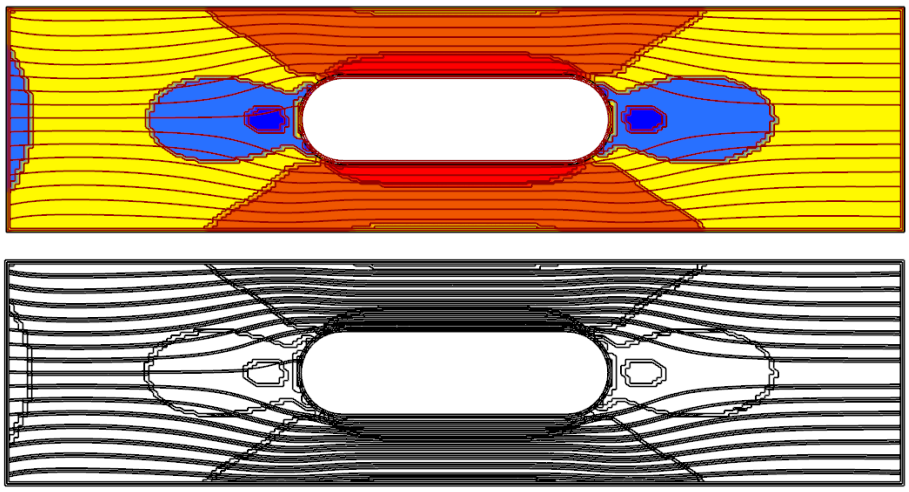

Figure 67: The stress field results obtained in Karamba3D® (top) and the constructed interior using the method for the rectangle with slot specimen (bottom)

Similarly, the G-code file is obtained from the method to be transferred to the 3D printer. There exist three specimens for this set. One of them have 58% linear infill structure, one of them have 58% diagonal infill structure and the last one has 58% stress modified infill structure. The manufactured geometries can be seen in Figure 68.


Figure 68: Rectangle with slot specimens with 58% infill density from top to bottom: linear, diagonal and stress modified

The names of the specimens seen on the stickers in the figures are different because these specimens are tested at different times. So, they are named differently.

As a final set, an s-shaped specimen is used. This design can be considered as more complex in terms of stress flow directions under tensile loading. Similar to the other test parts, the dimensions are determined randomly. The details of the geometry can be seen in Figure 69.

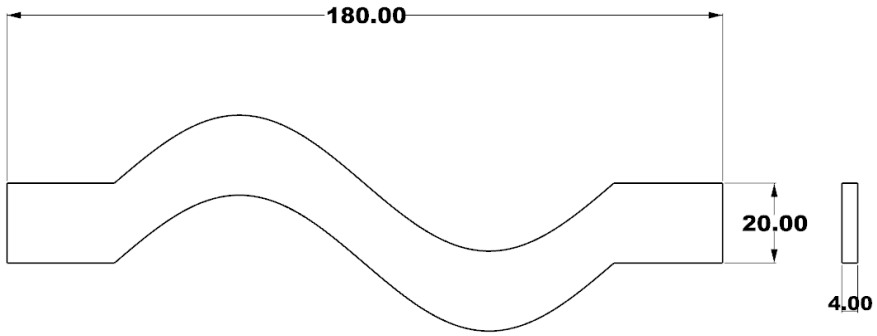


Figure 69: The details of the s-shaped specimen (All dimensions are in mm)

The s-like shape of this geometry is constructed by using a sine function defined in the Grasshopper3D®. The function blocks can be found in the below figure.

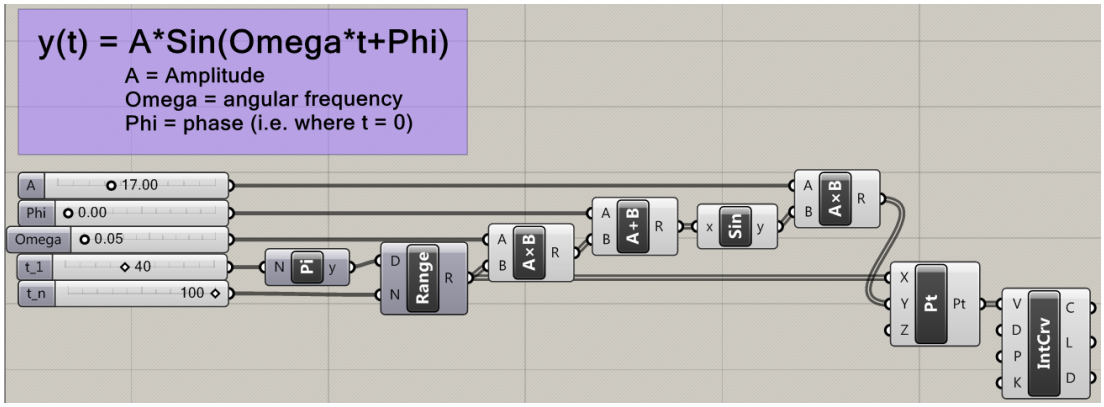


Figure 70: Block functions used to construct the s-shaped geometry

The gage section of the specimen, i.e., s-shaped region is drawn by using the sinusoidal function. For this specimen, the stress field results and the constructed geometry with modified interior can be seen in Figure 71.

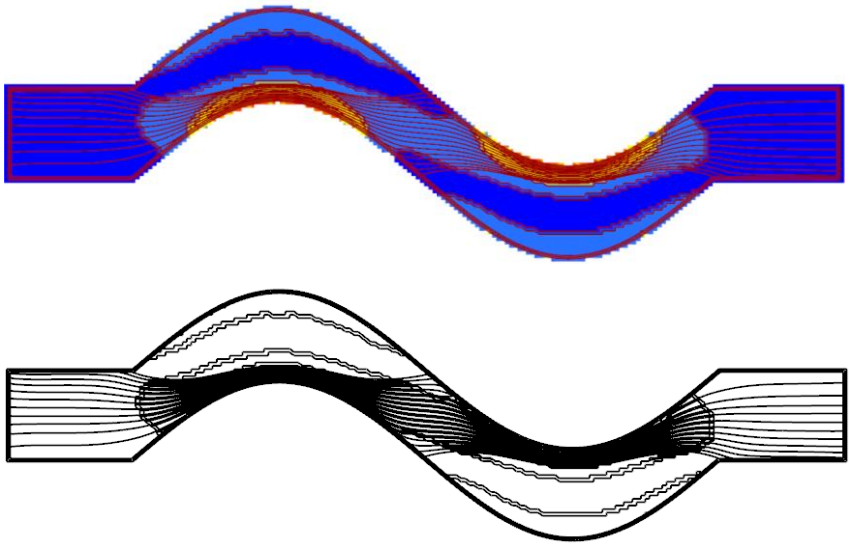

Figure 71: The stress field results obtained in Karamba3D® (top) and the constructed infill geometry for s-shaped specimen (bottom)

There exist five specimens manufactured for this set. The first one is manufactured with 100% infill density. The second and the third ones are manufactured by using 58% linear and 25% diagonal infill densities, respectively. The last two specimens are manufactured with 58% infill density with stress modified structure. These specimens manufactured for this set can be seen in Figure 72.

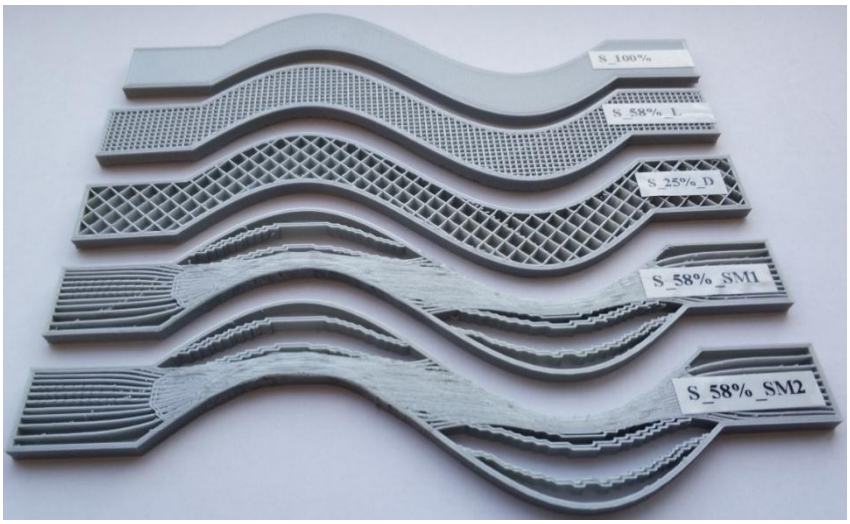


Figure 72: The s-shaped specimens with 100%, 58% linear, 25%diagonal, 58% stress modified and again 58% stress modified (from top to bottom) infill structures

All these sets of specimens are exposed to the tensile tests to verify the validity of the method for these kinds of specimens. The details of the test performances can be found in the next topic.

### 5.3 Test Performances of Different Geometries

To prove the validity of the method for more complex geometries, again tensile tests are performed for the 3D printed parts under the same specified loading. As for ASTM D638 Type 1 specimen, tests are conducted by Instron 8802 Servohydraulic Fatigue testing machine by considering the ASTM D638 tensile testing standard. The aim of the tests is to prove the validity of the method on complex parts' strength and load carrying capacity improvement.

As a first set, the artifacts named as “rectangular with neck” are considered. As previously mentioned, there exist five specimens; two of these geometries have linear and diagonal infill structures, which are used as reference geometry for the comparison. The other three have stress modified infill structures obtained by using the proposed method. All of the geometries have 58% density infill structure. The details of the geometries can be found in previous topic.

Tensile tests are performed for these specimens at specified test speeds given in ASTM-D638 testing standard. The test configurations of all these specimens are similar. Thus, it is enough to show one of the test configuration, which can be seen in Figure 73. The results obtained from the tensile tests are summarized in Table 12.

Figure 73: Tensile test configuration of the rectangle with neck specimen with 58% infill density having diagonal structure

Table 12: Tensile test results of the specimens with 70% stress modified infill structure

| Specimen # | Ultimate Load [N] | Extension at Ultimate Load [mm] | Mass [g] | Max Load / Weight Ratio [N/N] | Infill Structure |
|---|---|---|---|---|---|
| 1 | 1674 | 1.50 | 21.35 | 7.99 | 58% Linear |
| 2 | 1214 | 3.77 | 21.33 | 5.80 | 58% Diagonal |
| 3 | 3036 | 2.11 | 20.59 | 15.03 | 58% Stress modified |
| 4 | 2039 | 1.99 | 17.16 | 12.11 | 58% Stress modified |
| 5 | 2517 | 1.92 | 18.92 | 13.56 | 58% Stress modified |

The load vs. extension data for rectangle with necks geometries with 58% infill density can be seen in below figure.

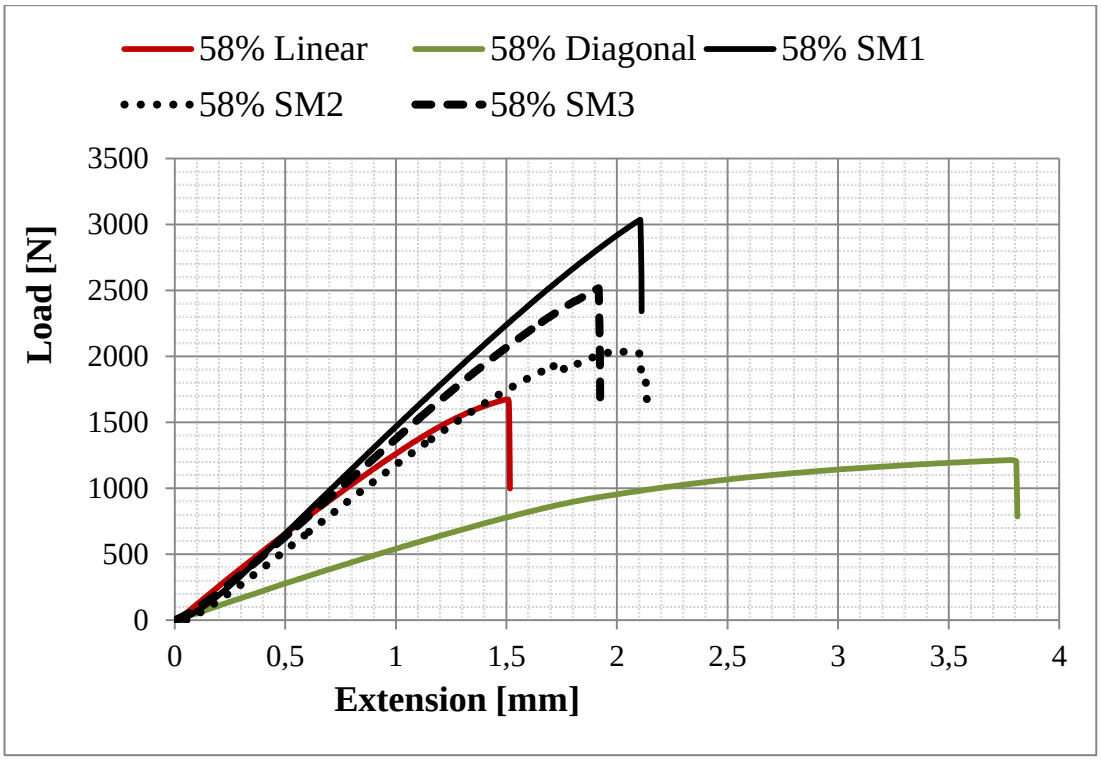


Figure 74: Load vs. extension plots of rectangle with necks specimens with 58% infill density

When the above load vs. extension curves are examined it can be said that the PLA material has ductile behavior for the geometry with diagonal infill. It behaves as brittle for other geometries, although the stress field results are obtained by considering the Von Mises theory which is generally used for ductile materials throughout the method development. Even if the Von Mises theory is used for the method, it can still be used for our case because only the tensile loading is considered which makes the first principal stresses are more effective. So, the Von Mises stresses are nearly equal to principal stress values for this plane stress case. Besides, two FEAs are performed in Abaqus® for the rectangle with necks geometry. One is performed by considering the Von Mises theory and the other is performed by using the maximum principal stress theory. The results can be seen in following figures.

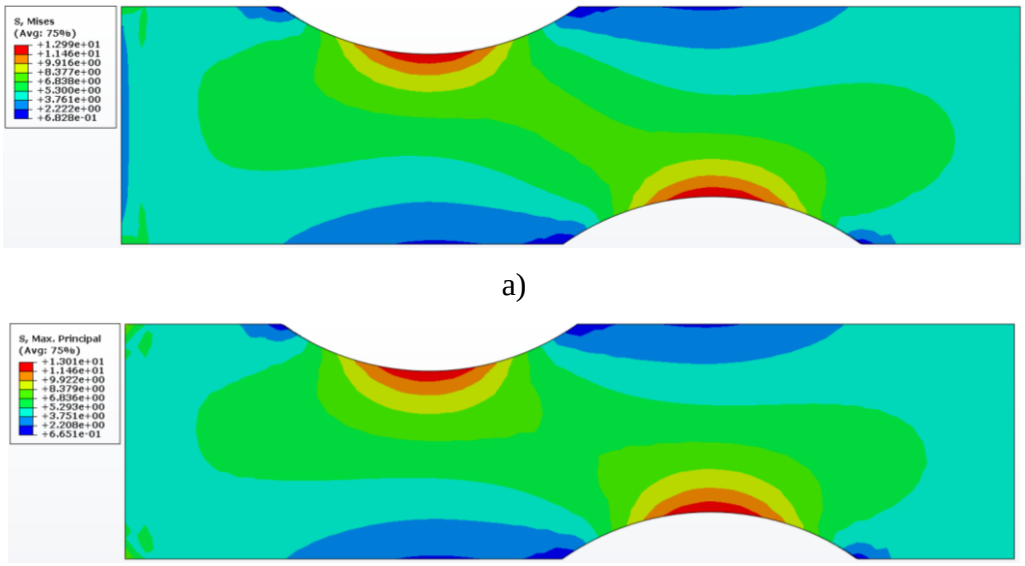


Figure 75: Stress field results obtained in Abaqus® FEA software by considering a) Von Mises theory and b) maximum principal stress theory

When the above figures are examined, it can be obviously said that the obtained stress field results are very similar, visually. Furthermore, these stress field results are very similar with ones obtained in Karamba3D® by considering the Von Mises failure theory. Because of that only the stress field regions' boundaries are used to modify and construct the interior structure of the geometries, this method can still be used for the strength improvement works. Moreover, the maximum stress values which define the colored stress regions are very similar for two of the stress field results in b)

Figure 75. The method can also be adjusted for ductile or brittle material by switching the theory behind the stress field results. Both the Von Mises stress field results and maximum principal stress field results can be visualized in Karamba3D®.

As a result of the tensile tests, as expected, even if they have the same infill density, the load carrying capacities of the specimens are different. Specimen 1 (SP 1) has the linear infill density structure. It fails at 1674 N load while it has 1.5 mm elongation at the ultimate point. However, SP2 which has diagonal infill structure fails at 1214 N load; its elongation is 3.77mm at ultimate point, which is larger than SP 1. This is rational according to theory of elasticity [10]. In theory, while the linear

structures carry more load, they elongate less the than diagonal structures. Furthermore, it can be inferred from the table that SP3 has the maximum load carrying capacity. All the specimens with stress modified infill structure constructed using the proposed method have higher load carrying capacities than the specimens with standard infill structures. SP3 has 81.36% higher load carrying capacity than the one with linear infill. SP4 and SP5 also have 21.82% and 50.36% higher load carrying capacities, respectively. As an average, the specimens with stress modified infill structures have 51.17% higher load carrying capacity than a standard specimen with linear infill structure. When the results of the tests are examined, it can be seen that the load carrying capacities of the specimens with stress modified infill fluctuate significantly. The reason behind this fact is the weights of the specimens. As a result of the tests, the artifacts with stress modified infill structures have larger load carrying capacity/weight ratio.

The failure modes can be seen in Figure 76 provided below.

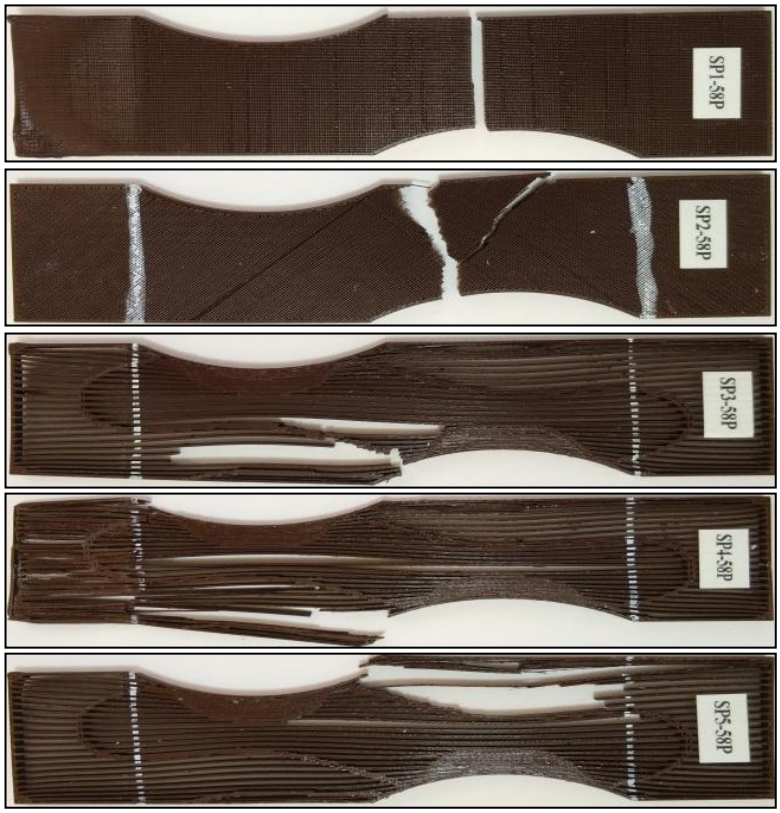


Figure 76: Failure modes for specimens with; 58% linear infill; 58% diagonal infill; 58% stress modified infill for last three

It can be obviously said that the test results are reliable when the failure modes are considered. The specimen with linear infill structure has pure tension failure while the specimen with diagonal infill structure has pure shear failure as expected. Although there is no complete separation into two parts for the specimens with modified interior structure, failure occurs near the neck regions where the maximum stress occurs.

As a second set, rectangular shape specimens are used again. However, the specimens have slot shapes at the center of the artifacts. These specimens are named as rectangular with slot. There exist three test specimens manufactured for this set. One of the artifacts has 58% density linear infill structure. Besides, other has 58% diagonal infill structure. The final one has 58% stress modified interior structure. As previous ones, this final specimen's interior is modified by using the proposed method. All these three specimens can be seen in the figures given in the previous topic.

Tensile tests of this set are also performed by considering the ASTM D638 tensile testing standard although the specimens of this set are not the standard ones. All the specimens are exposed the tensile testing in similar configuration. One of these test configurations can be seen in Figure 77.

Figure 77: Test configuration for the rectangular with slot specimens

The specimens of this set are exposed to tensile tests by using the same tensile testing machine. The obtained results from the tensile tests are summarized in Table 13.

Table 13: Tensile test results of rectangle with slot specimens

| Specimen # | Ultimate Load [N] | Extension at Ultimate Load [mm] | Mass [g] | Max Load / Weight Ratio [N/N] | Infill Structure |
|---|---|---|---|---|---|
| 1 | 1165 | 1.66 | 12.00 | 9.90 | 58% Linear |
| 2 | 616 | 1.53 | 11.56 | 5.43 | 58% Diagonal |
| 3 | 3355 | 1.56 | 19.24 | 17.78 | 58% Stress modified |

The load vs. extension plots of these specimens can be seen in below figure.

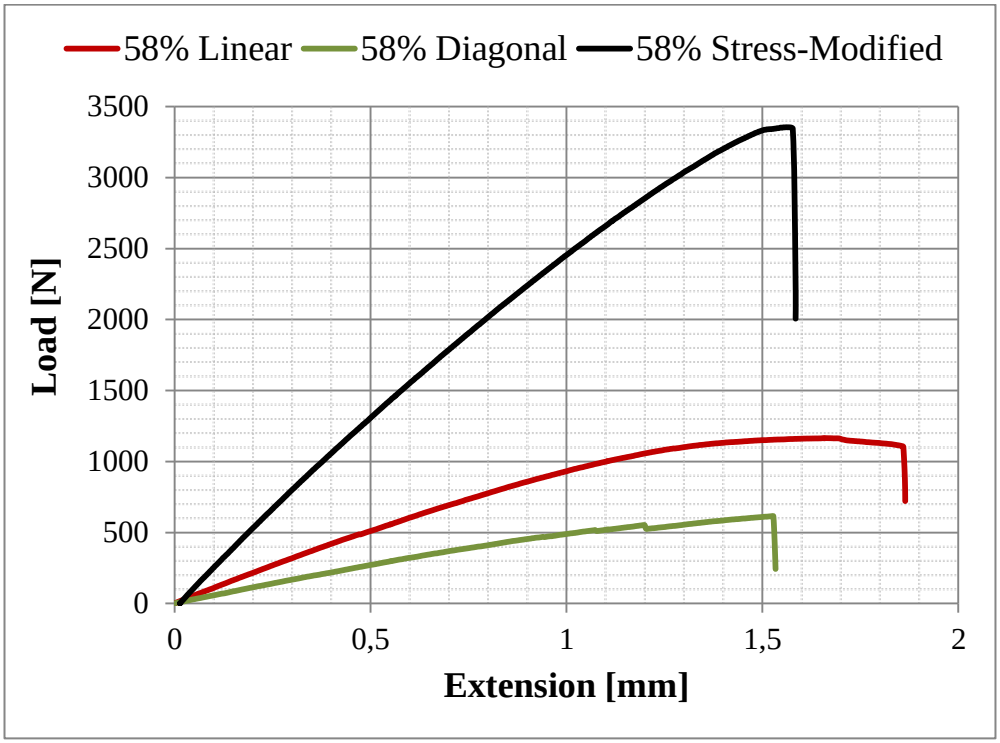


Figure 78: Load vs. extension plots of rectangle with slot specimens

From the load vs. extension plot, it can be observed that the material behaves as brittle for the geometry with stress modified infill structure obtained by using the proposed methodology like rectangle with necks geometries. However, ductile behavior is observed for the geometry with linear infill structure. Similar to previous case performed for rectangle with neck geometries, the method can also be used for strength improvement considerations for slotted geometries under tensile loading. Two FEAs are also performed for this set by considering both Von Mises theory and the maximum principal stress theory in Abaqus® FEA software. The obtained stress field results can be seen in following figures. When the figures are considered, it is obvious that the stress field results are very similar to each other. Because of that only the stress field regions' boundaries are used to construct the stress modified infill structure, the method can be used for the geometries with slot-like interior details.

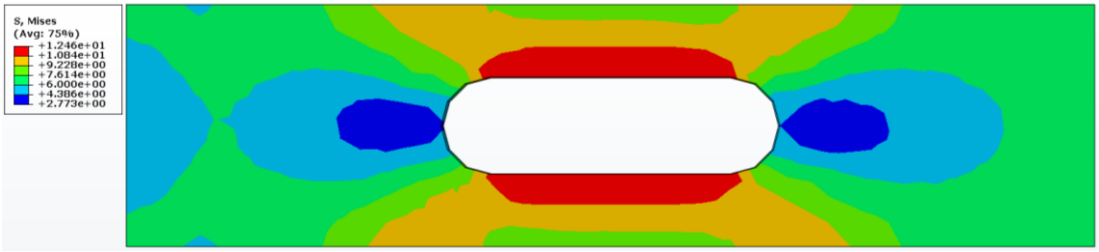


a)

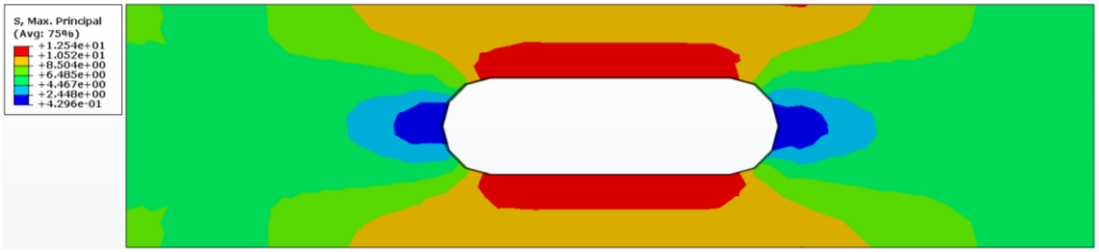


b)

Figure 79: Stress field results obtained in Abaqus® FEA sotware for rectangle with slot geometries by considering a) Von Mises theory and b) maximum principal stress theory

Besides, the stress values obtained for the colored regions are also very similar to each other for these two stress fields which makes the usage of the proposed methodology reasonable.

When the results of the tensile tests are considered, it can be seen that the method proposes a way to improve the mechanical behavior of the parts under tensile loading. Among the first two specimens, the first specimen which has 58% linear infill structure has the largest load carrying capacity and the largest ratio of the maximum load per weight. However, the extension value of this specimen is surprising. It also has the largest extension value. For this set of specimens, as similar with the previous ones, the largest load is carried by the specimen with stress modified infill. About 187% increase in the load capacity is obtained for this specimen. Actually, it is better to consider the maximum load per weight ratio. Although the density values for the specimens are the same, there are differences between the masses of the specimens. This can be due to the printing quality of the specimen. This can also result from the fact that the different color filaments are used for manufacturing processes for these specimens, which can be seen in Figure 68 given in the previous topic. In the case of maximum carried load per weight ratio, nearly 79.6% increase is obtained also for the specimen with stress modified interior.

For method verification, the failure modes of the specimens are also a significant issue. The failure modes resulting from the tensile tests of these specimens can be seen in Figure 80.

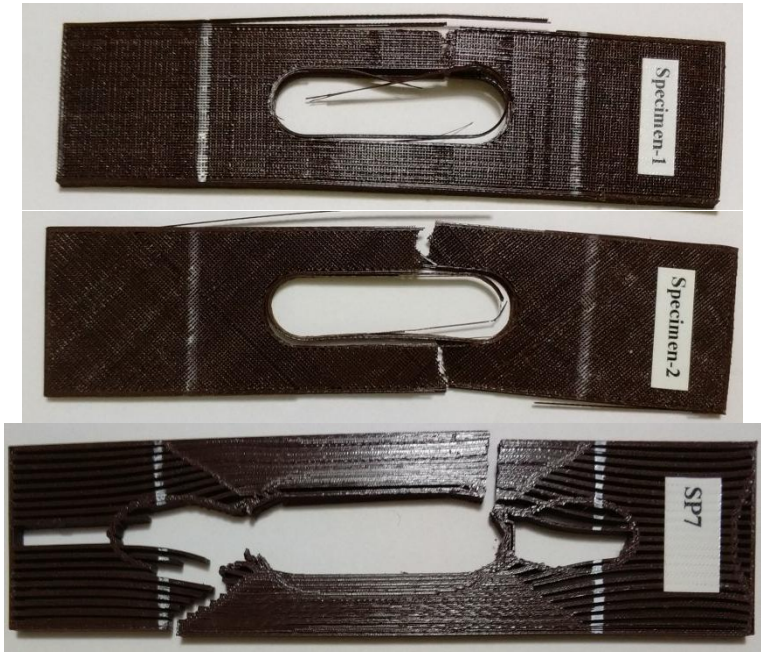


Figure 80: The rectangle with slot specimens with infill types: 58% linear, 58% diagonal and 58% stress

From the failure modes of the specimens, it can be said that the failure occurs near the maximum stress regions. The specimen with linear infill type has pure tension failure mode and the specimen with diagonal infill type has pure shear failure type which can be seen in Figure 80.

The last test specimen set has also five specimens. One of these specimens has 100% infill density which means the specimen is manufactured as fully filled. One of them has 25% diagonal infill structure and one has 58% linear infill structure which is used to compare the results of the other 58% density infill specimens. The last two have 58% stress modified interior structures. The specimens are named as S-shaped specimens. These specimens are also random design specimens. The details about them can be seen in Figure 69given in the previous topics.

All the specimens of this set have similar test configurations constructed according to ASTM D638 tensile test standard. One example of the configurations can be seen in Figure 81.

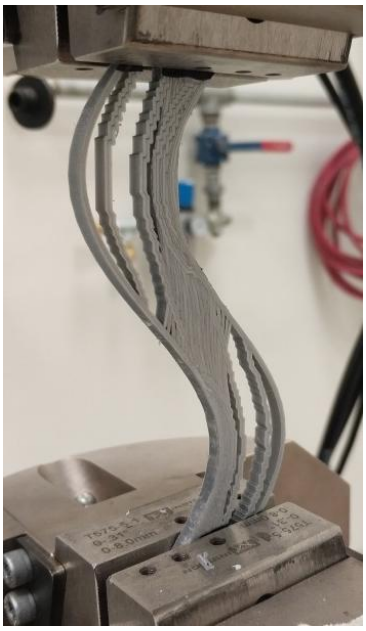

Figure 81: Tensile test configuration for s-shaped specimens

For this specimen set, again, the same tensile testing machine is used. The results obtained from the tensile tests are given in

Table 14.

Table 14: Tensile test results of the S-shaped specimens

| **Specimen #** | **Ultimate Load [N]** | **Extension at Ultimate Load [mm]** | **Mass [g]** | **Max Load / Weight Ratio [N/N]** | **Infill Structure** |
|---|---|---|---|---|---|
| 1 | 84 | 5.24 | 6.05 | 1.56 | 25% Linear |
| 2 | 311 | 1.49 | 10.78 | 2.94 | 58% Linear |
| 3 | 1079 | 2.89 | 17.99 | 6.11 | 100% |
| 4 | 530 | 3.06 | 9.53 | 5.66 | 58% Stress modified |

| | | | | | |
|---|---|---|---|---|---|
| 5 | 525 | 2.72 | 9.57 | 5.59 | 58% Stress modified |

The load vs. extension curves of these specimens can be seen in below figure.

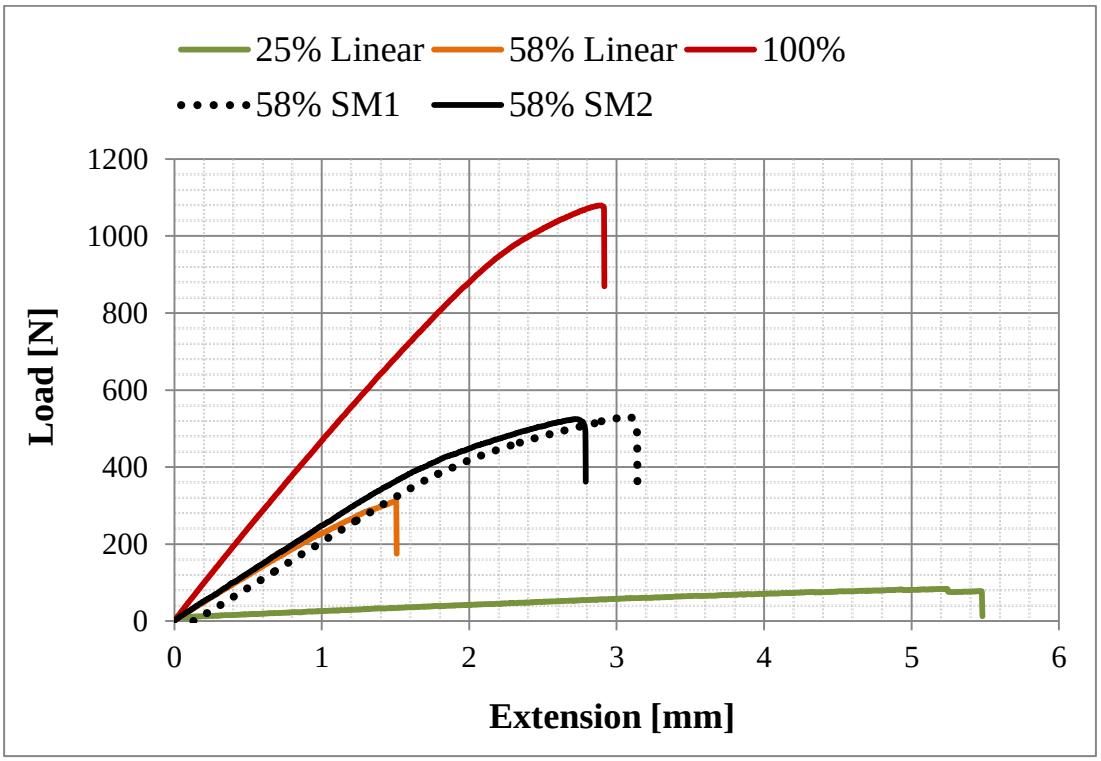


Figure 82: Load vs. extension plots for S-shaped geometries with 58% infill density

When the load vs. extension plots of the s-shaped geometries are examined, it can be clearly said that the PLA material behaves as brittle material for these geometries. Similar results are also valid for the s-shaped geometries. As in the case of rectangle with necks and rectangle with slot geometries, the stress field results obtained by considering the Von Mises theory, which is used for ductile material failures, and the maximum principal stress theory, which is used for brittle material failure.

It can be inferred from the test results that the proposed method can also be utilized to improve the mechanical behavior of s-shaped specimens under tensile loading. For the maximum load carrying part, the method provides about 69.6% increase. The specimens with stress modified infill structures have about 91.32%

larger maximum load carrying capacity per weight ratio. There exist again differences in the mass values of the specimens with same infill density. The failure modes of the specimens can be seen in Figure 83.

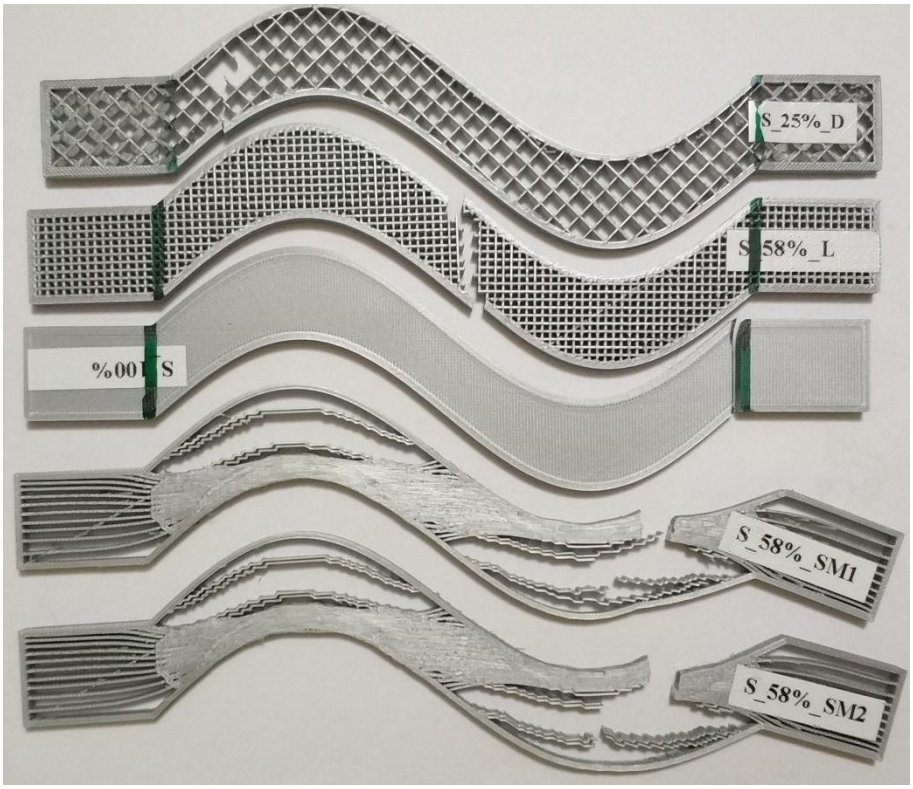


Figure 83: Failure modes of s-shaped specimens

Except for s-shaped specimen with 100% infill, other results are valid for these set. The failure occurs at the end of the grip section which makes the result invalid. When the other specimens are examined, it can be seen that the failure occurs at the regions where the maximum stress occurs for the specimens with stress modified infill in contrast with the other specimens with standard infill structures.

### 5.4 Discussion and Conclusion

Throughout the chapter, the specimens which are not the standard test specimens are used to observe the effects of the method on the mechanical behaviors under tensile loadings. Since these specimens are not standard specimens, the

extensometer used for ASTM D638 Type 1 specimens cannot be used for non-standard ones. For these test cases, the maximum carrying load per weight ratio is also considered since the weights of the specimens with the same density values are different. In theory, the masses of the specimens with the same infill density should be the same. However for our cases, the differences in the mass values can result from many parameters such as room temperature, alignment of the building plate, temperature of the nozzle, printing speed, deadlocks in the nozzle head, etc. Room temperature affects the viscosity of the material from nozzle head which can affect the amount of material extruded through the nozzle. Also, the nozzle temperature affects the extruded material amount. There can be some particles which blocks the material flow through the nozzle. Moreover, some excess material exists in the geometry where the geometry is printed with higher speeds. So, this situation increases the mass value of it. The accuracy of the printing can also affect the material in terms of dimensional accuracy. The final dimensions of the same specimens are different in small amount so, the masses should be different for this case. The alignment of the building plate can also affect the mass values. If there is some misalignment in the building plate, some excess material can bond the geometry at unwanted regions. So, this can increase the mass. Also, some material can be removed by the nozzle head due to misalignment which decreases the mass. Moreover, building plate temperature can affect the mass values of the artifacts. In some printed specimens, there exist some warpage which results from the improper building plate temperature. This causes again that the nozzle head removes some material from warpage regions. Besides, the environmental conditions for material affect the mass. For some specimens, the used material is affected by the moisture due to long time usage. So, the moisture affects the material quality which also affects the mass of the printed specimen. To prevent the mass differences of the same geometries with the same infill density values, maximum load per weight ratios are used to make the comparisons.

There are five specimens which are named as rectangle with necks specimens for the first set. In this set, the consideration is the stress regions near the neck details of the geometry. The specimen dimensions are determined with the consideration of

the dimensions of the building plate of the 3D printer. After the design stage is completed, the interior structure of the geometries is modified using the Von Misses stress field results obtained from a FEA performed by Karamba3D®. Moreover, the stress flow lines are used to construct the toolpaths for AM process. Then, the manufactured specimens are tested with tension loads to observe the effects of the method. From the results, it is observed that the method gives about 51% increase in the load carrying capacity of this set. It also results in 59.8% improvement on the maximum load capacity per weight ratio.

As a second set, the specimens named as rectangle with slot are used to observe the effect of the method on slotted geometries. There exist five specimens for this set. Two of them have 58% linear infill structure, other two have 58% diagonal infill structure and the last one has 58% stress modified infill structure. These specimens are also processed with the proposed method and are exposed to tensile testing. As a result of the tests, the method offers about 187.98% increase in maximum load carried. It also improves the maximum carrying load per weight ratio as 79.6%.

The s-shaped specimens are used as a last set which includes also five specimens, whose infill structures are 100% infill, 25% diagonal infill, 58% linear infill and two 58% stress modified infill. These specimens are considered to observe the effect of the method on mechanical behaviors of curved specimens. After the method is employed, these specimens are also exposed to tensile testing. From the results, it is observed that the method gives about 69.6% strength increase under tensile loading. The maximum load carrying per weight ratio is increased by 91.32% when the method is utilized.

While PLA material is considered as ductile material, the failure modes of all the geometries with stress modified infill structures constructed by using the proposed method show that the material behaves as brittle material for these complex geometries. However, Von Misses theory is used for the FEAs, which is generally used for the ductile material failure. Although Von Mises theory is considered throughout the method, the proposed methodology can still be used for strength improvement considerations. Because of that only the tensile loads are considered,

the effective stresses are the first principal stresses for the geometries. For the plane stress case which is also valid for my case, Von Misses stresses are nearly equal to first principal stresses. Moreover, the stress field results obtained in Abaqus® FEA software by considering both of the specified failure theories are very similar to each other. Because of all these reasons, the proposed method can still be used to improve the strength properties of the geometries under tensile loadings. Besides, the failure theory considered behind the FEAs can be easily switched between the Von Mises results and the maximum principal stress field results in Karamba3D®. Because of that, this proposed method can be used for geometries manufactured by using both the ductile and the brittle materials.

In conclusion, it is verified that the method can be used also for more complex geometries than the standard tensile test specimens. By using the method, the maximum load carried by the specimens under tensile loading can be improved in the range from 51% to 187% for the specimens used through this chapter. Besides, the maximum carried load per weight ratio can be increased to the range from 59.6% to 91.3 %. For 2.5D complex geometries, the proposed method gives an opportunity to improve the mechanical behavior of the parts under tensile loadings.

# CHAPTER 6

# CONCLUSIONS

## 6.1 General Conclusions

In this thesis study, a new design and fabrication pipeline for FFF 3D printers is proposed, which let us improve the strength of the additively manufactured objects. The method describes a new automatic fabrication pipeline for the open source FFF 3D printers starting from the design stage to G-code file generation. It directly slices the models by considering the quasi-static FEA results of the parts under the tensile loading conditions in order to construct the interior structure i.e., infill pattern of the artifacts. Although the traditional CAM software of the 3D printers constructs homogenous infill structures by using linear, diagonal, honeycomb, etc. shaped interiors; the proposed method gives an opportunity to construct heterogeneous interior structures by considering the results of FEAs, which simply improves the durability of the 3D printed parts.

Throughout the work a standard tensile test geometry which is described in the ASTM-D638 standard is used with the non-standard random geometries. ASTM D638 is a tensile test standard defined for the specimens manufactured by using plastic materials. Type 1 specimen geometry defined in this standard for extruded or molten plastics is used in scope of the method development process. The random geometries whose dimensions are determined with the consideration of the limits of the used 3D printer's building domain are used to prove the validation of the method for complex geometries. Rhinoceros3D® is used as CAD software for the design step. For the method, it is enough to draw the outer boundaries and the interior details of the geometry in 2D plane. The drawn wireframe geometries are used as inputs for the method. The algorithm of the method is developed by using Grasshopper3D® which is an algorithm generator for Rhinoceros3D®. It uses

functions as blocks. By creating block-chains, any algorithm can be constructed. After the design stage is done, the boundaries for the supports and the loads should be defined for FEA. Throughout the work, the artifacts are fixed from one end while the load is applied from the other end as described in ASTM D638. This step is important for the FEA case. The quasi-static FEAs are performed by using Karamba3D® which works as a plug-in on Grasshopper3D®. From the FEAs, Von Mises stress field results and the lines connect the first principal stress direction vectors are obtained, which are the source for the inhomogeneous interior structure under the tensile loading. Although the Von Mises stress field results which are generally considered for the ductile materials are obtained, the failure modes of the specimens with stress modified infill structures are brittle ones. In theory, it is recommended that the maximum principal stress field results should be used for the brittle materials. In the scope of this work, the stress field results under only tensile loadings are considered. For this case, the first principal stresses are effective, generally. Actually the case considered in this thesis is plane stress case. For plane stress cases, the first principal stress is equal to Von Mises stress. Because of this situation, the stress field results obtained by considering the Von Mises theory and maximum principal stress theory should be similar. From the FEAs performed in Abaqus®, it can be observed that these fields are similar to each other which can be observed in the related figures given previous chapters. So, this method can still be used for strength improvement considerations. Besides, the theory behind the FEA can be changed easily in the Karamba3D®. By changing the result visualization type as Von Mises or maximum principle stresses, this method can be used for the ductile or brittle materials, respectively. The heterogeneous interior is constructed by obtaining the lines related with the first principal stress direction vectors, offsetting them with a specified distance and trimming them by using the stress field region boundaries obtained from the FEA. The infill densities of the regions are determined according to the colors of the regions, which depend on the stress values of these fields. As a final step, the method generates G-code files for the specimens with modified infill structure for fabrication of them.

Within the scope of this work, the tensile testing is used to stimulate the loading condition in the FEA. Tests are performed by considering the ASTM-D638 testing procedure for the plastics. It is used to prove the reliability of the method. As can be inferred from the test results, the method provides nearly 45% strength increase for the ASTM D638 Type 1 specimens. For complex geometries, the strength increase is observed together with the maximum load per weight ratio. The proposed method provides load carrying capacity improvement in the range from 51% to 187% for them. It also provides improvement on the maximum carried load per weight between 59% and 92%. Based on the performed tests, it is obvious that the infill density is more effective on the strength of the parts than the infill pattern, which is a similar observation with the studies in the literature.

When the test result tables are considered, it is obvious that the mass values of the same geometries with the same infill densities are different. There can be many parameters exist to affect the mass values of the same geometries with same density percentages. As described in Chapter 5, there can be some particles remaining in the nozzle head which blocks the molten material flow. Due to the blocked flow, the extruded material value can be smaller than the required. Besides, the temperatures of the building plate or nozzle head can be improper for printing environment. For example, there are some warpage on the geometries which can be due to the improper temperature of the building plate. Because of the warpages, nozzle head can remove some amount of material from the last extruded layer. Moreover, environmental conditions such as moisture can affect the material properties which reduce the print quality. As similar with the improper building plate temperature, existing misalignments of the building plate can results in the amount of material reduction by the nozzle head. Finally, the printing speed can affect the mass values. 3D printer leaves some excess materials in the geometry for higher printing speeds. This issue increases the weight of the parts.

To sum up, the proposed automatic method provides an opportunity to improve the mechanical behaviors of 2.5D geometries under tensile loading. By using this method, the durability of either standard or non-standard complex parts can be improved with the help of the modified heterogeneous infill structure where

the geometries are fabricated using an open source FFF 3D printer. In scope of this study, ductile materials with brittle ones can be taken into consideration.

## 6.2 Recommendations for Further Studies

Throughout this study, the proposed method is developed for only 2.5D geometries under tensile loadings. The improvements listed below can be done for further studies.

- Method can be further improved for more intricate 2.5D geometries. For these types of geometries, the differences between the usage of different failure theories can be observed more clearly.
- Instead of tensile loading, method can be developed to be used with 2.5D geometries for different loading conditions such as bending, torque, etc. For this case, again the selection of the proper failure theory can be more significant.
- Different parameters such as printing time, printing speed, etc. can be taken into consideration for further improvements of the method. The temperature effects can also be taken into consideration to prevent the mass differences of the same geometries with the same infill density values.
- Method can be improved to be used for 3D geometries. This will require much more scripting and computational tasks. The improvement in this way is possible by using other FEA software because of the insufficiency of Karamba3D® for 3D cases. By using more advanced levels of scripting, the method can also be automatized by using the well-known FEA software such as Abaqus®.
- Method can be modified to improve the strength of the geometries by considering the fatigue loading scenarios. Optimum interior structure and the density values can be tried to be found.
- The geometries and the infill structures of the specimens used in Stauben's work can be used by applying the proposed method. This

makes it possible to compare the Stauben's work with the proposed one more properly.

- For all the geometries, stress fields are obtained by considering the Von Mises stress theory. This theory is used generally for ductile materials. While, the material behaves as ductile for the geometries with standard infill structures, it behaves as brittle for the specimens with stress modified interior structures constructed by using the proposed method in this thesis study. Some other theories such as the maximum principal stress theory can be used for the geometries with stress modified infill structures whose materials behave like brittle materials. Although the proposed method can be used, usage of stress field regions obtained from the FEA software by considering the proper failure theories for ductile and brittle materials can make this work more reliable.
- If there exist open-source 3D printers which utilize the metal materials, this work can be enlarged by usage of them.

## REFERENCES


[1] Vicente, M.F., Calle, W., Ferrandiz, S., Conejero, A. (2016). Effect of infill parameters on tensile mechanical behavior in desktop 3D Printing. 3D Printing and Additive Manufacturing, pp. 183-192.

[2] Johansson, F. (2016). Optimizing Fused Filament Fabrication 3D Printing for Durability (Master's Thesis) Retrieved from: http://www.diva-portal.se/smash/get/diva2:940935/FULLTEXT02.pdf .

[3] What is additive manufacturing?. (2016). Retrieved from http://additivemanufacturing.com/basics/

[4] Steuben, J.C., Iliopoulos, A.P., Michopoulos, J.G. (2016). Implicit slicing for functionally tailored additive manufacturing. Computer Aided Design, pp. 107-119.

[5] Feeney, D. (2013, August 29). FFF vs. SLA vs. SLS: 3D printing. Retrieved from http://www.sd3d.com/fff-vs-sla-vs-sls/

[6] What is 3D printing? Retrieved from: https://www.3dhubs.com/what-is-3d-printing#technologies

[7] Kerns, J. (2017). What's the Difference Between Stereolithography and Selective Laser Sintering. Retrieved from: https://www.3dhubs.com/what-is-3d-printing#technologies

[8] Boschetto, A., Giordano, V., Veniali, F. (2013). 3D roughness profile model in fused deposition modelling. Rapid Prototyping, pp. 240–252.

[9] Krolczyk, G., Raos, P., Legutko, S. (2014). Experimental analysis of surface roughness and surface texture of machined and fused deposition modeled parts. The Journal Tehnički vjesnik, pp. 217-221.

[10] Kuo, C.C., Su, S.J. (2013). A simple method for improving surface quality of rapid prototype. Indian Journal of Engineering and Material Sciences, pp. 465–470.

[11] Aditya, C., Akshay, G., Ravindra, J., Abhijit, N. (2017): Acetone Vapor Smoothing: A Post-processing Method for 3D Printed ABS Parts, pp.123-127, ISSN:2321-2705

[12] Lucknow. A., I., E., T., Gorakhpur, M., M., M.,U., T., Gorakhpur, G. (2014). An Analysis of Surface Roughness Improvement of 3D Printed Material. International Journal for Scientific Research & Development, Volume 2, Issue 7. ISSN (online): 2321-0613

[13] Kensuke Takagishi, Shinjiro Umezu. Development of the Improving Process for the 3D Printed Structure. Scientific Reports, 2017; 7: 39852 DOI: 10.1038/srep39852

[14] Wang, W., Zanni, C., and Kobbelt, L. (2016). Improved Surface Quality in 3D Printing by Optimizing the Printing Direction. EUROGRAPHICS 2016, Wiley

[15] Lanzetta, M., and Sachs, E. (2003). "Improved Surface Finish in 3D Printing Using Bimodal Powder Distribution", Rapid Prototyping Journal, Vol. 9 Issue 3 pp. 157 - 166

[16] Zhao, H., Gu, F., Huang, Q., Garcia, J., Chen, Y., Tu, C., Benes, B., Zhang, H., Cohen-Or, D., Chen, B. (2016). Connected Fermat Spirals for Layered Fabrication. ISBN: 978-1-4503-4279-7/16/07.

Retrieved from: http://dx.doi.org/10.1145/2897824.2925958

[17] Fodran, E., Koch, M., & Menon, U. (1996). Mechanical and dimensional characteristics of fused deposition modeling build styles. Solid Freeform Fabrication Proc. pp. 419-442.

[18] Sahu, R.K., Mahapatra, S., Sood, A.K. (2013). A study on dimensional accuracy of fused deposition modeling (FDM) processed parts using fuzzy logic. J Manuf Sci Prod 13(3). Pp. 183–197

[19] Sudin, M.N., Shamsudin, S.A., Abdullah, M.A. (2016). Effect of part features on dimensional accuracy of FDM model. APRN Journal of Engineering and Applied Sciences, pp. 8067-8072.

[20] Samantha S. (2015). 3D Printing & Dimensional Accuracy. Retrieved from: https://re3d.org/3dprintingdimensionalaccuracy/

[21] Simsek, S., Yaman, U. (2017). Dimensional Accuracy Improvement of Fused Filament Fabrication Holes Utilizing Modified Interior.

[22] Ingavale, P., Tak, A., Khopatkar, C., Barve, V., Bhure, S., Rajurkar, A. (2015, March 4st). Effect of 3D Printing Parameters on Dimensional Accuracy & Shrinkage

on Printed Parts. National Conference: Modeling, Optimization and Control (NCMOC).

[23] Kitakis, K., Alabey, P., Kechagias, J., Vaxevanidis, N. (2016). A Study of Dimensional Accuracy Obtained by Low Cost 3D Printing for Possible Application in Medicine. 20th Innovative Manufacturing Engineering and Energy Conference (IManEE 2016). DOI: 10.1088/1757-899X/161/1/012025

[24] Islam, M., N. (2013, July 3). An Investigation of Dimensional Accuracy of Parts Produced by 3D Printing: Proceedings of the World Congress on Engineering, Vol I. London, U.K.

[25] Kechagias, J., Stavropoulos, P., Koutsomichalis, A., Ntintakis, I., Vaxevanidis, N. (2014). Dimensional Accuracy Optimization of Prototypes produced by PolyJet Direct 3D Printing Technology. Advances in Engineering Mechanics and Materials, ISBN: 978-1-61804-241-5

[26] Mendricky, R (2016). Accuracy Analysis of Additive Technique for Parts Manufacturing. MM Science Journal. Pp: 1502-1508,
doi: 10.17973/MMSJ.2016_11_2016169

[27] Lu, L., Sharf, A., Zhao, H., Wei, Y., Fan, Q., Chen, A., Savoye, Y., Tu, C., Cohen-Or, D., Chen, B. (2014). Build-to-last: strength to weight 3D printed objects. ACM Transactions on Graphics.

[28] D. Adams & C. J. Turner (2017): An implicit slicing method for additive manufacturing processes, Virtual and Physical Prototyping, DOI: 10.1080/17452759.2017.1392684

[29] Tam, K., M., M., T., Mueller, C., T. (2017).Additive Manufacturing along Principal Stress Lines. 3D Printing and Additive Manufacturing, Volume 4, Number 2. Doi: 10.1089/3dp.2017.0001

[30] Baikerikar, P., J., Turner, C., J. (2017, August). Comparison of As-Built FEA Simulations and Experimental Results for Additively Manufactured Dogbone Geometries. Proceedings of the ASME 2017 International Design Engineering Technical Conferences and Computers and Information in Engineering Conference, IDETC/CIE 2017, USA. DOI: 10.1115/DETC2017-67538

[31] What is Rhino. Retrieved from: http://www.visualarq.com/info/what-is-rhino/ (Date accessed: 30.07.2017)

[32] ASTM D638-2010: Standard Test Method for Tensile Properties of Plastics

[33] Online forum: http://www.grasshopper3d.com/ (Date accessed: 08.09.2016)

[34] The Grasshopper Primer. Retrieved from: http://grasshopperprimer.com/en/0-about/1-grasshopper-an-overview.html

[35] What is Abaqus?. Retrieved from: http://mashayekhi.iut.ac.ir/sites/mashayekhi.iut.ac.ir/files//u32/presentation2_0.pdf

[36] Timoshenko, S. Theory of Elasticity. (McGraw Hill, California, 1934), pp. 11–46.

[37] Young, W., C. and Budynas, R., G. Roark's Formulas for Stress and Strain. (McGraw Hill, New York, 2002)

[38] WRL File Extension. Retrieved From: https://www.file-extensions.org/wrl-file-extension (Date accessed: 18.08.2017)

[39] Millipede, Online forum: http://www.grasshopper3d.com/group/millipede (Date accessed: 24.02.2017)

[40] Millipede Manual, 2014: User Manual

[41] Karamba3D, 2016: User Manual

[42] Slicer, 2013: User Manual

[43] Kim, H. (2017, May 31). Boundary Curves from Mesh Colors [Online forum comment]. Message posted to http://www.grasshopper3d.com/forum/topics/boundry-curves-from-mesh-colors?commentId=2985220%3AComment%3A1762127